

Assessing the Impacts of Silver Nanoparticles on the Growth, Diversity, and Function of Wastewater Bacteria

by

Christina Lee Arnaout

Department of Civil and Environmental Engineering
Duke University

Date: _____

Approved: _____

Claudia Gunsch, Supervisor

Mark Wiesner

Heileen Hsu-Kim

Joel Meyer

Dissertation submitted in partial fulfillment of
the requirements for the degree of Doctor of Philosophy in the Department of
Civil and Environmental Engineering in the Graduate School
of Duke University

2012

ABSTRACT

**Assessing the Impacts of Silver Nanoparticles on the Growth,
Diversity, and Function of Wastewater Bacteria**

by

Christina Lee Arnaout

Department of Civil and Environmental Engineering
Duke University

Date: _____

Approved: _____

Claudia Gunsch, Supervisor

Mark Wiesner

Heileen Hsu-Kim

Joel Meyer

An abstract of a dissertation submitted in partial fulfillment of
the requirements for the degree of Doctor of Philosophy in the Department of
Civil and Environmental Engineering in the Graduate School
of Duke University

2012

Copyright by
Christina Lee Arnaout
2012

Abstract

Silver nanoparticles (AgNPs) are increasingly being integrated into a wide range of consumer products, such as air filters, washing machines, and textiles, due to their antimicrobial properties [1]. However, despite the beneficial applications of AgNPs in consumer products, it is likely that their use will facilitate the release of AgNPs into wastewater treatment plants, thereby possibly negatively impacting key microorganisms involved in nutrient removal. For this reason, it is important to characterize the effects of AgNPs in natural and engineered systems and to measure the antimicrobial effect of AgNPs on wastewater microorganisms. Polyvinyl alcohol coated AgNPs have already been linked to decreased nitrifying activity and it is important to determine if AgNPs coated with other materials follow similar trends [2]. Furthermore, it is likely that with repeated exposure to AgNPs, microbial communities could evolve and develop resistance to Ag. Thus, a long-term effect of Ag nanoparticle exposure could be a reduction of the efficacy of such products in a similar fashion to the development of microbial antibiotic resistance [3]. Therefore, it is critical that the impacts of these materials be ascertained in wastewater treatment systems to prevent long-term negative effects.

The objectives of this dissertation were to: 1) characterize the effect of several different AgNPs on the ammonia oxidizing bacterium (AOB) *Nitrosomonas europaea* and investigate possible mechanisms for toxicity, 2) test the effects of consumer product AgNPs on a wide range of heterotrophic bacteria, 3) evaluate the effects of AgNPs on

bench scale wastewater sequencing batch reactors, and finally 4) assess the impacts on soil microbial communities which have been amended with wastewater biosolids containing AgNPs.

Nitrosomonas europaea was selected as the model ammonia oxidizing bacterium (AOB) for this study because AOB carry out the first step in the nitrification process and are known to be sensitive to a wide range of toxicants [4]. The antimicrobial effects of AgNPs on *N. europaea* were measured by comparing nitrite production rates in a dose response assay and analyzing cell viability using the LIVE/DEAD® fluorescent staining assay. AgNP toxicity to *N. europaea* appeared to be largely nanoparticle coating dependent. While PVP coated AgNPs showed reductions up to 15% in nitrite production at 20 ppm, other AgNPs such as gum arabic (GA) coated showed the same level of inhibition at concentrations of 2 ppm. Inhibition appears to occur through a cascade of mechanisms. First, a post-transcriptional disruption of the ammonia monooxygenase (AMO) and hydroxylamine oxidoreductase (HAO) encoding genes occurs by either dissolved Ag or ROS interference. This caused a decrease in nitrification ability in the cells that were not completely lysed (2 ppm GA AgNP and 2 ppm PVP AgNP treatments). The degree of nitrification disruption is dependent on AgNP characteristics, such as zeta potential and coating, which mediate how fast the AgNP will release Ag⁺ and induce ROS production. Finally, at high enough concentrations, total membrane loss

and release of internal cellular matter occurs, causing cell death (2 ppm Citrate AgNPs, 20 ppm GA and PVP AgNPs).

In the second part of this dissertation, the effects of AgNP containing consumer products (namely health supplements) were compared to pure AgNPs. To this end, bacterial toxicity assays were carried out on well-studied heterotrophic bacteria. Model Gram-positive and Gram-negative bacteria (*Bacillus subtilis* and *Escherichia coli*, respectively) were selected to assess any differences in sensitivity that may occur with the exposure to AgNPs. A third model Gram-negative bacterium (*Pseudomonas aeruginosa*) was chosen because of its ubiquitous presence in the environment. Growth curve assays and LIVE/DEAD staining indicated that the consumer product AgNPs had the most significant effect on growth rates, but not membrane integrity. Overall, *P. aeruginosa* was most negatively affected by all AgNPs with nearly 100% growth inhibition for all 2 ppm AgNP treatments. TEM imaging also confirmed cell wall separation in *P. aeruginosa* and *E. coli*. The effects on *B. subtilis*, the Gram-positive bacterium, were not as severe but toxicity was observed for several AgNPs at 2 ppm concentrations. Reduced toxicity to *B. subtilis* may have been a result of the thick peptidoglycan layer with thiol groups where metal species could attach and grow into aggregates [5]. Previous studies have shown that *B. subtilis* membrane walls bind more readily with ionic metals than Gram positive bacteria and the variance in AgNP dissolution rate may resulted in the inconsistency in growth functions [6]. TEM imaging indicated that AgNPs were not as

penetrative to *B. subtilis* as they were to the Gram-negative bacteria. Membrane integrity assays did not show one type of AgNP to strongly cause membrane loss, but all AgNPs did impart some cell damage at concentrations of 2 ppm or greater. In general, trends in this studied showed that toxicity to heterotrophic bacteria was dependent on the type of AgNP used and Gram-negative bacteria were more likely to be internally disrupted than Gram positive bacteria.

For the third section of this dissertation, the effects of pure AgNPs on complex microbial wastewater reactors were also tested. Eight bench-scale sequencing batch reactors were operated with an 8 h hydraulic retention time and constant aeration. Reactors were fed synthetic wastewater and treatment efficiency was measured by monitoring effluent concentrations of chemical oxygen demand (COD), NH_4^+ , and NO_3^- . After reaching steady state with 90%+ removal of COD and ammonia, the reactors were spiked with 0.2 ppm gum arabic and citrate coated AgNPs with 3 pulse spikes of different time lengths (14, 6, and 2 d), and then a 0.2 ppm continuous spike for three solids residence times (33 d). Treatment efficiency was monitored and results showed significant increases in ammonia and COD immediately following the first spike. COD removal appeared to be sensitive to AgNP spikes and decreased by approximately 20 to 30% within 4 h after each Ag spike. Ammonia removal was more strongly affected by Ag from AgNO_3 than AgNPs. In general, the treatment efficiencies dropped immediately after the pulse spikes but were able to recover similarly to COD removal. At the 14 d pulse spike, ammonia

removal changed from 98% to 97%, 83%, and 32% for citrate AgNPs, GA AgNPs, and Ag as AgNO₃, respectively, at the end of the first cycle. Reactors were able to recover in 3 to 5 d and return to steady state removal. Investigation of microbial community using terminal restriction fragment length polymorphism (T-RFLP) showed community shifts as AgNP spikes continued. These may have been a result of adaptation to the heavy metal input. Diversity indices of AgNP treated SBRs also decreased relative to the control SBR, signifying the narrowing of the bacterial community.

The last part of this dissertation examines the effects of land-applied biosolids spiked with AgNPs on soil microbial communities. Terrestrial mesocosms containing wetland plants were set up in the Duke Forest and applied with Class A biosolids mixed with PVP AgNPs or Ag as AgNO₃. Mesocosms were allowed to grow for 50 d and soil samples were taken below spiking, the day after, and 50 d after. Our microbial community analyses using T-RFLP conclude that soil bacterial communities will be altered if Ag and AgNP spiked biosolids are land applied. Overall, distinct shifts in microbial community were observed in Ag treated samples after 1 d that were statistically different from the biosolids and no biosolids controls. After 50 d, the AgNP induced clustering was not as obvious, possibly because the communities had time to adapt to environmental changes. T-RFLP fragments were used to identify which species of bacteria were present using ribosomal database matching. Fragment matching indicated that the *Proteobacteria* community decreased initially and *Firmicutes* become more dominant. We did not

observe any decrease in diversity, but rather an increase, possibly due to the bacteria supplemented by the biosolids slurry, which appears to be more diverse than the natural soil microbial community. Denitrifying bacteria, which are important for nitrogen cycling in soil, may have been negatively impacted AgNPs since they fall under the *Proteobacteria* phylum.

Overall, this dissertation asserts that AgNPs have a toxic effect on bacteria, which can be even more than pure Ag as AgNO₃, due to their unique physical and chemical properties like size, Stern layer charge, coating composition, and stability. Based on the types of AgNP used in consumer products, it may be possible to predict which AgNPs may be more detrimental wastewater treatment, but not all AgNPs will have the same effect. AgNPs at concentrations of 0.2 to 2 ppm were shown to be inhibitory to nitrifying bacteria, heterotrophic bacteria, and the mixed microbial community found in wastewater SBRs. Consumer product AgNPs were also proven to be of concern to environmental engineers since their toxicity was at level or sometimes higher than laboratory made AgNPs. Future studies regarding AgNPs should include an investigation of the prevalence of Ag resistance in wastewater to assess how resilient wastewater microbes are to Ag. The results obtained herein should also be expanded to other types of AgNPs and microorganisms of ecological importance.

Dedication

This dissertation is dedicated to my parents, Samir and Linda Arnaout, for their undying support and love. Thank you for never letting me give up my career aspirations and for always offering me advice and encouragement. I wouldn't be in this place in my life without you.

Contents

Abstract.....	iv
List of Tables	xiii
List of Figures.....	xiv
Acknowledgements.....	xvii
1. Introduction.....	1
1.1 Introduction and Problem Definition.....	1
1.2 Research Hypotheses and Approach.....	3
2. Literature Review.....	6
2.1 Definition of AgNPs, Sources and Human Risk.....	6
2.2 AgNP Chemistry and Characterization.....	9
2.2.1 Synthesis and Structure.....	11
2.2.2 Dissolution, Complexation and Speciation.....	12
2.3 Possible Pathways of Microbial Inactivation.....	14
2.4 Ag as a bactericide.....	16
2.5 AgNPs in WWTPs.....	17
2.7 Ag interactions with complex media such as wastewater.....	19
3. Impacts of Silver Nanoparticle Coating on the Nitrification Potential of <i>Nitrosomonas europaea</i>	21
3.1 Introduction.....	21
3.2 Materials and Methods.....	23
3.3 Results and Discussion.....	29

4 Toxicity of Silver Nanoparticles found in Consumer Products on Growth and Function of Three Model Bacteria	43
4.1 Introduction.....	43
4.2 Materials and Methods.....	45
4.3 Results and Discussion	51
5 Assessing the effects of Ag Nanoparticles on Biological Nutrient Removal in Bench-Scale Activated Sludge Sequencing Batch Reactors	67
5.1 Introduction.....	67
5.2 Materials and Methods.....	69
5.3 Results and Discussion	76
6 Soil Bacterial Community Dynamics in Terrestrial Mesocosms treated with Biosolids Containing Ag Nanoparticles.....	88
6.1 Introduction.....	88
6.2 Materials and Methods.....	90
6.3 Results and Discussion	95
7 Conclusions and Engineering Significance	104
References.....	119
Biography.....	138

List of Tables

Table 1: Physical and chemical properties of CEINT and consumer product AgNPs	55
Table 2: Order of Ag addition to SBRs	72
Table 3: Label guide for SBR T-RFLP sample	84
Table 4: Diversity indices of Ag treated SBRs	86
Table 5: R statistic similarity values for terrestrial mesocosms	96
Table A6: Ratio of Ag to nanoparticle coating and concentrations tested with <i>N. europaea</i>	110
Table A7: Primer sequences used for qRT-PCR.	113
Table A8: Dissolved Ag concentration after 4 h exposure period in AOB medium with <i>N. europaea</i>	114

List of Figures

- Figure 1: Nitrogen cycle of wastewater (Adapted from Zeng et al. [96]) 17
- Figure 2: Percent reduction in nitrification rate in AgNP treatments compared to no Ag control, as a function of total Ag concentration (A) and dissolved Ag concentration (B). Error bars indicate standard deviation values between 6 replicates. The targeted total Ag concentration was not statistically different from the measured total Ag concentration.. 32
- Figure 3: Nitrite production rate vs. treatments containing cysteine addition. Asterisks indicate statistical significance ($p < 0.05$). Error bars represent the standard deviation of triplicate samples. 34
- Figure 4: LIVE/DEAD microscopy results - percent of cells with compromised membranes. Pure Ag^+ ion at 0.2 ppm (not shown) disrupted almost all membranes, with $93 \pm 19\%$ membranes broken. Asterisks indicate statistical significance ($p < 0.05$) between no Ag samples and AgNP treatment samples. Error bars represent the standard deviation of triplicate samples. 37
- Figure 5: TEM images of no Ag control (A), 0.2 ppm Ag^+ as AgNO_3 (B), 2 ppm citrate AgNP treatment (C), 2 ppm gum arabic AgNP treatment (D), and 2 ppm PVP AgNP (E). 39
- Figure 6: Gene expression of *merA* relative to 16S rRNA reference gene. Higher concentrations of AgNPs (20 ppm) were significantly up-regulated in fold change. Error bars represent the standard deviation of triplicate samples. 41
- Figure 7: Illustration of effects of Ag^+ from AgNPs in *N. europaea*. As Ag^+ concentration reaches approximately 20 ppb, nitrification is inhibited and cell death and lysis is reached at 60 ppb..... 42
- Figure 8: Total and dissolved Ag concentration for gum arabic (GA), citrate (CA), MS (Mesosilver), SS (Sovereign Silver), and SB (Silver Biotics) AgNPs. Ionic Ag (Ag as AgNO_3) was also run as a positive control sample. Error bars represent the standard deviation of duplicate samples..... 52
- Figure 9: TEM images at 200 kV of three different consumer product AgNPs: (A) Mesosilver, (B) Silver Biotics, (C) Sovereign Silver. 54
- Figure 10: Percent reduction in growth rate for gum arabic (GA), citrate (CA), MS (Mesosilver), SS (Sovereign Silver), and SB (Silver Biotics) AgNPs. Ionic silver (Ag as AgNO_3) was also run as a positive control sample. Asterisks indicate statistical

significance ($p < 0.05$) between no Ag samples and AgNP treatment samples. Error bars represent the standard deviation of triplicate samples.	58
Figure 11: Trends in reduced GSH/GSSG ratio in <i>P. aeruginosa</i> cultures. Error bars represent the standard deviation of triplicate samples.	59
Figure 12: Percent membranes compromised for gum arabic (GA), citrate (CA), MS (Mesosilver), SS (Sovereign Silver), and SB (Silver Biotics) AgNPs. Ionic Ag (Ag as AgNO ₃) was also run as a positive control sample. Asterisks indicate statistical significance ($p < 0.05$) between no Ag samples and AgNP treatment samples. Error bars represent the standard deviation of triplicate samples.	61
Figure 13: TEM images of <i>P. aeruginosa</i> for control cells (A), 0.2 ppm Ag as AgNO ₃ treatment (B), citrate (C), gum arabic (D), Silver Biotics (E), Mesosilver (F), and Sovereign Silver AgNPs treatments (G). Ionic Ag (Ag as AgNO ₃) was also run as a positive control sample. All samples were examined at 80 kV.	63
Figure 14: TEM images of <i>B. subtilis</i> for control cells (A), 0.2 ppm Ag as AgNO ₃ treatment (B), citrate (C), gum arabic (D), Silver Biotics (E), Mesosilver (F), and Sovereign Silver AgNPs treatments (G). Ionic Ag (Ag as AgNO ₃) was also run as a positive control sample. All samples were examined at 80 kV.	64
Figure 15: TEM images of <i>E.coli</i> for control cells (A), 0.2 ppm Ag as AgNO ₃ treatment (B), citrate (C), gum arabic (D), Silver Biotics (E), Mesosilver (F), and Sovereign Silver AgNPs treatments (G). Ionic Ag (Ag as Ag) was also run as a positive control sample. All samples were examined at 80 kV.	65
Figure 16: SBR schematic showing influent and effluent pumping, aeration, and mixing which were controlled by timers.	70
Figure 17: Total and dissolved concentration of Ag measured from AgNP, Ag as AgNO ₃ and control SBRs. Error bars represent the standard deviation of duplicate samples.	79
Figure 18: COD and ammonia removal percentages in SBRs during pulse and continuous inputs.	82
Figure 19: Nitrite and nitrate concentrations in SBRs during 0.2 ppm pulse and continuous Ag spikes.	83
Figure 20: Bray-Curtis similarity indices of Ag treated SBRs.	85
Figure 21: PC-ORD ordination diagram showing clustering of all communities and samples. Day 0 = 8/25/09, Day 1 = 8/26/09, and Day 50 = 10/14/09.	97

Figure 23: Phyla of bacteria found in terrestrial mesocosms, sorted by treatment and date. “CNTL” = control boxes, “AG” = treated with Ag as AgNO₃ and biosolids slurry, “PVP” = treated with PVP AgNPs and biosolids slurry, “SLUR” = treated with only the biosolids slurry..... 102

Figure A24: TEM imaging of AgNPs used. Right to left: Citrate coated, gum arabic coated, and PVP coated AgNPs. Please note the aggregation state of PVP particles. Individual particles can be seen but surface area was drastically reduced in these aggregates. 110

Figure A25: Gene expression of *amoA* relative to 16S rRNA reference gene. No treatments significantly changed with exposure to AgNPs. Error bars represent the standard deviation of triplicate samples..... 114

Figure A26: Gene expression of *hao* relative to 16S rRNA reference gene. The pure Ag⁺ as AgNO₃ treatment was significantly up-regulated. Error bars represent the standard deviation of triplicate samples. 115

Figure B27: Growth rates of bacteria treated with AgNPs. Asterisks indicate statistical significance ($p < 0.05$) between no Ag samples and AgNP treatment samples. Error bars represent the standard deviation of triplicate samples. 116

Figure B28: Primary peak weight percentage vs. particle radius (nm) of all AgNPs..... 116

Figure B29: Ordination diagram of T-RFLP communities, sorted by day..... 117

Figure B30: Ordination diagram of T-RFLP profile clusters, sorted by treatment 118

Acknowledgements

First and foremost, I would like to thank my family and fiancé for their enduring love and support. Sam and Linda Arnaout, thank you for listening to me during the high and low points of my PhD journey and for always giving me the encouragement to continue and persevere. Diane Arnaout, thank you for being my protector, rationalizer and biggest supporter. Philip, thank you for being the stability I needed during this unstable time. Your support has meant so much to me and you always gave me excellent advice when I needed it. I am so thankful that you were able to come to Duke Law while I was at Duke Graduate School.

I would like to show my sincere appreciation to my adviser, Dr. Claudia K. Gunsch, for her support and advice throughout my dissertation research. She has been a patient mentor to me, not only regarding academic matters, but also career guidance. Her thoughtful and analytical mind guided me whenever I hit a bump in the road, and I truly admire her ability to balance work and family. I feel so lucky to have had her as my Ph.D. adviser and I hope she knows my endless gratitude.

I want to thank the members of my Ph.D. committee as well for their guidance and support. Dr. Hsu-Kim always welcomed my frantic questions at 3 pm regarding Ag speciation and I appreciate all of her advice. Without her and her lab, I would have greatly struggled to quantify and understand the complexation of silver in my

experiments. Dr. Wiesner always challenged me with his thoughtful and conceptual questions throughout my Ph.D. His inquisitive nature led me to explore new areas of my research that were very beneficial to the development of my dissertation. Dr. Meyer taught me about microbial stress responses and guided me on several of my microbial glutathione experiments. I am very grateful for his knowledge and assistance.

Last but certainly not least, I want to show my deep appreciation for the graduate students who help me succeed in graduate school. Without their advice and support, I would have struggled my whole way through my dissertation. First, Kaoru Ikuma taught me everything I know about laboratory practice. I am grateful for her endless encouragement and willingness to discuss research matters at any time. I also want to thank Amrika Deonarine, Andreas Gondikas, and Tong Zhang for helping me with all things chemistry (and life too). I want to thank the Gunsch Lab group for raising interesting discussions in journal club. I especially want to thank Carley Gwin for maintaining my sequencing batch reactors for me while I was writing my dissertation.

1. Introduction

1.1 Introduction and Problem Definition

The use of nanomaterials in industrial applications and consumer products has been increasing steadily as novel applications related to their unique properties are discovered. However, in general, little is known about the environmental fate, transport, and toxicity of nanomaterials. Nanoparticle properties can change significantly depending on their method of synthesis, shape, size and coating. Thus, it is critical to determine how these materials can impact natural and engineered settings (e.g., surface waters as well as water and wastewater treatment plants (WWTPs)). Some nanomaterials have been shown to: 1) exhibit features similar to known toxicants; 2) have the potential to interact with other toxicants and mobilize them and; 3) inhibit the growth of environmentally sensitive microorganisms [7]. However, the full extent of these issues is unknown for many different classes of nanoparticles.

Silver nanoparticles (AgNPs) in particular are increasingly gaining attention due to their antimicrobial properties [8, 9]. Many new applications for AgNPs have recently been developed, including AgNP embedment in bacterial cellulose wound dressings, water filters, and surface coatings for biofilm prevention [10-12]. AgNPs have also been measured in WWTPs and sludge biosolids in the form of Ag sulfide nanoparticles [13]. There is increasing concern that AgNP loading to WWTPs may disrupt sensitive biological nutrient removal processes, such as nitrification, and ultimately lead to WWTP

failure [14]. Therefore, there is a significant need to characterize AgNPs, determine their interaction with complex media and ascertain how their presence affects the growth of sensitive wastewater microorganisms.

Because ionic silver (Ag^+) is known to be toxic to bacteria, algae and a variety of other organisms, the general hypothesis for this dissertation is that the presence of AgNPs will also negatively impact ecologically important microbial functions by releasing ionic Ag as their coatings dissolve [15-17]. The overarching goal of this dissertation project was to investigate the impact of AgNPs on wastewater treatment. Specifically, their effects were measured by monitoring sensitive microorganisms (i.e. ammonia-oxidizing bacteria and activated sludge cultures) in wastewater treatment by examining the growth inhibition and mechanism of toxicity of AgNPs. The effects on bacterial community structure were also assessed in bench scale activated sludge sequencing batch reactors (SBRs) and land application of biosolids. By keeping track of divergences in microbial population, this study determined the possible upsets associated with AgNP release into natural and engineered environments.

The specific research objectives of this doctoral research were to:

1. Assess the impacts of AgNPs on pure culture heterotrophic bacteria and identify possible mechanisms of inactivation.

2. Evaluate the antimicrobial effects of AgNPs and investigate mechanisms of inactivation on a model wastewater nitrifying autotroph, *Nitrosomonas europaea*.
3. Quantify impacts of AgNPs in bench scale SBRs mimicking wastewater operation.
4. Examine differences in microbial community structure following land-application of AgNP containing biosolids.

1.2 Research Hypotheses and Approach

The impacts of AgNPs were evaluated by monitoring bacterial inhibition in pure culture studies, changes in microbial community structure, and the disruption of basic nutrient removal processes in more complex environments. The analysis included a comprehensive Ag mass balance as well as a mechanistic examination of microbial inhibition. Objective 1 was carried out by testing the effects of two lab-created AgNPs (gum arabic and citrate coated) and three consumer product AgNP supplements on pure cultures of *Pseudomonas aeruginosa*, *Escherichia coli*, and *Bacillus subtilis*. Liquid cultures were exposed to concentrations ranging from 0.2 to 2 ppm of AgNPs and growth curves were measured by monitoring optical density. Membrane integrity assays were performed by exposing late log phase cultures to AgNPs, then LIVE/DEAD fluorescence intensity was measured via 96-well plates. Extensive transmission electron microscopy

(TEM) imaging was completed to evaluate the morphological differences of bacteria exposed to AgNPs. Total and dissolved Ag measurements were taken at different time points to assess the relationship between toxicity and Ag speciation and concentration. Lastly, reduced and oxidized glutathione was measured in bacterial cultures to measure the oxidative stress caused by AgNPs.

Objective 2 was carried out by dosing *Nitrosomonas europaea*, a model wastewater nitrifying bacterium, with three different lab-created AgNPs (gum arabic, citrate, and PVP coated). Nitrification rate were measured and cell morphology was compared using membrane integrity assays and TEM imaging. Cysteine rescue experiments were performed to determine if excess thiol presence could quench Ag toxicity caused by the AgNPs. Finally, quantitative reverse transcription polymerase chain reaction (qRT-PCR) was completed to determine if nitrification and metal resistance genes were affected by AgNP addition. Total and dissolved Ag measurements provided relationships between AgNP concentration and toxicity. The findings from this objective have been published in *Environmental Science and Technology* [18].

Objective 3 was accomplished by operating bench scale SBRs seeded with activated sludge from the North Durham WWTP. The reactors were fed synthetic wastewater and allowed to reach steady state for 120 d. Four conditions were tested on the SBRs: a no Ag control, 0.2 ppm gum arabic coated AgNPs, 0.2 ppm citrate coated AgNPs, and 0.2 ppm

Ag^+ as AgNO_3 . Reactors were first fed with pulse inputs (14 d, 6 d, and 2 d in length) and then continuously fed Ag for 3 solids residence times (39 d). Treatment efficiency of the SBRs was monitored approximately every 3 d or 1 SRT after spiking. Chemical oxygen demand (COD), ammonia, nitrate, and nitrite were all monitored. Samples were taken periodically to measure the amount of total and dissolved Ag in the reactors. DNA was isolated from reactor cell biomass and terminal restriction fragment length polymorphism (T-RFLP) of 16S SSU rDNA and nitrification genes was utilized to visualize shifts in microbial community.

Objective 4 was achieved by applying terrestrial mesocosm boxes with class A biosolids mixed with PVP coated AgNPs or Ag^+ as AgNO_3 . Soil samples were taken from mesocosm and DNA was extracted for T-RFLP analysis. Ordinations and similarity analyses were used to determine if the microbial community shifted with the addition of Ag. Ribosomal database matching was also carried out to determine which bacterial phyla were dominant after Ag spikes.

2. Literature Review

2.1 Definition of AgNPs, Sources and Human Risk

The definition of a nanotechnology, as defined by the Environmental Protection Agency (EPA), is as follows: “research and technology development at the atomic, molecular, or macromolecular levels using a length scale of approximately 1–100 nm in any dimension; the creation and use of structures, devices, and systems that have novel properties and functions because of their small size, and the ability to control or manipulate matter on an atomic scale.” Specifically, a nanoparticle is defined as a particle consisting of 10 to 10⁵ atoms that is utilized for its unique size characteristics, which can fulfill a variety of functions, such as serving as biosensors, nanoelectric materials, and also antibacterial consumer products [19, 20]. One class of nanoparticles that is specifically utilized for its antibacterial properties is nano Ag; a group of Ag molecules surrounded by a stabilizing coating, which is usually formed through the reaction of a Ag salt and a reducing agent [21].

The use of ionic Ag as an antimicrobial agent spans back to ancient Egyptian times, where it was utilized for its antiseptic properties [22]. More recently, Ag nanoparticles (AgNPs) are increasingly being used in replacement of ionic Ag because of their chemical and bactericidal properties. AgNPs can be manufactured with a variety of coatings to increase stability which has facilitated their incorporation into a wide range of consumer products including wound dressings, air filters, washing machines, textiles, and

baby pacifiers [23]. The list of consumer products is also expanding to include cosmetics, cleaning solvents, and athletic activity equipment [24, 25]. Because AgNPs range from 1 to 100 nm, researchers suspect that they may infiltrate the cell membrane of a microorganism, then release ionic Ag directly into the microbe [26]. Recent studies have also tried to quantify the amount of total Ag present in several consumer products, and a concentration range of 1.4 to 270,000 $\mu\text{g Ag g/product}$ was found [27]. Because of the high variation in Ag concentration present in consumer products, it is difficult to find estimations of the total Ag and nano Ag being added to consumer products. Benn et al. [28] found that AgNP containing socks leached up to 68 $\mu\text{g Ag/g sock}$ in water with gentle agitation, while Geranio et al. [29] measured up to 377 $\mu\text{g/g}$ with the application of detergent.

In addition to consumer products, AgNPs have been integrated into an array of manufacturing and industrial settings for their unique chemical properties or to prevent microbial growth. Yu et al. [30] found that AgNP/TiO₂ “nanosponge” composite photocatalysts were superior in UV light photocatalytic activity when compared to TiO₂ nanosponges, because of their uniform AgNP distribution and electron interactions between AgNPs and TiO₂. AgNPs and other metal nanoparticles could also have a future in gene therapy and other medical applications. DNA-conjugated AgNPs are in development for recognition, transfer and manipulation of genes because of their unique optical and catalytic properties [31]. AgNPs and AuNPs (gold) functionalized with

ampicillin increased antibacterial activity and uptake of the antibiotics into multiple-antibiotic-resistant strains of bacteria including *Pseudomonas aeruginosa* [32]. The incorporation of AgNPs into sulfonated polyethersulfone (SPES) membranes would make this type of membrane available for aseptic usage in food industries, biomedical engineering, and hospital machinery [33].

The EPA has set some limits on the concentration of Ag allowable in environmental settings, such as the secondary maximum contaminant level of 100 ppb in drinking water [34]. The EPA has also examined the amount of Ag found in biosolids, a waste product from the wastewater treatment process, where leftover sludge that has settled out of wastewater is dewatered, dried, and sometimes sold as a fertilizer for non-human consumption plants. A variety of biosolids from different wastewater treatment plants were tested, and the average concentration measured via inductively coupled plasma atomic emission spectroscopy (ICP-AES) was 23 ± 31 mg Ag/kg biosolids, but samples ranged from 1.94 to 856 mg/kg [35]. The ceiling concentration for Ag in sludge/biosolids has not been established; currently, only As, Cd, Cu, Pb, Hg, Mo, Ni, Se, and Zn are regulated in title 40, part 503 of federal regulation [36].

Human risk assessment of consumer product AgNPs has become a wide topic of discussion, including evaluations of cosmetic usage by German consumers, leaching of AgNPs into food from AgNP coated food containers, and human health risks of

aerosolized AgNPs [37-39]. Researchers have recently begun to evaluate the deposition of AgNPs in the human body and their toxicology on contact with internal organs. Fröhlich et al. [24] found that the complexities of the esophageal and digestion tract, such as inherent pH, mucus composition/excretion, and gastrointestinal flora, complicated the prediction of AgNP uptake from consumer products. Samberg et al. [40] studied a variety of AgNPs and their effects on human epidermal keratinocyte (HEK) skin cells. They observed uptake of AgNPs into cytoplasmic vacuoles and overall inflammation, but low mortality of HEKs [40]. The effects of AgNPs on fertility have also come into question. Asare et al. [41] compared the cytotoxicity of AgNPs (20 and 200 nm) to TiO₂ nanoparticles in testicular cells and concluded that the AgNPs were more likely to induce oxidative stress, DNA mutations, and apoptosis.

2.2 AgNP Chemistry and Characterization

Since AgNPs can be fabricated and designed optimally for nearly any size, shape, and function, there is an inherent amount of variability in their toxicity, which depends on their interaction with complex media such as wastewater, soil, and surface water. Before examining the different types of AgNPs made, it is important to understand how AgNPs can be characterized and the terminology used in most publications. The detection of different sizes, shapes, aggregates and species of Ag released by AgNPs is variable in AgNP literature, since several different methods are preferred. One of the most frequently used method of Ag concentration is inductively coupled plasma mass spectrometry (ICP-

MS) which can be used to measure total Ag, or dissolved Ag, by filtering the sample through a filter with < 2 nm pore size [42-45]. Another available used Ag detection method is atomic adsorption, which measures the light emitted from gaseous state free ions [46]. Zook et al. [47] argues that ICP-MS and AA are not sufficient for estimating Ag left in AgNPs after AgCl has formed, in addition to its inability to characterize Ag oxidation. Instead, they suggest using localized surface plasmon resonance (LSPR) UV-vis absorbance to identify non-AgCl species by examining absorbance spectra [47].

Other properties of AgNPs that are frequently measured are the hydrodynamic diameter, the zeta potential (ZP), and the polydispersity index (PDI). The ZP is important for measuring the colloid stability of the AgNP suspension, which reveals how likely the sample is to aggregate by measuring the surface charge of the slipping plane [46]. ZP values close to 0 mV tend to aggregate more and be less stable in suspension form, while samples around ± 30 mV have considerable electrostatic repulsion, which stabilizes them. The PDI is a measure of the homogeneity in a suspension, and a higher PDI typically indicates a more diverse sample that is less homogenous, which could affect toxicity [48]. Lastly, hydrodynamic diameter is frequently used to describe the size of aggregates found in AgNP suspensions, rather than the individual particle size, which can be estimated by transmission electron microscopy (TEM) [49, 50].

2.2.1 Synthesis and Structure

AgNPs can be created in a variety of manners and customized to meet the needs of the application. Surface charge, size, and polydispersity are all factors that can be controlled. Electrostatically stabilized AgNPs, such as citrate stabilized AgNPs, are created by reducing Ag nitrate in water with sodium citrate [51]. Sodium dodecyl sulfate (SDS) and cetyltrimethylammonium chloride or bromide (CTAC, CTAB) stabilized AgNPs also fall under the electrostatically stabilized AgNP group [52]. Sterically stabilized AgNPs, such as poly(N-vinylpyrrolidone) (PVP) stabilized AgNPs, can be produced by heating Ag chloride and PVP with a solvent to induce surface attachment, or photoreduction of Ag nitrate in the presence of PVP [53, 54]. Sur et al. [55] showed that AgNPs can also be functionalized with compounds such as lactose and glucose to encourage uptake into living cancer cells.

There is no consensus on the best stabilizing coating. Researchers appear to be divided, possibly because of the wide range of media and conditions in which the AgNPs were used. Tejamaya et al. [56] found PVP AgNPs to be the most stable over 21 d in media containing chloride, yet our own study found PVP AgNPs to be the most aggregated after only 4 h. One explanation for the aggregation in PVP AgNPs used in the present study is that the particles were synthesized at a suboptimal PVP:AgNO₃ ratio. Wang et al. [57] found that a PVP:AgNO₃ ratio greater than 1.5 was ideal for colloid stabilization. More information regarding our study can be found in Chapter 3 of this dissertation.

2.2.2 Dissolution, Complexation and Speciation

The dissolution, complexation, and speciation (DC&S) of Ag and AgNPs are important factors that dictate the toxicity and availability of Ag to interact with biota. Studies thus far seem to agree that DC&S are a function of the AgNP stabilizing coating, which will interact with ions found in the matrix. Piccapietra et al. [58] recently studied the DC&S of carbonate stabilized AgNPs in varying the ionic strength, pH, and humic substance concentration of freshwater. They found pH to be a strong predictor of AgNP stability and dissolution, which was based on the pKa values of carbonate, and increasing electrolyte concentration amplified the degree of agglomeration [58]. Interestingly, aggregation and destabilization of AgNPs did not seem to be affected by increasing humic substance concentration, due to the dual negative charges of humics and the carbonate coating that repel each other [58]. Kittler et al. [59] studied the dissolution of citrate and PVP stabilized AgNPs over 125 d, and found that “aged” nanoparticles exhibited the most toxicity to bacteria, due to the release of ionic Ag. This has specific implications for storage of AgNP suspensions and indicates that AgNPs should be synthesized and used immediately after. Zhao et al. [60] found that the toxicity of AgNPs to *Daphna magna* was greatly dependent on the dissolution rate of the AgNPs tested. The ionic strength of the medium in which the AgNPs are suspended plays a large role in the aggregation state and dissolution of the AgNPs. Several studies have established that the higher the ionic strength, the more destabilized the AgNPs are, which has lead to the development of new AgNPs to improve stability [61-63].

Destabilization can lead to less overall surface area for contact dissolution and less toxicity of the AgNPs or more toxicity if the coatings are replaced with ions from the liquid, leading to higher dissolution [64, 65]. Stebounova et al. [66] discovered that the initial starting AgNP concentration also has an effect on the amount of aggregation and dissolution. They found that there is a “critical concentration” in which polymer coated AgNPs will begin to aggregate and settle out as a result of surface destabilization [66]. Sondi et al. [67] found that a Daxad 19 (a high-molecular-weight naphthalene sulfonate formaldehyde condensate sodium salt) coating was capable of withstanding high ionic strength.

Speciation and oxidation state of Ag released from AgNPs are of interest to researchers because they dictate what forms of Ag will be in the environment and how toxic the Ag will be. Synchrotron speciation of Ag oxide AgNPs in a kaolin suspension identified the presence of Ag chlorides, which has also been recorded in several other Ag speciation studies [68-70]. Synchrotron/ X-ray Absorption Near Edge Structure (XANES) has also been utilized to determine where and in what form the Ag is bonding in alfalfa plant, which provides some information about the mode of toxicity [71]. In summary, this section highlights the complicated nature in predicting DC&S of AgNPs. It suggests that each AgNP situation be examined case by case since the particle characteristics will depend on several environmental factors that should be taken into account.

2.3 Possible Pathways of Microbial Inactivation

Although ionic Ag is a known antimicrobial agent, the exact mechanism of toxicity to a variety of organisms is likely dependent on the organism it has come into contact with and thus will vary. Despite this fact, studies have shed light on the pathways that lead to microbial inactivation by AgNPs. Heavy metal toxicity to bacteria has been studied extensively, and the unique chemical reactions, such as metal binding to organics, precipitation, complexation, and ionic interaction, all play a key role in microbial inactivation [72]. Toxicity is also very closely related to several environmental chemistry factors such as pH, ionic strength, organic compound presence such as natural organic matter, and metal cation occurrence [72]. While heavy metals are essential for several biochemical pathways in bacteria, such as membrane-mediated ion transport, excess metals can overtake cell-buffering capacity and lead to oxidative damage. Heavy metals such as lead and mercury will bind with free thiol complexes used by bacteria as antioxidants or enzymes [73]. In order to bind with remaining heavy metals, the cells will begin to produce excess reactive oxygen species, such as hydroxyl radical (HO \cdot), superoxide radical (O $^{2\cdot-}$) or hydrogen peroxide (H $_2$ O $_2$), which are destructive in nature and can break down RNA, DNA, proteins, and membrane lipids and could ultimately lead to cell death [74]. All of these variables dictate what form of Ag is present and how it will come into contact with microbes.

As a result of heavy metal toxicity, bacterial resistance mechanisms have developed in many forms to alleviate stress. Energy drive efflux pumps can mediate cadmium and arsenic toxicity by flushing out heavy metals to the exterior of the cell [75]. Oxidation or reduction reactions can also be employed to convert the metal from a more toxic to less toxic speciation as seen in anaerobic sludge treatment by iron-oxidizing bacteria [76]. Bacteria have also been shown to synthesize extracellular polymers, which can complex with metals such as lead and nickel, in order to eliminate heavy metals from infiltrating the cell [77]. Binding of heavy metals with surface compounds on bacteria has also been documented as a defense mechanism to prevent intracellular penetration [78, 79]. If the metal has been transported inside the cell, there are further defense systems in place to prevent damage from metal complexation. Most notably, the importance of the potassium efflux channel and glutathione metabolite production has been well studied in *P. aeruginosa* and *E. coli* [80, 81]. Reduced glutathione (GSH), a tripeptide containing an thiol group, is an antioxidant found in high concentrations in a variety of types of cells, ranging from bacteria to mammalian cells. Some cells utilize GSH in the event that a toxic substance enters, and it is then oxidized to glutathione disulfide (GSSG). GSSG can then be converted back to GSH if the cell has the glutathione reductase enzyme where coenzyme NADPH is utilized [82]. Other heavy metal defense systems also exist, such as biomethylation of mercury, selenium, and thallium [83-85].

2.4 Ag as a bactericide

The bactericidal nature of Ag has been well established in previous literature [86, 87], but the toxicity of AgNPs appears to differ greatly depending on nanoparticle size and coating [16, 88]. Studies have begun to examine the dissolution of AgNPs from consumer product surfaces to determine how much of microbial inhibition is caused by ionic Ag or the AgNPs themselves [28]. Ag has previously exhibited a lethal effect on bacterial membranes and caused release of intracellular material [89]. Ag has also been shown to cause leakage of glutamine, mannitol, and other metabolites [90]. Earlier literature has similarly indicated that Ag can bind with DNA and RNA and disrupt genomic functions [91, 92]. The toxic nature of Ag ions can be decreased with the addition of sulfur containing compounds such as cysteine or thiols found in natural organic matter. Although ionic Ag has been well characterized as antimicrobial, the harmful effects of AgNPs on bacteria are still not completely understood. [93, 94]. Jin et al. [95] has utilized high-throughput screening to examine the influence of specific ion found in water on AgNPs and their effects of bacterial toxicity. They concluded that the addition of divalent cations, in the form of magnesium or calcium hardness, reduced toxicity to Gram-positive *Bacillus subtilis*, but not Gram-negative *Pseudomonas putida*, which had higher mortality [95].

Current literature is beginning to examine the linkages between AgNP toxicity and thiol groups present in bacteria. As previously mentioned, the addition of cysteine to a reaction

has been shown to bind with free Ag. Yeast cells of *Candida* and *Saccharomyces* genera have been shown to utilize metallothioneins, cysteine rich proteins, to bind heavy metals and detoxify. Navarro et al. [17] saw that with equimolar concentrations of cysteine to AgNPs, photosynthesis disruption was alleviated in *Chlamydomonas reinhardtii*. No research has been published yet showing that the addition of cysteine to AgNPs and bacteria will decrease heavy metal induced bacterial stress.

2.5 AgNPs in WWTPs

Even if AgNPs are only present at very low concentrations in wastewater influent, it is possible that their innate antimicrobial properties could alter important microbial functions. Nitrification is an essential wastewater process where NH_4^+ is converted to N_2 through a series of biodegradation pathways, as shown below in Figure 1:

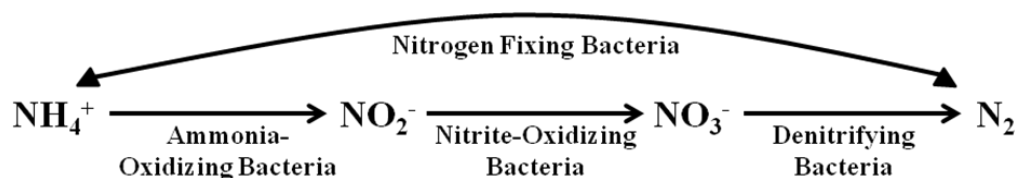


Figure 1: Nitrogen cycle of wastewater (Adapted from Zeng et al. [96])

The microorganisms shown above are responsible for nitrogen removal in wastewater and their disruption may lead to poor water quality. Nitrifying bacteria in the genera *Nitrosomonas* and *Nitrobacter* are of particular interest because they are inefficient

growers that can easily be outcompeted by heterotrophic bacteria especially in the presence of chemical stressors [97]. Nitrifiers, which are chemolithotrophs that derive their energy source from inorganic electron donors, are very sensitive to their environmental conditions such as pH (optimum pH is 7-8), salt concentration, and dissolved oxygen [98]. Their inactivation pathway has been established as the suppression of the membrane-bound enzyme ammonia monooxygenase (AMO) and heavy metals are known to cause this inhibition [99]. Due to the high sensitivity of nitrifiers, they have proven to be good model organism for prediction of nitrification disruption and ultimately WWTP failure. Studies have shown that *Nitrosomonas* spp. displayed a tenfold increase in toxicity from organic contaminants when compared to toxicity on aerobic heterotrophs [100]. In previously published work, polyvinyl alcohol coated AgNPs at concentrations of 0.5 ppm have been linked to a decrease of nitrifying activity in mixed nitrifying bacterial communities commonly found in municipal wastewater treatment plants (WWTP) [2]. While small concentrations of AgNPs such as 0.5 ppm may not be significant today, increased utilization in consumer products warrants further evaluation to determine potential impact. Although studies have begun to examine the antimicrobial effects of AgNPs on wastewater bacteria, this dissertation research focuses on studying several AgNPs at different concentrations. Then, all microbial inhibition data will be compared across all AgNPs so that size and coating dependent toxicity can be evaluated.

Lee et al. [101] suggest that heavy metals such as copper inhibit suspended and attached growth of nitrifying bacteria in bench-scale reactors. Copper and Ag appear to have a very similar pattern of interaction in a variety of microorganisms and can be used interchangeably in some cases. Copper resistance genes have been shown to be closely related to Ag resistance in *Candida albicans* [102]. *Sphaerotilus natans*, a filamentous bacterium, has been shown to remove copper and Ag in wastewater treatment [103]. Ag has also been shown to compete with copper for intracellular binding sites of *E. coli* [104]. For these reasons, it is essential that the toxicity of AgNPs on nitrifiers in wastewater be further ascertained since other heavy metals have been shown to cause upsets in wastewater treatment.

2.7 Ag interactions with complex media such as wastewater

The exact concentration of AgNPs in wastewater is still unknown due to difficulties in measurement, and as a result, studies have begun to try to answer important research questions regarding the interaction of AgNPs in complex media. Since one of the suggested antimicrobial mechanisms of AgNPs is the release of ionic Ag after the particle coating dissociates, researchers have started to examine nanoparticle coating interactions with solution properties such as pH, ionic strength, and dissolved organic carbon concentration [7]. Gao et al. [105] conducted experiments where AgNPs were added to different types of water (e.g. deionized, river water) and Ag ion concentrations were measured using inductively coupled plasma mass spectroscopy (ICP-MS). Preliminary

results indicate that coating dissolution varies depending on water characteristics and the coating used on the particle [105]. In another study performed by Fabrega et al. [106], high humic acid and pH levels showed an increase in aggregation, a decrease in dissolution of the coating, and a decrease in antimicrobial efficacy. Recent literature has also concluded that the fabrication of the AgNPs can play a large role in toxicity level. For example, if a process such as electrical spark discharge is used to create a colloidal AgNP suspension, which entails a charge being forced through Ag electrodes, there is a high output in the solution of ionic Ag [107].

Ag sulfide nanoparticles were recently detected in wastewater treatment plants and sludge has been identified as a likely place for Ag sulfide complexation because of its inherently high thiol concentrations [13, 108]. These data suggest that Ag that flows into a WWTP is likely to end up in biosolids waste due to its high concentration of thiol groups [109]. Lack of further research in AgNP interaction confirms the research gap present in understanding the impacts of AgNPs in the environment and more specifically, wastewater. Even though research has begun to investigate the effects of AgNPs, significant research gaps still remain and there is a great need to quantify their impact in wastewater microbial communities.

3. Impacts of Silver Nanoparticle Coating on the Nitrification Potential of *Nitrosomonas europaea*

This work was accepted for publication in *Environmental Science and Technology*, 2012

3.1 Introduction

The use of nanomaterials in industrial applications and consumer products has been increasing steadily as novel applications related to their unique properties are discovered. In particular, silver nanoparticles (AgNPs) are a commonly used class of nanoparticles with known antimicrobial properties. AgNPs have been embedded in bacterial cellulose wound dressings, water filters, and surface coatings for biofilm prevention [10, 11, 110]. Many different types of AgNPs have been manufactured [111] and, in general, little is known about their environmental fate, transport, and toxicity. While the bactericidal nature of ionic silver (Ag^+) is well established [86, 87], the toxicity of AgNPs appears to differ greatly depending on size and coating [16, 88], and the mechanisms of toxicity are poorly understood. Recent studies have examined the dissolution properties of AgNPs from consumer product surfaces to determine if the source of microbial inhibition is from Ag^+ or the AgNPs themselves [28]. Research has shown that the dissolution of Ag^+ from AgNPs varies greatly as a function of AgNP surface area and coating stability [112, 113].

Because of their use in consumer products, wastewater is a likely place for AgNPs to be found. Ag sulfide nanoparticles were recently detected in wastewater treatment plants and sludge has been identified as a likely sink for Ag sulfide complexation because of its high thiol concentrations [13, 108]. In general, very few studies have compared the effects of

different classes of AgNPs on ecologically important bacteria in wastewater treatment [70, 114]. Nitrifying bacteria in the genera *Nitrosomonas* and *Nitrobacter* are of particular interest because they are inefficient growers that can be easily outcompeted by heterotrophic bacteria [97]. The disruption of ammonia oxidizing bacteria (AOB) is of specific concern because they carry out the first step in nitrification which consists of oxidizing ammonia to hydroxylamine (NH₂OH) using the *amoA* gene which codes for ammonia monooxygenase (AMO) [115]. Their inactivation pathway has been established as the suppression of membrane-bound AMO and heavy metals as well as other contaminants are known to cause this inhibition [116, 117]. The *hao* gene, also located in the cell membrane, codes for hydroxylamine oxidoreductase (HAO) and carries out the second conversion from hydroxylamine to nitrite [118]. Due to their high sensitivity, nitrifiers are commonly used for predicting the impact of contaminants on nitrification disruption and ultimately wastewater treatment failure. Studies have shown that *Nitrosomonas* spp. displayed a tenfold increase in toxicity from organic contaminants when compared to aerobic heterotrophs [100].

While there have been several studies which have examined the consequences of AgNP exposure on wastewater bacteria, the results therein are divergent [119, 120]. We speculate that while the mechanisms of inhibition may be similar for different types of AgNPs, the divergent results reported to date may be linked to the differences in AgNPs properties such as their method of synthesis, shape, size distribution and coating. Thus, the objectives of this study were to determine the differential impacts of AgNPs with

three different coatings: gum arabic (GA), citrate, and polyvinylpyrrolidone (PVP). *Nitrosomonas europaea* was selected as the model AOB because it is known to be a key player in wastewater nitrification and has been widely used in nitrification literature [121, 122].

3.2 Materials and Methods

AgNP Characterization. GA, citrate, and PVP stabilized AgNPs were tested in this study. These three particle types were selected because they are synthesized using common stabilization methods likely to be used for AgNPs found in consumer products [123-125]. For information on AgNP synthesis, transmission electron microscopy (TEM) images, and zeta sizing of AgNPs, please refer to the “*AgNP Synthesis*” section in the supporting information. Briefly, citrate AgNPs were synthesized by reducing Ag nitrate in water with sodium citrate [126]. Particle size characterization by TEM shows that the average particle size was 25.2 ± 9.3 nm. GA AgNPs were synthesized by reducing Ag nitrite with water and GA. The average particle size of these particles given by TEM imaging was 27 ± 6.5 nm. PVP AgNPs were purchased from Nanostructured & Amorphous Materials, Inc. (Houston, TX). The average particle diameter was measured as 21 ± 17 nm by TEM inspection. A probe sonicator was used to suspend PVP AgNPs in DI water as described in Meyer et al. [127]. All AgNP used herein have been widely used and characterized by researchers within the Center for the Environmental Implications of NanoTechnology (CEINT). More information regarding characterization of AgNPs used in this study can be found in Yin et al. [128] and Meyer et al. [127].

Cell Growth and Preparation. *N. europaea* (ATCC 19718) was grown in 1 L of AOB medium containing 0.2 g/L MgSO₄-7H₂O, 20 mg/L CaCl₂-2H₂O, 87 mg/L K₂HPO₄, 405 mg/L KH₂PO₄, 0.01 mg/L Na₂MoO₄-2H₂O, 0.017 mg/L MnSO₄-H₂O, 0.0004 mg/L CoCl₂-7H₂O, 0.17 mg/L CuCl₂-2H₂O, 0.01 mg/L ZnSO₄-7H₂O, 1 mg/L chelated iron and 3.33 g/L (NH₄)₂SO₄ [129]. The ionic strength of the growth medium was calculated to be 0.097 M and the pH was maintained at 7.5 throughout the experimental period. To maintain aerobic conditions, cells were constantly stirred at 600 rpm using a magnetic stir bar. All reactors were maintained in the dark at room temperature (~21°C). Periodic transfers to R2A agar plates were performed to check for contamination. For use in subsequent experiments, late log cells (OD₆₀₀ ~0.070) were harvested by centrifugation at 8200 rpm for 30 min using an Eppendorf Centrifuge 5804 (Westbury, NY). Cells were washed with 40 mM KH₂PO₄ buffer (pH 7.8) and then pelletized again.

Batch Reactor Preparation. Nitrite production experiments were carried out in batch reactors consisting of 250 mL Erlenmeyer flasks each containing 100 mL of the previously described AOB growth medium. All flasks and growth medium were heat sterilized by autoclaving at 121°C and 15 psi for 20 min prior to the beginning of each experiment. AgNPs were added in stock solution form, suspended in nanopure water immediately before inoculation with *N. europaea*. AgNP concentrations used in the experiments were 0.2, 2 and 20 ppm. This range was selected based on preliminary experiments performed using concentrations ranging from 20 ppb to 200 ppm.

Concentrations at or below 200 ppb (total Ag) showed no statistically significant effect on nitrification compared to the no Ag control ($p < 0.05$) whereas the 200 ppm concentration resulted in 100% cells with membrane compromised and complete nitrification loss (data not shown). Nitrification experiments were carried out by resuspending the bacterial cell pellet (as described previously in the Cell Growth and Preparation section) in 15 mL of 40 mM KH_2PO_4 buffer. One mL of resuspended cells was added to each batch reactor and the protein content in each sample before treatment was determined by digesting 0.75 mL of cell sample with 3 N NaOH for 24 h at 4°C (modified from Arp et al. [130]). The Micro BCA™ Protein Assay Kit (Rockford, IL) was then used to quantify protein concentration, following the manufacturer's protocol. The average starting concentration of protein was $75.3 \pm 8.6 \mu\text{g/mL}$ and the OD_{600} was 0.07 as previously described [131]. Triplicates of each treatment condition were prepared. Negative controls consisting of batch reactors without AgNPs were also prepared. Reactors containing 0.2 ppm Ag^+ as AgNO_3 were used as a positive control. Complete nitrification inhibition was observed at 0.2 and 2 ppm Ag^+ as AgNO_3 . 0.2 ppm Ag^+ as AgNO_3 was selected as the positive control because it was the lowest concentration of Ag^+ as AgNO_3 that eliminated nitrification potential and was not statistically different from 2 ppm Ag^+ treatment ($p < 0.05$). The reactors were continuously stirred at 600 rpm in the dark at room temperature ($\sim 22^\circ\text{C}$). The dissolved oxygen concentration in the reactors was $9.5 \pm 1 \text{ mg/L}$. Total and dissolved Ag were measured in triplicates at the beginning and end of each experiment. One mL samples were collected from each reactor hourly and used for nitrite concentration quantification using NitriVer® 3

Reagents (Hach, Loveland, CO). All experiments lasted 4 h. A 4-h exposure period was selected based on previously published studies [132-134]. In order to rule out the toxicity of the AgNPs coatings themselves, nitrite production inhibition was also quantified for the coating compounds independently. Because the manufacturer did not provide the amount of coating of the PVP AgNPs, a range of concentrations was used to test PVP toxicity. More details are provided in Table A6 of the supporting information concerning AgNP coating concentrations used in the present study.

Analytical Methods. Total Ag and dissolved Ag were quantified using an Agilent 7700 inductively coupled plasma mass spectrometer (ICP-MS, Santa Clara, CA). Total Ag is defined as the concentration of all Ag species originating from the AgNP. To obtain total Ag measurements, AgNPs were dissolved by adding nitric and hydrochloric acid as described. Dissolved Ag is defined as the fraction of Ag filtrate that can be passed through a 3-kDa pore size membrane. To measure dissolved Ag, the filtrate was completely acidified with nitric and hydrochloric acid using a method modified from Wang et al. [135]. Samples were acidified in 2% HNO₃ and 0.5% HCl concentrated acid for 24 h. Ten mL of total Ag samples were used for each analysis. To measure dissolved Ag, 3.5 mL of sample from each treatment were placed on an Amicon® Ultra-4 Centrifugal Filter Unit (Millipore, Billerica, MA) and centrifuged at 7,000 rpm for 35 min. Ag concentration was then quantified in the filtrate (<3 kDa) using the previously described protocol for total Ag [127]. In all cases, total Ag measurements taken at the

beginning and end of the experimental period were not statistically different ($p < 0.05$) from the total targeted Ag range (0.2-20 ppm).

Cysteine Rescue. Because L-cysteine has been shown to strongly bind with Ag [93], it was selected as a thiol donor compound for Ag rescue experiments. These experiments were carried out similarly to the nitrite production experiments outlined previously, except that L-cysteine was added to batch reactors directly before Ag addition at a 1:1 ratio of L-cysteine:Ag concentration. Nitrite production was monitored as described previously. The integrity of cell membranes (described below) was also examined. A control with L-cysteine only was also run independently to ensure L-cysteine did not impart any toxicity to *N. europaea*. GA and citrate AgNPs were tested at 2 ppm while PVP AgNPs were tested at 20 ppm. These concentrations were selected because they were the lowest concentrations where toxicity was observed in terms of effect on nitrite production rates.

Membrane Integrity Testing. Membrane integrity was quantified using the LIVE/DEAD® fluorescent staining assay as previously outlined [136, 137]. All membrane integrity tests were performed at the end of the 4 h exposure of *N. europaea* to AgNPs. Cells of *N. europaea* from nitrite generation experiments were also harvested and pelletized for thin-section TEM imaging. Cell preparation and imaging was carried out at Duke's Shared Materials Instrumentation Facility (Durham, NC). After embedding cells, epoxy resin slices were inspected by TEM. More details concerning microscopy

protocols and procedures are provided in the *Transmission Electron Microscopy (TEM)* section of the supporting information.

qRT-PCR. Gene expression of *amoA* (gene encoding for AMO; the first enzyme in the ammonia breakdown pathway [138]), *hao* (gene encoding for HAO; responsible for hydroxylamine to nitrite conversion [139]), and *merA* (gene encoding for mercuric reductase, noted for heavy metal stresses [131]) were monitored by two-step quantitative reverse transcriptase PCR (qRT-PCR). Briefly, *N. europaea* cells were washed and resuspended in the previously described AOB growth medium, then exposed to AgNPs for 4 h. Samples were taken for RNA extraction when a statistically significant difference in nitrite production rate was noticed ($p < 0.05$). This time point was chosen to determine if the first noticeable loss in nitrification was due to a transcriptional or post-transcriptional bacterial mechanism. Tested treatments were 2 and 20 ppm for all AgNPs since 0.2 ppm did not have a significant effect on nitrification. A no Ag treatment was used as a negative control while the positive control consisted of 0.2 ppm Ag as AgNO₃. RNA extraction protocol and PCR conditions are provided in the *qRT-PCR* section of the supporting information. Gene transcript quantification was completed using relative quantification as described by Peirson et al. [140]. The *16S rRNA* gene was used as the reference gene for normalization. Primer sequences and annealing temperatures for target genes in *N. europaea* are listed in *qRT-PCR* section of the supporting information. Fold change was calculated by comparing Ag⁺ and AgNP treated samples to no Ag control

samples. Upregulated expression and down-regulated expression will show fold change > 1 and < 1 relative to the control, respectively.

Statistical Analysis. The unpaired, two tailed student's t-test was used to identify statistical differences between control samples and treated samples. Results were considered statistically different when p-value < 0.05 .

3.3 Results and Discussion

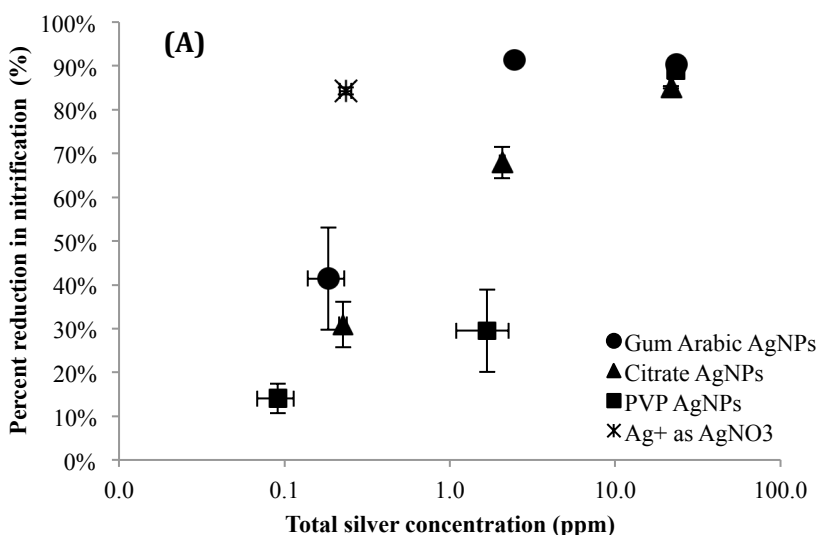
Dissolution of Ag⁺ from AgNPs. At time zero, Ag⁺ was below the ICP-MS detection limit of 10 ppt. However, at the end of the exposure period, dissolved Ag concentration varied (summary shown in supporting information Table A8). At the lowest target concentration (0.2 ppm total Ag), the dissolved Ag concentrations were 2.1 ± 0.9 , 6.3 ± 3.4 , 0.6 ± 0.8 ppb for the PVP, GA and citrate coated AgNPs, respectively. These concentrations are well below the 0.2 ppm Ag⁺ treatment (45.4 ± 3.1 ppb). For the 2 ppm treatments, citrate AgNPs had the highest amount of dissolved Ag (63.5 ± 2.2 ppb), while the GA and PVP AgNPs had lower concentrations (16.1 ± 9.5 and 21.6 ± 8.3 ppb, respectively). At the highest target concentration (20 ppm), all of the samples were releasing Ag⁺ at levels equal to or higher than the 0.2 ppm Ag⁺ control. Ag concentrations were statistically similar for citrate and PVP AgNPs (150.0 ± 3.2 and 160.9 ± 10.3 ppb, respectively), while GA AgNPs samples had a lower concentration of dissolved Ag (37.9 ± 1.3 ppb). It should be noted that Liu et al. [65] found that air saturation of 9.1 mg/L increased Ag⁺

dissolution rate because of O₂ AgNP surface oxidation. Therefore, Ag⁺ dissolution rates may be different in our experiments because of our high dissolved oxygen concentration.

Dynamic Light Scattering (DLS) estimated hydrodynamic diameters of approximately 25 and 68 nm for GA and citrate coated AgNPs, respectively, while PVP coated AgNPs showed two diameter peaks at 30 and 128 nm, indicating some aggregation after initial suspension. More details concerning DLS experiments can be found in the *AgNP Synthesis* section of the supporting information. It is noteworthy that PVP AgNPs used in this study aggregated substantially compared to the other two AgNPs. This result may be attributed to the destabilization of the sterically stabilized PVP coating. This result is somewhat surprising as PVP coatings have been proven to be very stable in water suspensions due to the hydrophilic nature of PVP [141]. Similarly, Badawy et al. [62] found that PVP AgNPs were far less likely to aggregate with changing pH and ionic strength when compared to citrate AgNPs. One explanation for the aggregation in PVP AgNPs used in this study is that the particles were synthesized by NanoAmor with a suboptimal PVP:AgNO₃ ratio. Wang et al. [57] found that a PVP:AgNO₃ ratio greater than 1.5 was ideal for colloid stabilization.

Nitrification Inhibition. Nitrite production was significantly inhibited at concentrations of 2 and 20 ppm for GA and citrate AgNPs, and 20 ppm for PVP AgNPs when compared to the no Ag control ($p < 0.05$) (Figure 1). No statistically significant inhibition was observed in the 0.2 ppm AgNP treatments. Citrate and GA AgNPs showed the highest

degree of inhibition on nitrification rate at 2 ppm ($67.9 \pm 3.6\%$ and $91.4 \pm 0.2\%$ reduction in nitrification rate, respectively) while PVP AgNPs inhibited to a lesser degree (29.5 ± 9.4). At the 20 ppm concentration, PVP AgNPs reduced nitrite production by $89 \pm 1.3\%$. For both PVP and citrate AgNPs, higher inhibition of nitrification was observed at 20 ppm compared to the 2 ppm exposure ($p < 0.05$) suggesting that toxicity may be a function of dosage. The inhibition levels observed at 20 ppm for all AgNPs were statistically similar to the reduction in nitrification observed in the 0.2 ppm Ag^+ positive control treatments ($p > 0.05$).



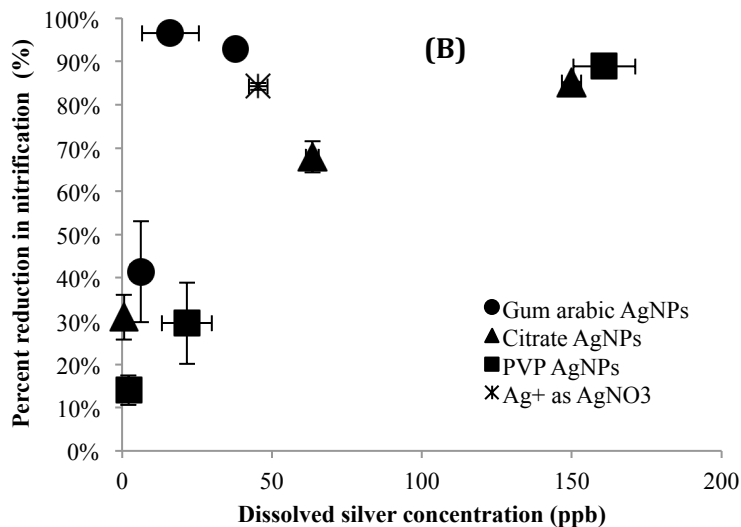


Figure 2: Percent reduction in nitrification rate in AgNP treatments compared to no Ag control, as a function of total Ag concentration (A) and dissolved Ag concentration (B). Error bars indicate standard deviation values between 6 replicates. The targeted total Ag concentration was not statistically different from the measured total Ag concentration.

Our data suggest that once the dissolved Ag concentration reaches a certain threshold (~10 ppb in the present study), nitrifying enzyme activity is repressed. AMO has previously been shown to be the most vulnerable enzyme to interference, above all other important nitrifying enzymes [36]. The intracytoplasmic location of AMO may be what renders it susceptible to interference, since AgNPs are likely to first interact with the cell surface. Furthermore, because AMO is known to be rich in copper, it may be chelated and deactivated easily by several compounds such as thioureas [142]. Thus, it is possible that the addition of Ag^+ from AgNPs may interfere with its copper bonds by either replacing copper with Ag or inducing production of chelators, both of which may alter AMO activity ultimately leading to a reduction in nitrification [143, 144]. Further experiments are needed to confirm these hypotheses. Reversibility experiments were attempted to

assess whether cells could recover from AgNP exposure. However, we were unsuccessful in separating AgNPs from cell biomass after attachment had occurred and therefore could not perform these experiments.

The relationship between nitrification inhibition and dissolved Ag concentration was not consistent across the three differently coated AgNPs tested in the present study. If dissolved Ag^+ release is the main cause for AgNP toxicity, based on the measured dissolved Ag concentrations discussed in the previous section, it would be expected that citrate AgNPs should have the highest inhibitory effect on *N. europaea* at a total concentration of 2 ppm. Similarly, at the 20 ppm concentration, both citrate and PVP AgNPs should have similar nitrification inhibition. However, this does not corroborate with our observations for the 2 ppm treatment. Rather, our data show that at total Ag concentrations of 2 ppm, GA AgNPs had the highest inhibition (Figure 2A) even though citrate AgNP treatments had higher dissolved Ag concentrations. At the highest total Ag concentration (20 ppm), GA and citrate AgNPs had statistically similar inhibition while PVP AgNPs exhibited a lower but still substantial degree of inhibition ($88.8 \pm 1.3\%$).

Quenching by L-Cysteine. L-cysteine, a strong metal chelator, was added to quench Ag^+ released from the AgNPs and to test the relationship between microbial inhibition and AgNP release of Ag^+ . The strong complexation of Ag^+ and L-cysteine has been long established [94, 116], but the affinity for AgNPs and L-cysteine is still under investigation. Navarro et al. [17] found that the addition of L-cysteine removed all AgNP

toxicity to *Chlamydomonas reinhardtii*, a unicellular algae found in freshwater. Similarly, the addition of the antioxidant N-acetylcysteine alleviated all oxidative stress in human hepatoma cells [145].

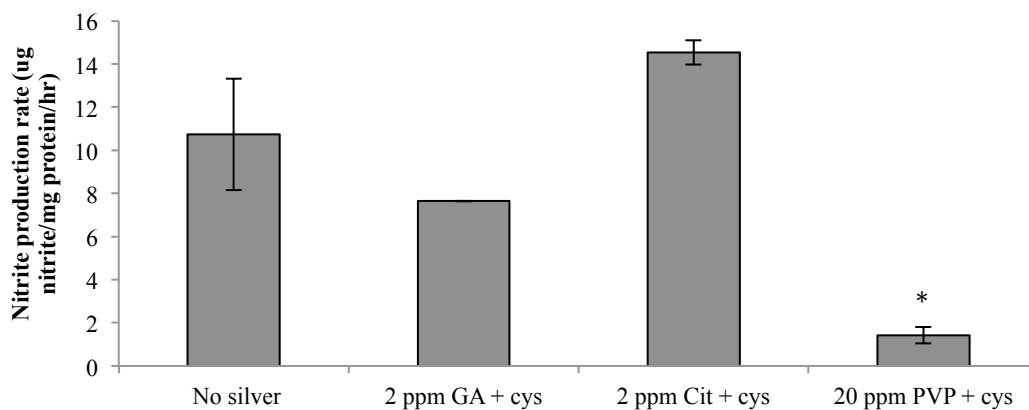


Figure 3: Nitrite production rate vs. treatments containing cysteine addition. Asterisks indicate statistical significance ($p < 0.05$). Error bars represent the standard deviation of triplicate samples.

In the present study, the addition of L-cysteine eliminated nitrification inhibition in all cases except for the 20 ppm PVP AgNPs exposure, which remained statistically different from the no Ag control ($p < 0.05$). These results suggest that for GA and citrate AgNPs (2 ppm), nitrification inhibition appears to be linked to Ag^+ (Figure 3). It should be noted that L-cysteine is also capable of quenching reactive oxygen species (ROS), which are known to be induced in bacteria by heavy metals. Xiu et al. [146] reported that the predominant source of AgNP toxicity to *E. coli* was Ag^+ rather than ROS generation. Similarly, we speculate that Ag^+ as opposed to ROS is a predominant pathway of toxicity in *N. europaea*, however, follow up experiments are needed to confirm the relative L-cysteine quenching for Ag^+ and ROS. In the presence of PVP AgNPs (20 ppm), other mechanisms may have interfered with L-cysteine and Ag^+ binding, such as by-products

during manufacturing of AgNPs. TEM images of the PVP AgNPs showed extraneous shards of matter that were added by the nanoparticle stock suspension, not related to the AgNPs themselves (Figure 5E). Thus, it is possible that L-cysteine was binding with these particles instead of quenching Ag^+ or AgNP induced ROS. However, since all toxicity was removed with the addition of L-cysteine in the other 2 AgNP samples, this makes a strong case that Ag^+ dissolved from the AgNPs and, possibly, ROS caused membrane and nitrification loss.

Impacts on Membrane Integrity. Cell membranes were examined using the LIVE/DEAD assay and TEM imaging to investigate whether AgNPs damaged membranes of *N. europaea*. Figure 4 shows results of membrane integrity testing and Figure 5 shows TEM imaging results. While membrane integrity was reduced by $93 \pm 19\%$ in the positive control treatments (0.2 ppm Ag as AgNO_3), no effects were observed in the presence of 0.2 ppm AgNPs ($p > 0.05$). This result was not unexpected as the Ag^+ concentrations were below the threshold interference concentration determined in nitrification experiments. TEM results showed that cells treated with 0.2 ppm Ag as AgNO_3 had a noticeable difference in their internal density. The internal matter appears more nodular and lighter in color, indicating less density. Although this effect may be an artifact of TEM staining preparation, because this was observed in a repeatable fashion, we speculate that *N. europaea* formed vesicles in response to Ag stress as others have hypothesized in the literature [147, 148]. AgNO_3 treated samples also had less defined membranes, possibly caused by Ag^+ ions interfering with the peptidoglycan layer and

cytoplasmic membrane, as previously seen in bacteria [89]. Follow up work including energy dispersive X-ray spectroscopy (EDX) should be performed to further verify Ag containing images. In the presence of 2 ppm AgNPs, membrane damage varied with nanoparticle coating. PVP and GA AgNPs showed no statistical difference from the no Ag control in the 2 ppm treatments in LIVE/DEAD assays ($p < 0.05$). This result was unexpected for the GA AgNPs as this treatment showed the highest decrease in nitrification rate at 2 ppm ($96.5 \pm 0.2\%$ reduction), suggesting inhibitory mechanisms other than membrane disruption may be more important for GA AgNPs. Ag^+ may dissolve from the GA AgNPs and attach to the membrane surface to interrupt membrane-bound AMO/HAO activity, but not completely lyse the membrane. TEM showed that the internal density of samples treated with 2 ppm GA AgNPs was lighter than no Ag controls, similar to the Ag^+ treatment. GA AgNPs were also observed on the membrane surface of *N. europaea*. This is interesting to note because these samples were washed extensively with ethanol in TEM preparation in order to remove AgNPs and other imaging disruptors. By contrast, TEM of the 2 ppm PVP AgNP treated samples did not appear different from no Ag controls, a finding which was expected as no significant nitrification or membrane disruption was noticed at this concentration. PVP AgNPs, which had the highest hydrodynamic diameter particles, had the smallest effect on membrane integrity and the most aggregation.

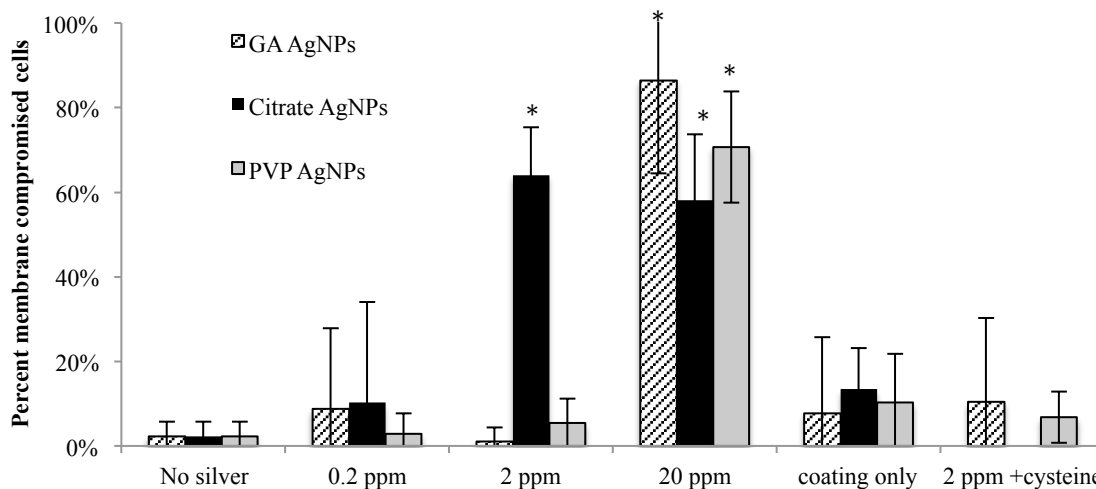


Figure 4: LIVE/DEAD microscopy results - percent of cells with compromised membranes. Pure Ag⁺ ion at 0.2 ppm (not shown) disrupted almost all membranes, with 93 ± 19% membranes broken. Asterisks indicate statistical significance ($p < 0.05$) between no Ag samples and AgNP treatment samples. Error bars represent the standard deviation of triplicate samples.

Citrate AgNPs showed significant membrane disruption at 2 ppm, with 64 ± 11% loss in membrane integrity. TEM samples treated with 2 ppm citrate AgNPs showed extensive membrane damage, which further corroborates the previously described membrane integrity results. The internal density of the cells did not appear to change, suggesting that the citrate AgNPs primarily lysed cell membranes. Overall, increased AgNP dosage was not correlated to an increase in membrane damage. Statistically similar membrane disruption rates were observed in the 2 and 20 ppm treatments for citrate AgNPs ($p > 0.05$). Higher concentrations of AgNPs (200 ppm) were also tested for GA and PVP AgNPs to test the dose dependence on membrane loss, and there were no statistical differences from 20 ppm treatments ($p < 0.05$) (data not shown). This suggests that *N.*

europaea can withstand a certain level of Ag^+ beyond which membranes are lysed and severe membrane loss occurs.

Another possible explanation for membrane loss in *N. europaea* is the surface charge interaction between AgNPs and the bacterial membranes. The measured zeta potential (ZP) values for citrate, GA, and PVP AgNPs in AOB medium were -23.0 ± 1.1 , -21.0 ± 1.3 , -11.6 ± 1.8 mV, respectively. These ZP values are in agreement with Kittler et al. [149] who found citrate coated AgNPs to be very negatively charged (ZP -30 mV) and PVP to be less negatively charged (-17 mV). Based on these results, it would be expected that PVP AgNPs would have the highest attraction for bacterial membranes. However our results show that PVP AgNPs are the least toxic. We speculate that this observation is a result of the higher stability and lower aggregation of the more negatively charged particles (citrate and GA AgNPs herein) which may have led to a higher available surface area for possible bacterial interaction.

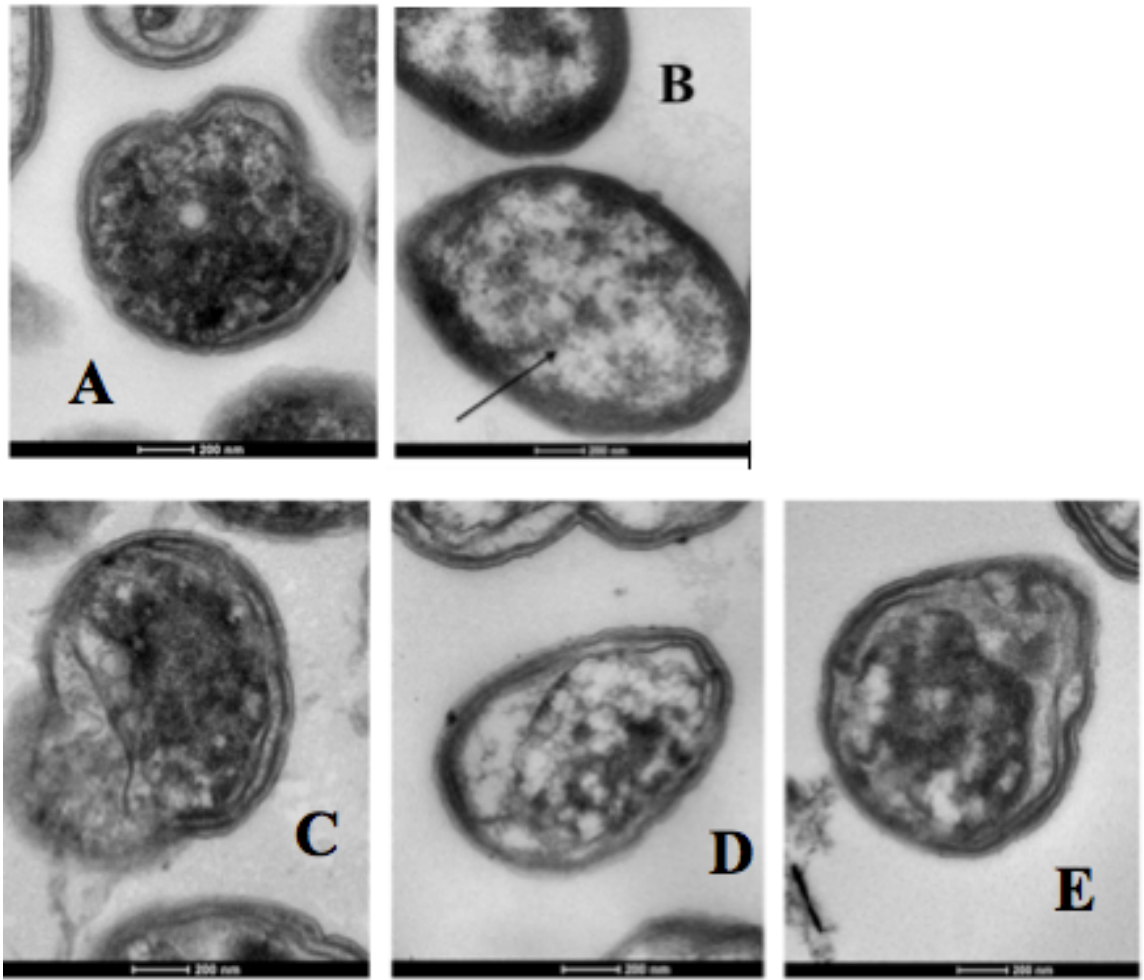


Figure 5: TEM images of no Ag control (A), 0.2 ppm Ag⁺ as AgNO₃ (B), 2 ppm citrate AgNP treatment (C), 2 ppm gum arabic AgNP treatment (D), and 2 ppm PVP AgNP (E).

Expression of functional genes in N. europaea after AgNP exposure. Gene expression analyses were carried out to assess whether AgNPs affected the expression of major functional genes by qRT-PCR. The expression of *amoA*, *hao*, and *merA* were tested with the two highest concentrations of AgNPs, where an effect on nitrification was noticed. The expression of *amoA* was not altered even in treatments where nitrification was inhibited suggesting that Ag does not affect *amoA* transcription (Supporting Information

A25). The expression of *hao* was only significantly up-regulated in the 0.2 ppm Ag⁺ by a fold change of 6.23 ± 1.15 (Supporting Information Figure A26). This observation suggests that the only transcriptional effects on nitrification are likely to occur in the expression of conversion of hydroxylamine to nitrite. However, because no significant effects were observed in the presence of the AgNPs, even at concentrations as high as 20 ppm, this effect is most likely not a major nitrification inhibition mechanism. The expression of *merA* varied across Ag treatments (Figure 6). In general, *merA* is used to reduce metals with NADPH and therefore this gene tends to be up-regulated in the presence of heavy metals [150]. Mercuric reductase enzyme is a flavin-containing disulfide oxidoreductase and is one of many strong antioxidants used to relieve oxidative stress in a variety of organisms [151, 152]. In the present study, *merA* was up-regulated in 4 treatments: 0.2 ppm Ag⁺ (fold change of 43.51 ± 12.82), 20 ppm citrate AgNP (206.16 ± 43.31), 20 ppm GA AgNP (34.03 ± 13.85), and 20 ppm PVP AgNP (74.39 ± 2.26). No up-regulation was observed in the 2 ppm AgNP treatments even though significant dissolved Ag were measured and nitrification inhibition was measured suggesting that *merA* is only activated under high dissolved Ag concentrations (~50-100 ppb in this study). Citrate and PVP AgNPs appear to have the strongest effect on *merA* up-regulation. These treatments also showed the highest Ag⁺ concentration suggesting there may be a correlation between these two parameters. These findings are consistent with the fact that citrate AgNPs were the most disruptive to cellular membranes with PVP and GA AgNPs following in toxicity.

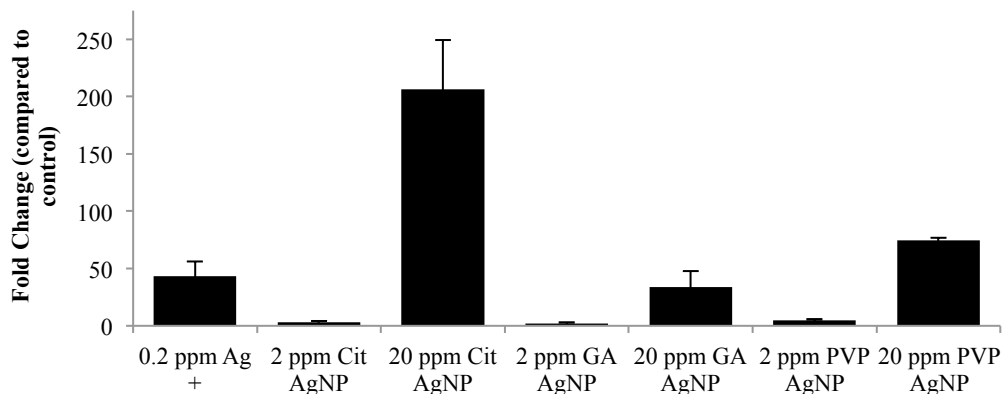


Figure 6: Gene expression of *merA* relative to 16S rRNA reference gene. Higher concentrations of AgNPs (20 ppm) were significantly up-regulated in fold change. Error bars represent the standard deviation of triplicate samples.

Order of AgNP induced inactivation in N. europaea. Our data show that distinct AgNPs have differential effects on *N. europaea*. AgNPs with differing coatings may vary in the relative importance of bacterial inactivation mechanisms, and not exclusively cause nitrification loss directly through membrane disruption, as suggested in previous literature [153]. The results from the present study suggest that there is an order of interaction, which dictates how cells will become inactivated and what mechanisms will cause their disruption. Figure 7 illustrates the interactions observed for *N. europaea*. Since the first steps of nitrification are mediated by membrane bound AMO/HAO, we expected to find a correlation between nitrification inhibition and either membrane disruption or the down-regulation of *amoA* and *hao*. However, our data suggest otherwise. The first mechanism of inhibition appears to be a post-transcriptional interference of AMO/HAO by either dissolved Ag or ROS, in treatments where membranes are not completely disrupted but nitrite production decreased (2 ppm GA

AgNP and 2 ppm PVP AgNP treatments). The disruption of nitrification is dependent on AgNP characteristics, such as zeta potential and coating, which will dictate how fast the AgNP will release Ag^+ and ROS production. As Ag^+ concentrations increase, metal regulation genes, such as *merA* are up-regulated. Finally, total membrane loss and release of internal cellular matter occur. We speculate that by examining AgNP coating type, Ag^+ dissolution rates and Stern layer surface charge, it may be possible to predict which AgNPs may be more detrimental to nitrifiers such as *N. europaea*. However, the results obtained herein must be expanded to other types of AgNPs and nitrifying organisms to further confirm our findings. In addition, further research studying AgNPs in more complex environments such as wastewater are needed to determine if similar observations are seen.

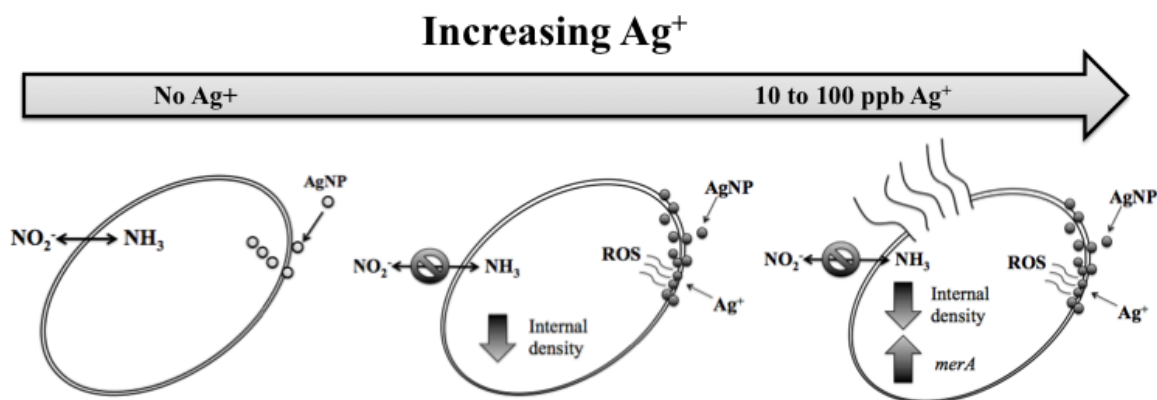


Figure 7: Illustration of effects of Ag^+ from AgNPs in *N. europaea*. As Ag^+ concentration reaches approximately 20 ppb, nitrification is inhibited and cell death and lysis is reached at 60 ppb.

4 Toxicity of Silver Nanoparticles found in Consumer Products on Growth and Function of Three Model Bacteria

4.1 Introduction

Nanomaterials such as silver nanoparticles (AgNPs) are increasingly being added to consumer products to increase their antimicrobial properties. AgNPs have already been integrated into a wide range of industries, including military service and medical fields, as well as commercially available products such as toys, supplements, and cosmetics [88, 154, 155]. Previous research has shown that AgNPs can slowly release ionic Ag, a known antimicrobial, as their coatings dissolve [59]. Preliminary studies also indicate that induction of reactive oxygen species (ROS) is responsible for cell damage and ultimately death [153, 156]. Thus, AgNPs may provide a constant source of toxicity to microbes over time, but their dissolution rate is largely dictated by the environmental matrix they are in as well as the physical chemical properties of the AgNPs themselves [157]. To meet the needs of these industries, a variety of coatings have been developed to customize the dissolution rate, size, and shape of the AgNPs, but the inhibitory effects of AgNPs on microbes is still inconsistent and only beginning to be compiled.

Consumer products containing AgNPs are of particular concern to wastewater treatment plants (WWTPs), which could disrupt nitrogen and carbon removal. Their antimicrobial characteristics are problematic for biological nutrient removal, which relies on heterotrophic bacteria for biochemical oxygen demand (BOD) removal and mainly autotrophic bacteria for ammonia removal (nitrification) [18, 70]. For this reason, it is

important to characterize the specific mechanistic effects of AgNPs on a variety of bacteria so toxicity implications can be quantified and ultimately predicted when new products are manufactured. Thus far, some studies have begun to investigate the impacts of AgNPs on pure culture heterotrophic bacteria, but very few findings have been published on the effects of AgNPs found in consumer products. It is still unclear whether laboratory manufactured AgNPs are representative of consumer product AgNPs, since their synthesis methods are proprietary information. Recently, some studies have quantified and characterized some AgNP containing consumer products, but results are divergent. Benn et al. [28] found that AgNP containing socks leached up to 68 μg Ag/g sock in water with gentle agitation, while Geranio et al. [29] measured up to 377 $\mu\text{g}/\text{g}$ with the application of detergent. The 5-fold difference in these values proves the difficulty in assessing the quantity of AgNPs in WWTPs and demonstrates the need for further research.

To gauge the benefits and risks of AgNPs in industries and engineered systems such as WWTPs, studies have begun to analyze the bactericidal mechanisms of AgNPs. The membranes of *Escherichia coli* were shown to be strongly disrupted by 50 ppm of Daxad 19 coated AgNPs and were found to be less resilient to AgNPs than *Bacillus subtilis* [158, 159]. Others have reported on Ag and gold nanoparticle biosynthesis by *Pseudomonas* in the extracellular supernatant produced by the bacteria [160, 161]. Although there have been numerous inquiries on the causes of lab manufactured AgNP toxicity, there have been limited studies on consumer products and none have studied the

effects of liquid dietary supplements containing AgNPs. The objectives of this study were to compare the antimicrobial activity of two laboratory manufactured AgNPs (gum arabic (GA) and citrate stabilized) to three AgNP dietary supplements (Mesosilver™, Sovereign Silver™, and Silver Biotics®). Two Gram-negative bacteria, *E. coli*, *P. aeruginosa*, and one Gram-positive bacterium, *B. subtilis*, were selected for this study since they are well studied and their genomes are sequenced.

4.2 Materials and Methods

Cell Growth and Preparation. *E. coli* K12 (ATCC 10798), *P. aeruginosa* PAO1 (ATCC 15692), and *B. subtilis* (ATCC 6633) were grown in 100 mL of Luria-Bertani (LB) broth containing 10 mg/L tryptone, 10 mg/L NaCl, and 5 mg/L yeast extract until reaching late log phase (OD₆₀₀ ~0.700). Cell cultures were spiked from single colonies isolated on LB agar plates. Cells were maintained by constant shaking at 150 rpm using a multi-flask shaker in a temperature-controlled incubator (~37°C). Samples were periodically taken for plating to check for contamination and to confirm proper morphology.

AgNP Characterization. Gum arabic (GA) and citrate (CA) stabilized AgNPs were the laboratory AgNPs tested in this study. These AgNPs were chosen for their commonly used stabilizing coating, which is generally accepted as being representative of coatings used in consumer product AgNPs [123-125]. Three Ag supplements, found at local food markets, were also tested – Mesosilver™ (Westampton, NJ), Sovereign Silver™ (Pompano Beach, FL), and Silver Biotics® (Alpine, UT). These supplements are abbreviated as

Mesosilver (MS), Sovereign Silver (SS), and Silver Biotics (SB) in this study. According to the product labels, these supplements are intended for human consumption and infection prevention. Ag as AgNO₃ (abbreviated AG in this study) was chosen as the positive control in all experiments. Particle size characterization by transmission electron microscopy (TEM) shows that the average particle size was 32.3 ± 0.5 and 15.5 ± 0.5 nm for GA and citrate AgNPs, respectively. More details regarding lab-made AgNPs and our TEM protocols can be found in the “*Transmission Electron Microscopy (TEM)*” and “*AgNP synthesis*” section of supporting information of our previous publication [18]. All laboratory AgNPs used in this study have been extensively characterized by others and us. Please refer to Yin et al. [128] and Meyer et al. [127] for further information on synthesis and characterization.

Analytical Methods. Total Ag and dissolved Ag were quantified in batch reactors composed of bacterial cells, LB medium and AgNPs. Total Ag concentration is defined as the amount of Ag in a given volume derived from the AgNPs. Total Ag concentrations were obtained by acidifying a known volume of sample with nitric and hydrochloric acid as previously described in Arnaout et al [18]. This study classifies dissolved Ag as the concentration of Ag that flows through a 3 kDa Amicon® Ultra-4 Centrifugal Filter Unit (Millipore, Billerica, MA) after centrifugation at 7,000 rpm for 35 min. Ag concentration of the filtrate (<3 kDa) was then quantified as previously defined for total Ag [127]. In all cases, total Ag measurements taken at the beginning and end of the experimental period were not statistically different ($p < 0.05$) from the total targeted Ag range (0.2-2 ppm).

Total Ag in consumer product samples was assessed using ICP-AES, prior to bacterial spiking. Concentrations were found to be 25.9 ± 2.1 , 10.9 ± 1.1 , and 11.29 ± 0.5 ppm for MS, SS, and SB AgNPs, respectively. Three mL of sample were taken for total and dissolved Ag measurements, in triplicates. Samples were acidified and then measured using ICP-MS.

Bacterial growth assays. Batch reactors were prepared in 250 mL Erlenmeyer flasks containing 100 mL of LB medium. Each reactor was inoculated with 1 mL late log phase *B. subtilis*, *P. aeruginosa* PAO1 or *E. coli* K12. All flasks were previously heat-sterilized by autoclaving at 121°C at 15 psi for 20 min. Aliquots of 200 μ L early phase bacterial cultures were added to wells in a clear 96 well Costar Clear Polystyrene plate (Corning, NY). Pure AgNPs were then added in stock solution form, directly to wells. If the bacteria were treated with consumer product AgNPs, the AgNPs were added directly as given by manufacturer. The concentrations of lab-manufactured AgNPs tested on the three model bacteria were 0.2 and 2 ppm. Three replicates of three different starting colonies were tested for each bacterium. Wells without AgNPs were run in parallel as negative controls. Reactors containing 0.2 ppm Ag as AgNO₃ were used as a positive control. To ensure uniform oxygen and nutrient distribution, plates were then incubated and shaken in Spectramax M5 plate reader (Sunnyvale, California) which maintained a temperature of 37°C and shook the plate vigorously every minute. After dosing each reactor with AgNPs, optical density readings at 600 nm were taken automatically every 20 min and a growth curve was produced after 24 h. All samples were collected under

aseptic bench top technique and optical density was measured at 600 nm using a Hach DR/4000 U spectrophotometer (Loveland, Colorado). Growth rate was calculated by selecting the linear range of growth curves (approximately 120 to 270 min) and growth rates were calculated from linear slopes. Percent reduction in growth rate was calculated based on treated and control growth rates.

Membrane Integrity. Membrane integrity was measured using the Invitrogen LIVE/DEAD® fluorescent plate assay (Grand Island, NY) as instructed by the manufacturer. Briefly, cells were washed, pelletized, and then resuspended in phosphate buffer solution (PBS) to reach $OD_{670} = 0.06$. One mL samples of cells were mixed with AgNPs to reach desired AgNP concentration, and then mixed on a horizontal shaker for 1 h. This time point was selected because growth inhibition was observed at approximately this time point. After 1 h, 100 μ L of cells were aliquoted into 96 well plates in triplicate and a propidium iodide/SYTO 9 mix was added for staining. Abiotic treatments at all tested concentrations were also run to determine if the medium, AgNPs or Ag^+ had any inherent autofluorescence. Samples were allowed to incubate for 20 minutes and then fluorescence was measured in triplicate on a Spectramax M5 plate reader (Sunnyvale, California). Experiments were repeated 3 times to ensure the same trends were seen for 3 different starting bacterial colonies. The manufacturer's protocol specifies an excitation wavelength centered at 485 nm, and fluorescence intensity measurements at 530 nm (green) and 630 nm (red). Standard curves of "live" and "dead" cells were run for every plate and type of bacteria to ensure proper measurements. "Dead" cells were treated with

isopropyl alcohol, prior to experimentation. Autofluorescence background was subtracted out of final data and then ratios of live/dead cells were calculated. Cell samples were also washed and pelletized after the 1 h exposure for thin-section TEM imaging. Thin film embedding preparation and imaging was done at Duke's Shared Materials Instrumentation Facility (Durham, NC). After embedding cells, epoxy resin slices were inspected by TEM. AgNP TEM imaging was carried out at 200 kV and bacterial imaging was done at 80 kV. More details regarding our TEM protocols can be found in the *Transmission Electron Microscopy (TEM)* section of the supporting information of our previous publication [18].

Reduced and Oxidized Glutathione. Samples for glutathione measurements were prepared from bacterial cultures with average density of 10^{10} cells/mL, as described in Kelly et al. [162]. *B. subtilis* contains no glutathione system so we were unable to measure its glutathione [163]. We were also unable to quantify glutathione in *E. coli*, because glutathione concentration was below detection in our samples. For *P. aeruginosa*, five mL of culture in late log phase were centrifuged at 5,000 RPM for 10 min. Cells were then washed, pelletized, and resuspended in PBS buffer. Due to the high amount of cells necessary for glutathione detection, all the cells from initial 5 mL of culture were added to 50 mL of LB medium following resuspension. Directly before inoculation, AgNPs were added and briefly mixed. The reactors were run in triplicate and continuously mixed on a horizontal shaker at 150 RPM for 1 h to allow exposure to AgNPs. AgNP treatment concentrations were chosen based on an examination of growth

inhibition data. The concentration of 2 ppm was selected since growth was significantly stunted but not stopped. The Bioxytech® GSH/GSSG-412 glutathione analysis kit (Oxis International, Portland, OR) was used to measure reduced (GSH) and oxidized glutathione (GSSG). To prevent interaction of Ag with any glutathione analysis reagents, samples were washed with centrifugation and resuspended with phosphate buffer. Cells were then ruptured using a Branson 1510 bath sonicator (Danbury, CT) for 10 min of total sonication time and iced intermittently to prevent heating during sonication. All further analyses were followed directly from Oxis Research reduced and oxidized glutathione manual.

Statistical Analysis. The unpaired, two tailed student's t-test was used to identify statistical differences between control samples and treated samples. Results were considered statistically different when P-value < 0.05.

4.3 Results and Discussion

Dissolution and Characterization of AgNPs. Both laboratory-created and consumer product AgNPs were characterized for dissolution, average radius, poly dispersity index, zeta potential, and total organic carbon (TOC). Samples were taken at the 1-h time point (when membrane integrity assays were completed) to assess the total and dissolved Ag concentration in each treatment. For all laboratory made Ag samples and concentrations, the dissolved Ag concentration remained below the ICP-MS detection limit (0.01 ppb), similarly to the control sample. This may indicate that free Ag, in the form of dissolved Ag was not present at detectible concentrations in our experiments. It is possible if there were minimal amounts of dissolved Ag in the samples, they were bound with chlorides in the LB medium, which had a strong Cl⁻ presence (171.1 mM). Interestingly, the dissolved Ag concentrations in the consumer product AgNPs were much higher and close to the Ag as AgNO₃ positive control concentration. Figure 8 shows the average concentrations and standard deviations for all AgNP treatments. The dissolved Ag concentrations measured in the 2 ppm treatments were 0.40 ± 0.00 , 0.43 ± 0.1 , and 0.36 ± 0.05 for MS, SS, and SB treated samples, respectively. The dissolved Ag:total Ag ratio was higher for the 0.2 ppm treatment than the 2 ppm treatment, which we also previously observed in our study with *Nitrosomonas europaea* [18]. This may be caused by the aggregation of the particles and the total surface area available for dissolution, which decreases in the presence of ions such as chloride and sulfide [164, 165]. Total Ag concentrations for all Ag and AgNP treatments were not statistically different across different types of bacteria ($p < 0.05$).

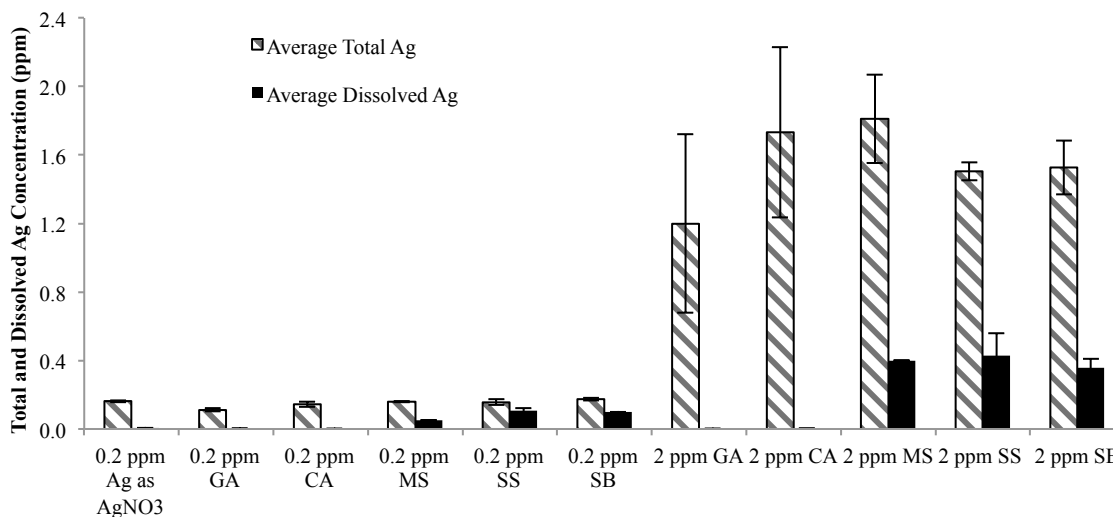


Figure 8: Total and dissolved Ag concentration for gum arabic (GA), citrate (CA), MS (Mesosilver), SS (Sovereign Silver), and SB (Silver Biotics) AgNPs. Ionic Ag (Ag as AgNO₃) was also run as a positive control sample. Error bars represent the standard deviation of duplicate samples.

The size of AgNPs is of great importance because of its effect on dissolution and total surface area available for interaction between AgNPs and bacteria. The difference in aggregate size given by ALV goniometer between the consumer product AgNPs was large – MS AgNPs had the average diameter of 39.6 nm while SS AgNPs had an average radius of 196.9 nm. Size and morphological differences were also assessed via TEM imaging (Figure 9). All consumer product AgNPs were asserted to be suspended in pure water, but TEM imaging revealed what looked to be coatings on all three of the AgNPs. This is not surprising since some of the consumer product suspensions were visually colored and further corroborated by TOC measurements. MS AgNPs had the most uniformity in shape (spherical) and were connected in long chains by a lower density substance that did not appear as dark as Ag. SB AgNP images showed a similar long chain of AgNPs but the individual particles were not as spherical or uniform. SS AgNPs

appeared to be in a cloudy substance, but uniform in size and shape. It was hard to distinguish the higher density Ag particles from the coating since there were large aggregates in most images. The average TEM particle sizes of the individually visualized particles were 10.2 ± 5.3 for MS AgNPs, 7.1 ± 8.1 for SB, and 12.6 ± 3.2 for SS. These values vary greatly from ALV and DLS measurements likely because these instruments could not distinguish between the large chain/cloud aggregates and the smaller individual particles observed in the TEM imaging. TOC measurements indicated that some organic compounds may have been present in consumer product AgNPs, but not to the same degree as the lab manufactured AgNPs.

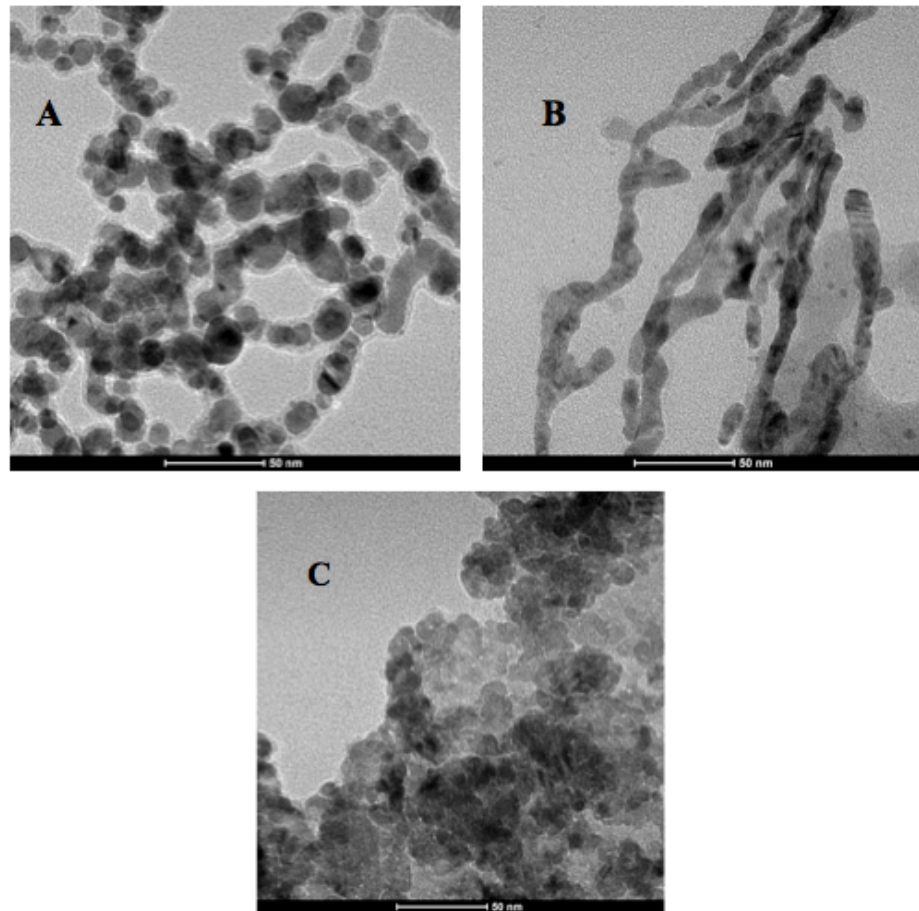


Figure 9: TEM images at 200 kV of three different consumer product AgNPs: (A) Mesosilver, (B) Silver Biotics, (C) Sovereign Silver.

Zeta potential values were relatively close for all AgNPs used in this study and ranged from -21 ± 1.3 for CA AgNPs to -30.3 ± 2.9 for MS AgNPs. These values indicate that the AgNP suspensions had a similar stability level and were likely to remain dispersed due to repelling external charge. The PDI for all the AgNPs was below 1, indicating relative monodispersity for all the AgNPs. This was further corroborated by the percent by weight of the primary peak radius measured via ALV goniometer. All AgNPs were more than 74% by weight their primary peak radius, with SB AgNPs having the most

monodispersity (99.7% by weight primary peak radius at 77.7 nm). Surprisingly, the consumer product AgNPs appeared to have a better monodispersity than the lab manufactured particles, based on their PDI. During experimentation, no significant aggregation was visually observed in LB medium over the 16 h experimental period. This may be due to the negative zeta potential charges of the AgNPs, which increased stabilization, and short durations of experimentation. SS AgNPs also had the highest TOC content of the consumer product AgNPs at 3.975 ppm. This was however much lower than the TOC in lab manufactured AgNPs, due the amount of stabilization solvents required to synthesize those particles.

Table 1: Physical and chemical properties of CEINT and consumer product AgNPs

Sample	Avg Radius	PDI	Primary Peak Radius	% Weight	ZP avg	St dev	TOC	St dev
Silver Biotics	76.23	0.98	77.67	99.7	-23.2	1.6	1.601	0.101
Mesosilver	19.78	0.92	39.83	84.3	-30.3	2.9	1.379	0.044
Sovereign Silver	98.45	0.77	55.28	85.0	-30.2	5.3	3.975	0.076
CEINT Ag GA	32.31	0.474	44.78	87.7	-23	1.1	690	16
CEINT Ag Cit	15.49	0.536	29.86	74.3	-21	1.3	703.2	19.0

Given by ALV (nm) (nm) (mV) n=6 (ppm)

Effects of AgNPs on growth rate. Growth of model heterotrophic bacteria was hindered for nearly all bacteria at 0.2 ppm, with the exception of *B. subtilis* primarily. Figure 10 shows the percent reduction in growth rate for all treatments. Growth inhibition was amplified with increasing total and dissolved Ag concentration for most AgNPs. Surprisingly, all AgNPs showed more toxicity to *E. coli* and *B. subtilis* at 0.2 ppm than

the ionic Ag treated sample. MS, SS, and SB treatments showed the highest reduction in growth rate to all bacteria, and prevented growth entirely at 2 ppm. The highest degree of inhibition was seen in the *P. aeruginosa* sample that was treated with 2 ppm of SS and SB AgNPs. Growth rate was decreased by $100\% \pm 0.4\%$ and $100\% \pm 0.6\%$ for SS and SB AgNPs, respectively. This result is likely due to the dissolved Ag concentrations found in these samples, which were higher in the consumer products than the lab manufactured AgNPs. No statistically significant inhibition was observed in *B. subtilis* at several concentrations including 0.2, 2 ppm CA, and 0.2 AG ($p > 0.05$). Growth of *E.coli* was significantly suppressed in all 2 ppm samples but especially by SS and SB, with $99\% \pm 0.1\%$ reduction in growth for SS, and $100\% \pm 0.1\%$ for SB. There was also no significant inhibition noticed for 0.2 ppm GA treatment of *P. aeruginosa*.

In general, the consumer products were more effective in stunting growth of all three bacteria than the lab manufactured AgNPs and Ag as AgNO_3 . Overall trends indicate that *P. aeruginosa* was the most affected by AgNPs while *E.coli* and *B. subtilis* had more inherent resilience to AgNPs. These results were surprising since the opportunistic pathogen, *P. aeruginosa* PAO1, is known to be able to make protective biofilms to decrease surface contact with AgNPs. Studies have shown however that liquid cultures of *P. aeruginosa* are less proficient at preventing heavy metal intrusion, via extracellular polymeric substances, which may explain the decreased resilience to AgNPs [166]. The amount of shaking and the short duration of experimentation was likely to inhibit the growth of biofilms on our samples. *B. subtilis* had the most variable growth curve data, a

result which could be a function of its Gram-positive membrane. *B. subtilis* ATCC 6633 has previously been shown to have the lowest minimum inhibitory concentration (MIC) when exposed to Ag crystalline structures, when compared to *S. aureus* ATCC 6538, *E. coli* ATCC 35218, *P. aeruginosa* ATCC 13525 [166]. It also has a peptidoglycan layer that is 25 times thicker than Gram-negative bacteria such as *E. coli* and full of thiol groups where metal species could attach and grow into aggregates [5]. In addition, *B. subtilis* membrane walls have also been shown to bind more readily with ionic metals than Gram positive bacteria and the variance in AgNP dissolution rate may result in the inconsistency in growth functions [6].

Overall, the toxicity of the AgNPs was enhanced in the presence of dissolved Ag concentration, but not dependent on it. There was a clear relationship between the dissolved Ag concentration and growth inhibition, but cells were still repressed by AgNPs even when no detectable dissolved Ag concentration was measured (GA and CA). These results suggest that there are other mechanisms at work, which cause toxicity to bacteria. Although the dissolved Ag was not in the bulk mixture for some of the AgNPs, it is possible that they were still adhering to bacterial surfaces and releasing Ag as their coatings dissolved. It is also likely that the AgNP properties had an effect on surface interaction of the AgNPs with bacteria. The dietary supplements had lower TOC content than the lab manufactured AgNPs, indicating that they had much less stabilizing coating than lab manufactured AgNPs, which may have increased Ag dissolution. It is also noteworthy that the consumer product AgNPs were more toxic even though their

aggregation was greater than the lab manufactured AgNPs and their general size was larger. However, we speculate that their high dissolved Ag concentration surpassed size differences in AgNPs and caused acute toxicity to all bacteria.

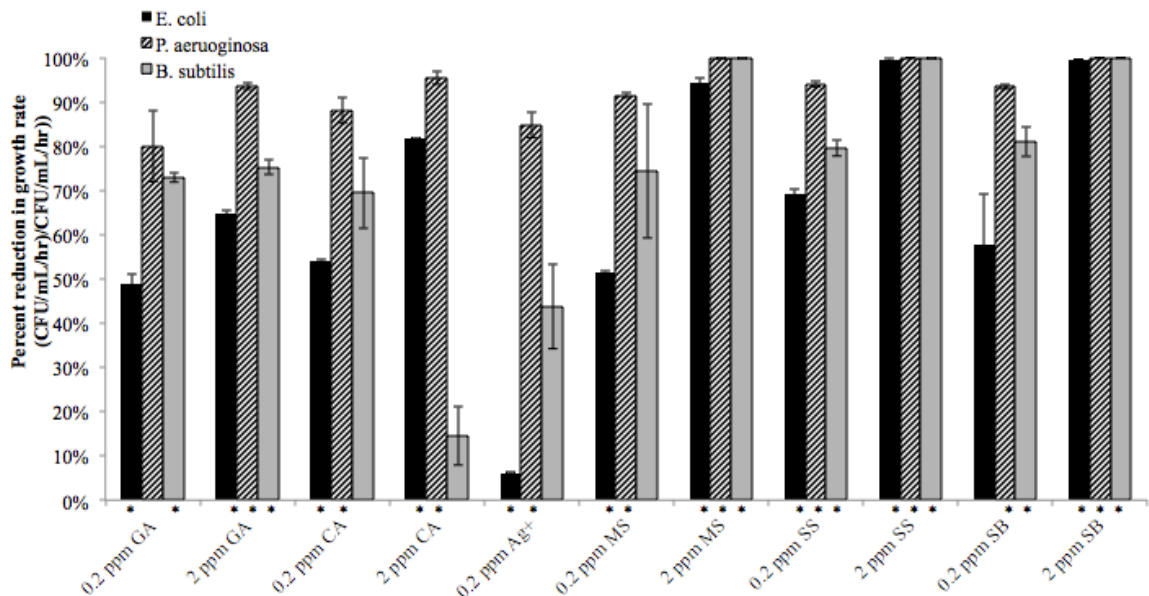


Figure 10: Percent reduction in growth rate for gum arabic (GA), citrate (CA), MS (Mesosilver), SS (Sovereign Silver), and SB (Silver Biotics) AgNPs. Ionic silver (Ag as AgNO₃) was also run as a positive control sample. Asterisks indicate statistical significance ($p < 0.05$) between no Ag samples and AgNP treatment samples. Error bars represent the standard deviation of triplicate samples.

GSH/GSSG Assay. The GSH/GSSG ratio was measured in *P. aeruginosa* cultures exposed to AgNPs for 1 h. Figure 11 shows GSH/GSSG ratios for all 2 ppm treatments. GSH/GSSG measurement is one method of determining the level of oxidative stress in bacteria, since some strains are capable of producing this tripeptide with a thiol group to bind with reactive oxygen species or heavy metals. The ratio of these two components can indicate whether the organism was inducing GSH production and quenching

oxidative stress. Although trends in GSH/GSSG ratios were observed in *P. aeruginosa* samples, GSH/GSSG ratios were not statistically different from the control samples ($p > 0.05$). The consumer product AgNPs caused an increase in the GSH/GSSG ratio, while the lab manufactured AgNPs and AG decreased GSH/GSSG. GSH may have been decreased by Ag-thiol binding, rendering GSH unavailable for the assay to detect since it uses a thiol scavenger-quenching agent to quantify GSH. Either way, the difference in GSH/GSSG ratios indicate that cells may have had a post-transcriptional response to the intrusion of AgNPs releasing dissolved Ag.

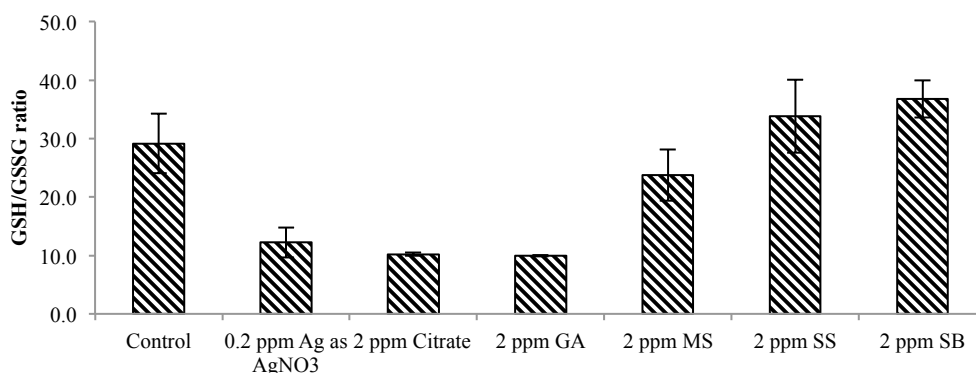


Figure 11: Trends in reduced GSH/GSSG ratio in *P. aeruginosa* cultures. Error bars represent the standard deviation of triplicate samples.

Impacts on Membrane Integrity and Cellular Morphology. Samples of bacteria were analyzed using the LIVE/DEAD assay and TEM imaging to assess what effects AgNPs had on their morphology. Percent membrane compromised cells is shown in Figure 12. Not surprisingly, higher concentrations of AgNPs are associated with higher percentages of membrane compromised bacteria. However, membrane integrity results did not have

as strong of a correlation with dissolved Ag concentration as with the growth rate results discussed earlier. This could indicate that AgNP characteristics including size and coating, which affect AgNP attachment to bacterial walls, may be mostly responsible for membrane loss. Since the AgNPs tested in this study had similar zeta potentials, it is possible that the Stern layer charge, which was not considerably different for all tested AgNPs, is the major trait that determines membrane attachment. Similar to growth rate data, the highest impacts on membrane integrity were measured in *P. aeruginosa* followed by *B. subtilis* and *E. coli*. A statistical difference in *P. aeruginosa* membrane loss was first observed at concentrations of 2 ppm GA, 0.2 ppm CA, and 0.2 ppm AG. Although growth rates of all three bacteria were severely inhibited by consumer product AgNPs, membrane integrity did not show the same trends. The highest percentage of compromised membranes was observed in 0.2 ppm AG treated *P. aeruginosa* sample, which contained $72 \pm 9\%$ “dead” cells. For *B. subtilis*, 0.2 ppm AG had the strong impact on membrane integrity ($61 \pm 3\%$ “dead” cells), but was followed very closely by the 2 ppm MS and SS treatments which caused $57 \pm 5\%$ and $55 \pm 2\%$ “dead” cells, respectively. Of the three consumer products, SB had the lowest effect with only $25 \pm 2\%$ “dead” cells in the 2 ppm treatment. Overall, every AgNP treatment tested significantly disrupted membranes at 2 ppm.

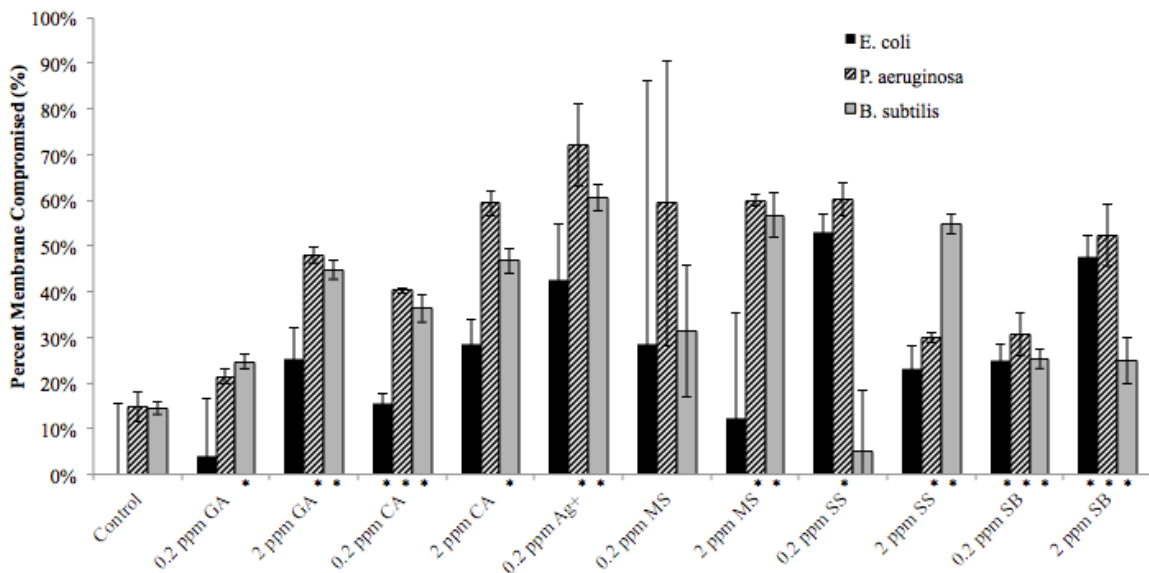


Figure 12: Percent membranes compromised for gum arabic (GA), citrate (CA), MS (Mesosilver), SS (Sovereign Silver), and SB (Silver Biotics) AgNPs. Ionic Ag (Ag as AgNO₃) was also run as a positive control sample. Asterisks indicate statistical significance ($p < 0.05$) between no Ag samples and AgNP treatment samples. Error bars represent the standard deviation of triplicate samples.

TEM images were examined to find differences in visual cell morphology (Figures 13-15). Investigation of *P. aeruginosa* TEM images of GA, SS, and MS AgNP treated samples showed many empty cells that had membrane damage and lacked internal matter, while CA and SB treated samples had increased membrane space between the cell membrane and internal matter. TEM imaging of *P. aeruginosa* also showed internal black dots in all of the Ag treated samples but we were not able to confirm that these dots corresponded to Ag with elemental mapping (energy-dispersive X-ray spectroscopy) due to our pre-treatment with Uranium. These black dots had a different morphology and size than the spiked AgNPs. They were smaller, uniform in size, and denser. Previous studies have reported biosynthesis of intracellular AuNPs by *Pseudomonas* spp. and extracellular

AgNPs by the fungi *Fusarium*, which could be what is observed in the images in this study as well [161, 167]. AgNPs were also found on the surface of the bacteria in the CA, GA, and SB images, which may have contributed to membrane loss in these samples. *B. subtilis* TEM imaging of AgNP treated cells did not reveal many differences from control cells. In general, internal structures and cell walls looked similar throughout all images. Replication and chains of bacteria were observed in all treatments, including the diplococci and streptococci orientation. No AgNPs could be found on the surface of *B. subtilis* nor inside the cells. One notable observation was the loss of internal cellular matter in the SB sample, indicating membrane loss. In the AG images, cells appeared to have uncharacteristically pentagonal shapes, rather than their usual smooth edges. This may have been caused by membrane disruption that did not result in complete membrane loss [9]. In general, *B. subtilis* was not as impacted by AgNPs as *P. aeruginosa*. *E. coli* showed similar characteristics as *P. aeruginosa* in response to Ag addition. AgNPs were observed on the membrane surface of all AgNP treatments with *E. coli*. Some treatments, including AG, GA, MS, and SS, showed internal cellular matter pulling away from cell membranes. Internal black dots were also identified in all of the Ag treatments, which may have been caused by Ag uptake and biosynthesis, which has been recorded in *E. coli* previously [168].

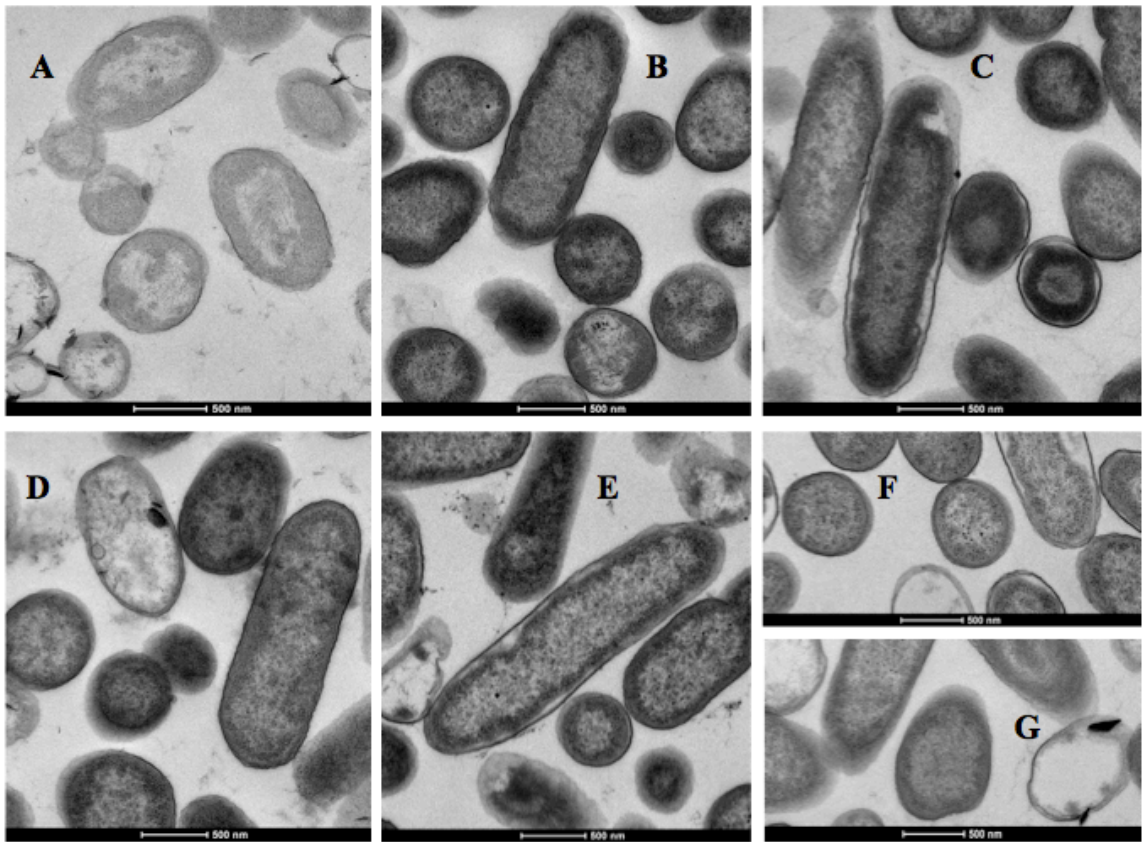


Figure 13: TEM images of *P. aeruginosa* for control cells (A), 0.2 ppm Ag as AgNO₃ treatment (B), citrate (C), gum arabic (D), Silver Biotics (E), Mesosilver (F), and Sovereign Silver AgNPs treatments (G). Ionic Ag (Ag as AgNO₃) was also run as a positive control sample. All samples were examined at 80 kV.

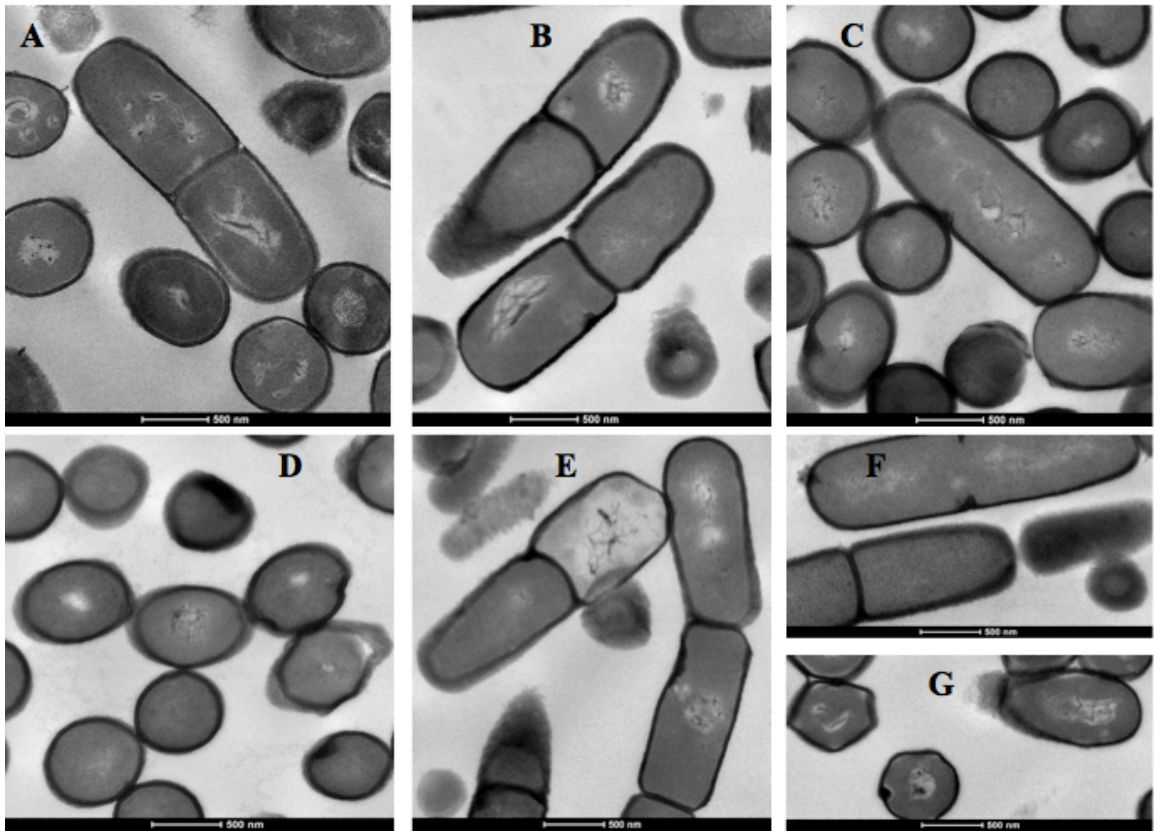


Figure 14: TEM images of *B. subtilis* for control cells (A), 0.2 ppm Ag as AgNO₃ treatment (B), citrate (C), gum arabic (D), Silver Biotics (E), Mesosilver (F), and Sovereign Silver AgNPs treatments (G). Ionic Ag (Ag as AgNO₃) was also run as a positive control sample. All samples were examined at 80 kV.

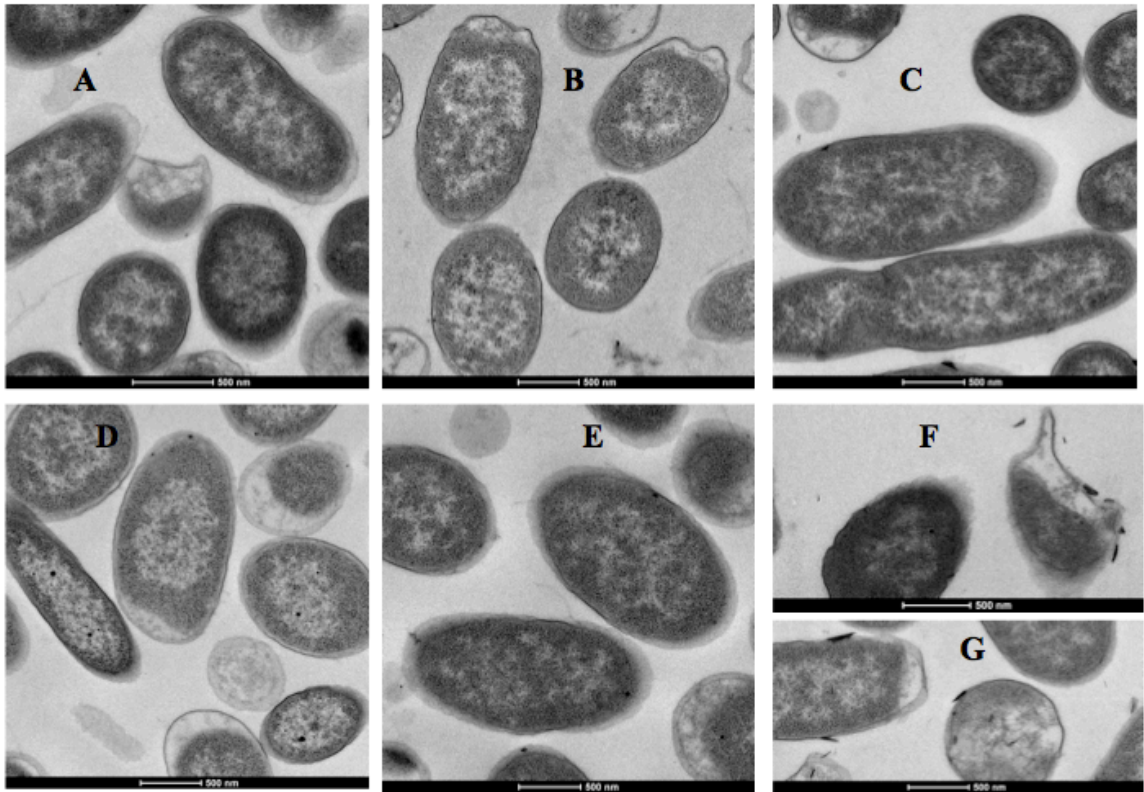


Figure 15: TEM images of *E.coli* for control cells (A), 0.2 ppm Ag as AgNO_3 treatment (B), citrate (C), gum arabic (D), Silver Biotics (E), Mesosilver (F), and Sovereign Silver AgNPs treatments (G). Ionic Ag (Ag as Ag) was also run as a positive control sample. All samples were examined at 80 kV.

Differential impacts of AgNPs on heterotrophic bacteria. Our data suggest that AgNP toxicity to heterotrophic bacteria is linked, but not exclusively, to dissolved Ag, which is in agreement with previous literature [14]. These results also highlight the importance of AgNP coating on bacterial interactions and inhibition. Consumer product AgNPs were found to be more toxic than lab manufactured AgNPs with similar physical and chemical properties. We hypothesize that the high dissolved Ag concentration found in consumer products was primarily responsible for the increased growth inhibition. This high dissolved Ag could have been caused by a low amount of stabilizing agent used in

consumer product AgNPs, which was corroborated by low TOC values measured in SB, SS, and MS samples. However, membrane integrity was not a function of the dissolved Ag concentration, and seemed to be linked to the attachment of AgNPs on the surface of the bacteria, as shown by TEM imaging. It also appears that the toxicity of AgNPs to heterotrophic bacteria is not primarily a function of the type of membrane, but rather to the individual properties of the bacterium, such as their ability to bind with heavy metals and their stress responses. Although the TEM imaging indicated similar mechanisms of inhibition for the Gram-negative bacteria, *E. coli* and *P. aeruginosa*, growth inhibition and membrane loss percentages were not congruent for the two bacteria. GSH measurements in *P. aeruginosa* were inconclusive in showing oxidative stress in cells, but trends did suggest that excess Ag could have been bound with GSH or causing the production of GSH. AgNPs did not as strongly affect the growth of the Gram-positive bacterium, *B. subtilis*, and TEM imaging did not show major damage to cells. However, the results attained herein demonstrate that AgNP containing consumer products are as toxic, if not more, than lab manufactured AgNPs. Further research needs to be carried out to expand this assessment to other bacteria and AgNP containing consumer products to verify the trends observed. An examination of the bioavailability of excreted consumer products would also be helpful for assessing toxicity of consumer product AgNPs.

5 Assessing the effects of Ag Nanoparticles on Biological Nutrient Removal in Bench-Scale Activated Sludge Sequencing Batch Reactors

5.1 Introduction

Ionic Ag is an established antibacterial agent and has been utilized for its antiseptic properties in consumer products such as washing machines, clothing, and children's toys [22, 154]. More recently, Ag nanoparticles (AgNPs) have replaced ionic Ag in consumer products because of their ability to slowly release ionic Ag as their coatings dissolve making them better suited for long term consumer product usage. Because manufactured AgNPs generally range from 10 to 100 nm, researchers speculate that they may be small enough to infiltrate the cell membrane of a microorganism, then release ionic Ag directly into the microbe as their coatings dissolve [26]. Since it is likely that some consumer products such as textiles will be washed, it is critical that the concentration of AgNPs in wastewater treatment plant (WWTP) influent be quantified and their impacts ascertained. Current reports show that there is a high variation in Ag concentration present in consumer products and it is difficult to find estimations of the total Ag and AgNPs being added to consumer products. Benn et al. [28] found that AgNP containing socks leached up to 68 μg Ag/g sock in water with gentle agitation, while Geranio et al. [29] measured up to 377 μg /g with the application of detergent.

Since these AgNP-containing consumer products are already in use, studies have begun developing methods for estimating speciation of AgNPs in complex media such as wastewater, where it will likely collect. Because one of the suggested antimicrobial

mechanisms of AgNPs is the release of ionic Ag after the particle coating dissociates, researchers are examining nanoparticle coating interactions with solution properties such as pH, ionic strength, and dissolved organic carbon concentration [7]. The characteristically high concentration of thiols in wastewater sludge has also led to the discovery of naturally occurring Ag sulfide nanoparticles in wastewater, which provides evidence that influent Ag is likely to be bound up with wastewater sludge thiols [109]. Nonetheless, because of their proven antimicrobial properties, even if AgNPs are only present at very low concentrations in wastewater influent, it is possible that AgNPs could alter important microbial functions. The disruption of biological nutrient removal, and especially nitrification, in wastewater treatment is of particular concern. Nitrifying bacteria including *Nitrosomonas* spp. can be easily inactivated by disruption of their membrane-bound enzyme ammonia monooxygenase (AMO) which could ultimately cause treatment failures in activated sludge treatment scheme [99].

The bactericidal nature of Ag has been well established in previous literature [86, 87], but the toxicity of AgNPs appears to differ greatly depending on size and coating [16, 88]. In previously published work, polyvinyl alcohol coated AgNPs at concentrations of 0.5 ppm have been linked to a decrease of nitrifying activity in mixed nitrifying bacterial communities commonly found in WWTPs [2]. While small concentrations of AgNPs such as 0.5 ppm may not seem significant considering current loading rates, increased utilization in consumer products warrants further evaluation to determine potential impact. Although a handful of studies have examined the antimicrobial effects of AgNPs

on wastewater bacteria, few have examined the effects on wastewater bacterial diversity and overall treatment efficiency. The objective of this project was to determine the effect of two AgNPs (citrate and gum arabic stabilized) on common treatment characteristics (namely in terms of COD and ammonia removal efficiency) and microbial community structure in sequencing batch reactors (SBRs) mimicking WWTP operation.

5.2 Materials and Methods

AgNP Characterization. GA and citrate stabilized AgNPs were used in this study. These particles were selected because they have been widely studied and because their coatings are representative of AgNPs used in consumer products, as previously described [18]. Citrate AgNPs were produced by reducing Ag nitrate in water with sodium citrate [126]. GA AgNPs were manufactured by reducing Ag nitrite with water and GA. The average particle sizes measured by transmission electron microscopy (TEM) were 32.3 ± 0.5 and 15.5 ± 0.5 nm for GA and citrate AgNPs, respectively. More information related to AgNP synthesis and characterization can be found in Yin et al. [128] and Meyer et al. [127]. In addition, the “*AgNP Synthesis*” section in the supporting information of Arnaout and Gunsch [18] has extensive information on TEM images, zeta sizing of AgNPs, and laboratory procedures.

SBR Design. Eight 3-L bench-scale SBRs were constructed out of square pieces of plexiglass (6 x 6 x 6 in, 1/8” thick), which were welded together using poly(methyl methacrylate). The peak volume in all reactors was 1.5 L and the volume after decanting

was approximately 0.5 L. SBRs were operated on an 8 h cycle, starting with 39 min of influent synthetic wastewater feeding, 6 h of aerating and vigorous mixing, 1 h of settling, and 30 min of decanting (Figure 16). A 13 d solids retention time (SRT) was chosen to ensure optimum conditions for nitrification and the reactors were run with a 5.3 h hydraulic retention time (HRT), which falls in the typical range for contact stabilization systems [169, 170]. The SRT was maintained by wasting sludge periodically to retain 2000-2500 mg/L of mixed liquor suspended solids (MLSS). The SBRs were fed synthetic wastewater (SWW) based on a recipe found in Zeng et al. [171], which had an average COD of 450 mg/L, average ammonia concentration of 40 mg/L and pH 7. All reactors were covered with aluminum foil to prevent any light photolysis. AgNPs were added in stock concentration form either directly to the reactors (for pulse additions) or into the influent medium (for continuous additions).

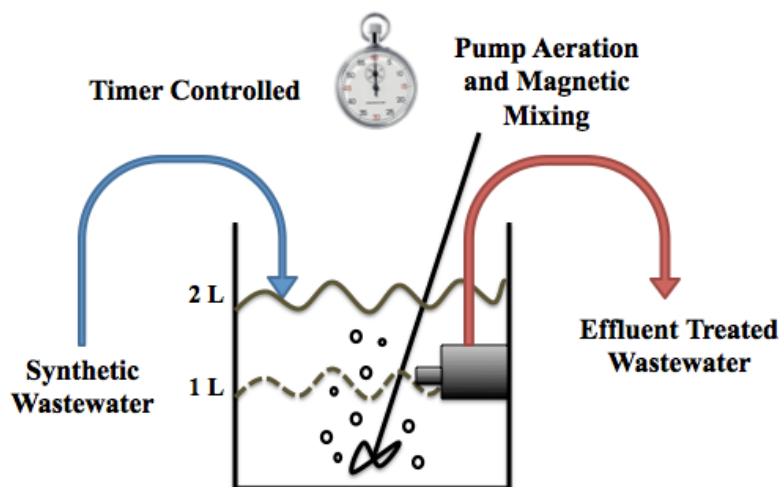


Figure 16: SBR schematic showing influent and effluent pumping, aeration, and mixing which were controlled by timers.

Air was fed into reactors via Tetra Whisper small aquatic aerators (Madison, WI) and feed water was pumped in via multi-head pumps (Cole Parmer, Masterflex L/S™, Vernon Hills, IL). The dissolved oxygen was maintained between 6 and 6.5 mg/L. The reactors were continuously mixed with large stir bars on stir plates at 700 RPM. The cycling of air, feed, and pumping was controlled by Intermatic TN311C timer-controllers (Grove, IL). Reactors were kept at room temperature (~17-20°C). The SBRs were initially spiked with 500 mL of activated sludge taken from the North Durham Water Reclamation Facility (Durham, NC). This plant currently treats up to 20 million gallons/day and utilizes biological nutrient removal systems to remove phosphorus, BOD, and ammonia. Prior to beginning the AgNP spikes, the SBRs were operated for 120 d with no Ag additions. After the reactors reached steady state, COD and ammonia removal, microbial community analysis was performed to ensure all reactors were operating similarly (please refer to *Microbial Analysis* section for information). At this stage, the SBRs were steadily removing 90% or more of COD and ammonia. Microbial community structure analysis was also performed on steady state SBRs and reactors were split into 2 groups of 4 reactors with the most comparable starting microbial community profiles. Please refer to “*T-RFLP analysis*” section for more information on pre-treated microbial community analysis. In total, four treatments were operated on the SBRs in duplicate consisting of: 1) – “control” with no Ag, 2) citrate AgNP, 3) GA AgNP, 4) Ag⁺. At the time of the initial Ag spike, the COD and ammonia removal rates were not statistically significantly different across all eight reactors.

AgNP Addition. 0.2 ppm was selected as the baseline concentration to test in SBRs. This value was based on our previous study, which showed that the effects of AgNP on the model wastewater microorganism, *N. europaea*, exhibited some toxicity at 0.2 ppm [18]. Table 2 shows the order of Ag addition to the SBRs. Ag were initially added in pulses at 0.2 ppm followed by a continuous addition. For the pulse input, AgNPs or Ag⁺ were added directly to the SBRs at the start of the morning cycles. Following each pulse input, the SBRs were allowed to adapt for different lengths of time. The first adaptation period was the longest (2 wks) to assess the recovery period needed by the SBRs, then shorter adaptation periods ranging from 2 to 6 d were selected. Following the pulse inputs, a continuous flow of Ag was added by spiking influent SWW with stock solutions of AgNPs and AgNO₃.

Table 2: Order of Ag addition to SBRs

Order of Addition	Spike Concentration	Type of Spike	Length of Spike
1	0.2 ppm	Pulse	14 d, 6 d, 2 d
2	0.2 ppm	Continuous	3 SRTs

Analytical Methods. To monitor COD and N removal efficiency, influent and effluent samples were collected approximately every 3 d as well as directly after each Ag spike. Four parameters were measured using HACH (Loveland, CO) reagents: COD (mercuric digestion method), ammonia (salicylate method), nitrite (diazotization method), and

nitrate (cadmium reduction method). Samples were taken directly from SBR effluent containers and tested within 30 mins. To measure the Ag concentration in the SBRs, samples were collected directly from the SBRs during treatment as well as from the treated SBR effluent. Samples for Ag spikes were taken at 1 min, 1 h, 6 h, 24 h, and at the end of the spike, while samples for continuous Ag spikes were taken at 24 h and every 7 d following the continuous spike. Effluent treated water samples were also collected for Ag analysis every 3 d. Ag analysis was performed as previously described in Arnaout and Gunsch [18]. Briefly, samples were diluted in an acid solution to digest stabilizing coatings and other compounds that could interfere with ICP-MS measurements. An Agilent 7700 inductively coupled plasma mass spectrometer (ICP-MS, Santa Clara, CA) was used to measure total and dissolved Ag. First, total Ag was measured by dissolving a sample of wastewater in 2% HNO₃ and 0.5% HCl concentrated acid for at least 24 h. Samples were separately taken to measure the amount of dissolved Ag in the wastewater. Dissolved Ag samples were defined as the fraction of Ag filtrate that can be passed through an Amicon® Ultra-4 Centrifugal Filter Unit (Millipore, Billerica, MA) and centrifuged at 7,000 rpm for 35 min. The filtrate was then acidified with nitric and hydrochloric acid using a method amended from Wang et al. [135].

DNA extraction and PCR Conditions. Biomass samples were collected periodically from the SBRs and micro-centrifuged for 1 min at 13,000 x g. Biomass samples were then immediately stored at -20°C until DNA extraction. Duplicate samples were extracted for each treatment using the UltraClean® DNA Isolation Kit (MoBio Laboratories, Solana

Beach, CA). All DNA extractions were performed following the manufacturer's protocol. Following extraction, DNA was stored in elution buffer at -20°C until used for downstream processing. A ND-1000 NanoDrop spectrophotometer (NanoDrop Technologies) was used to verify concentration and purity of DNA. PCR of the bacterial 16S SSU rRNA gene region was carried out by the methods described in Lukow et al. [172] with small adjustment. 6 – carboxyfluorescein (6-FAM) was used to fluorescently label the forward primer (27F) and 1392R was used as the unlabeled reverse primer [173]. Also, primers for bacterial [174] and archaeal ammonia oxidizer genes [175] were used to identify shifts in ammonia oxidizing bacterial communities. First, 5 µL of template DNA was used for each amplification in a 100 µL reaction. The presence of the correct length PCR amplicons was confirmed by visualization on a 1% agarose gel containing 0.1% ethidium bromide. PCR amplicons were further purified by following the manufacturer's protocol in the Qiagen PCR Purification Kit (Qiagen, Hilden, Germany). Final PCR product concentrations and purity was verified as described above using the NanoDrop.

T-RFLP Analysis. Restriction enzyme digests were carried out by following the protocol described in Lukow et al. [172]. Ten units of *MspI* (New England Bio-labs Inc., Beverly, MA, USA) was added to 100 ng of purified PCR product and the manufacturer provided buffer solution. The mixture was incubated for 3 h at 37°C, followed by an enzymatic inactivation at 65°C for 15 min. Samples were stored on ice prior to the spin column filtration desalting step. Fragment analysis was carried out using an Applied Biosystems

3100 capillary sequencer (Foster City, CA) with POP6 polymer and ROX-labeled MapMarker 1000 size standards (BioVentures, Inc., Murfreesboro, TN). All analyses were carried out at the Duke University DNA Analysis Facility (Durham, NC) following standard procedures. Applied Biosystems GeneScan v3.7.1 software (Foster City, CA) was used to interpret the raw data after electrophoresis. All samples were visually inspected for clean peaks and raw data was transferred into T-REX [176] in the resulting format: Dye/Peak, Sample File Name, Size, Height, Area, Data Point. T-REX aligned peaks and identified true peaks. Data analysis was performed in T-REX using the peak area feature, so that abundance and diversity could be examined. T-RFs smaller than 50 bp were not included in analysis, as to eliminate primer dimer fragments. The minimum peak height threshold was set at 50 relative fluorescent units. Data files were then imported into PAST statistical software to create Bray-Curtis principle coordinate graphs and cluster similarity (Hammer & Harper, D.A.T. 2006. Paleontological Data Analysis. Blackwell). For Bray-Curtis analysis, a transformation exponent of $c=2$ was selected. Eigenvalues were produced for coordinate plots. Diversity indices were calculated by transposing data into PAST and comparing taxonomic species with the Simpson 1-D index. The greater the resulting value, the more diverse sample is in species.

Statistical Analysis. The unpaired, two tailed student's t-test was used to identify statistical differences between control samples and treated samples. Results were considered statistically different when $p\text{-value} < 0.05$.

5.3 Results and Discussion

Dissolution of Ag from AgNPs. The concentration of total and dissolved Ag was measured in the SBRs to assess how quickly Ag dissolved from AgNPs, adsorbed to biomass, or was removed out of reactors (Figure 17). In general, total Ag concentrations during pulse inputs were near dosing concentration (0.2 ppm) immediately following spikes, and gradually decreased thereafter. Total Ag concentrations dropped in the SBR supernatant by at least 40% in 24 h. The total Ag concentrations in the wastewater after 1 h for the 14 d pulse spike were 96.8 ± 0.95 , 70.8 ± 10.9 , and 134.2 ± 10.8 ppb Ag for Citrate AgNPs, GA AgNPs, and Ag as AgNO₃, respectively. The dissolved Ag concentrations after 1 h were significantly lower, and measured 0.59 ± 0.01 , 0.58 ± 0.01 , and 0.16 ± 0.18 ppb Ag for Citrate AgNPs, GA AgNPs, and Ag as AgNO₃, respectively. These concentrations were not statistically significantly different when compared to the no Ag control concentrations ($p > 0.05$). Total and dissolved Ag concentrations in the no Ag control SBR were consistently lower than ICP-MS detection limit, and averaged 0.11 ± 0.17 ppb Ag over the 60 d operation time. After 24 h, the total Ag concentrations were 63.5 ± 5.6 , 8.89 ± 0.1 , and 79.2 ± 2.1 ppb Ag for Citrate AgNPs, GA AgNPs, and Ag as AgNO₃, respectively, showing a $34.3 \pm 4.6\%$, $87.3 \pm 1.3\%$, and $41 \pm 2.3\%$ reduction in total Ag measured compared to the 1 h time point. These results suggest that the AgNPs were adsorbing faster to biomass than Ag as AgNO₃, especially GA AgNPs, and dissolved Ag was basically eliminated after 1 h. It is like that dissolved Ag became AgCl species because the Cl⁻ concentration was approximately 150 mM.

The same trends were observed for the second and third 0.2 ppm pulse spikes; GA AgNPs had the greatest reduction in total Ag concentration, while citrate AgNPs and Ag as AgNO₃ levels were higher. Within 24 h after the second spike, total Ag concentrations had reduced by $28.4 \pm 9.5\%$, $77.4 \pm 0.4\%$, and $24.2 \pm 2.6\%$ for Citrate AgNPs, GA AgNPs, and Ag as AgNO₃, respectively. Levels in the Citrate AgNPs and ionic Ag control were statistically indistinguishable ($p > 0.05$). The average total concentrations over 30 d during the continuous addition were 9.28 ± 10.9 , 6.94 ± 4.2 , and 9.37 ± 12.9 ppb for Citrate AgNPs, GA AgNPs, and Ag as AgNO₃, respectively. Dissolved Ag concentration was undetectable. Similarly to that observed during the pulse addition experiments, GA AgNPs had the lowest total Ag concentration in the SBRs compared to the other treatments. Effluent total and dissolved Ag was also measured periodically to determine how much Ag was flowing out of the reactors. The effluent total Ag concentration was very low and averaged 0.24 ± 0.17 ppb Ag across all treatments. Ag levels were not statistically different from the no Ag control. Effluent dissolved Ag concentrations were undetectable by ICP-MS.

Overall, total Ag concentration decreased most rapidly in SBRs receiving GA AgNPs in their influent. This result is surprising since GA AgNPs are typically known to be very stable due to their steric and electrostatic stabilized coating which keeps them well dispersed [177, 178]. In previous experiments, we found that GA and citrate AgNPs had similar zeta potentials, suggesting that their dispersion should have been similar [18]. However, it is possible that the properties of the GA coating caused adsorption to sludge

biomass in the wastewater matrix. The hydrophobic and hydrophilic properties of the polymer coating may have bound to biomass more readily [54]. Since effluent total Ag concentrations were so low, it is likely that Ag and AgNPs persisted in the sludge biomass but became less bioavailable as they bound with wastewater ligands. Similarly, Hou et al. [179] found that 90% of citrate AgNPs stayed in SBRs and subsequent treatment cycles would thus be exposed to those AgNPs until sludge wasting occurred. Kiser et al. [180] also found that AgNPs were removed not only by aggregation and sedimentation, but also by biosorption onto heterotrophic sludge biomass. Since dissolved Ag concentrations were minimal in the SBRs, it is unlikely that any free Ag^+ was present in the SBRs. Rather, the Ag as AgNO_3 or Ag^+ released from AgNPs may have been combined with the abundance of chloride or sulfide groups normally present in sludge biomass [181].

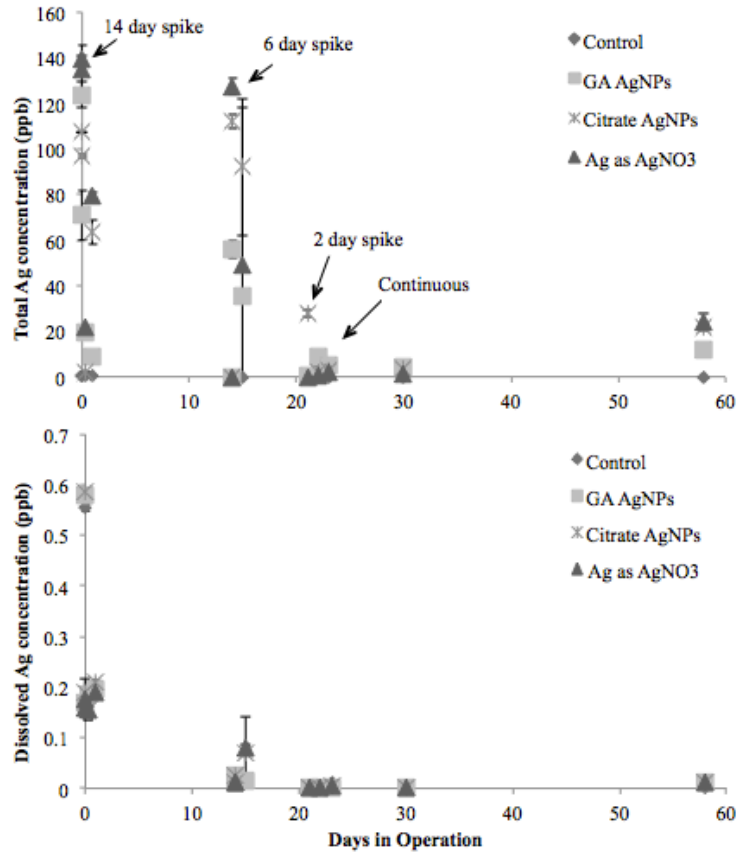


Figure 17: Total and dissolved concentration of Ag measured from AgNP, Ag as AgNO₃ and control SBRs. Error bars represent the standard deviation of duplicate samples.

Reactor Treatment Efficiency. The presence of AgNPs and Ag as AgNO₃ in wastewater SBRs was found to significantly impact heterotrophic and autotrophic activity in the SBRs ($p < 0.05$). The removal efficiencies of COD and ammonia decreased immediately after pulse additions, but stabilized with 3-5 d. This may be linked to the total Ag concentration that decreased in all treatments by at least 40% in 24 h after the first pulse addition. If biosorption was occurring and AgNPs were attaching to extracellular

polymeric substances (EPS) found in sludge biomass, it is likely that their biocidal potential was reduced.

COD removal was moderately affected by AgNPs, especially following the first pulse addition. Removal percentages dropped from 99% to 71, 80, and 90% for citrate AgNPs, GA AgNPs, and Ag as AgNO₃, respectively, at the end of the first treatment cycle following the pulse addition. However, after 3 d, the COD removal recovered and efficiencies were 92, 95, and 92% for citrate AgNPs, GA AgNPs, and Ag as AgNO₃, respectively, which were not statistically different from the control ($p > 0.05$). The same trend was seen for the second and third 0.2 ppm pulse additions, with treatment efficiencies of 77, 81, and 79% following the third 0.2 ppm pulse addition. Overall, Ag from AgNO₃ did not affect COD removal significantly more than citrate or GA AgNPs. This trend may be due to a handful of reasons. Ag from AgNO₃ may have bound quickly with chlorides and sulfides, reducing toxicity to heterotrophic bacteria that are mainly responsible for COD removal [182, 183]. It is also possible that the heterotrophic bacterial community was slowly adapting to the Ag addition, similar to antibiotic resistance [3]. The continuous spike of 0.2 ppm Ag and AgNPs did cause a slight drop in treatment efficiency after the first cycle from 96% to 77, 81, and 79% for citrate AgNPs, GA AgNPs, and Ag as AgNO₃, respectively, but the reactors were able to recover and remove COD by 90% or more after 3 d. This improvement in recovery may have been linked to a more drastic shift in microbial community structure in response to the constant

flow of AgNPs. Please refer to the “*Effects of AgNPs on Microbial Community*” section for a more detailed discussion on community dynamics.

Ammonia removal was more strongly affected by Ag as AgNO₃ than AgNPs. In general, ammonia removal efficiencies dropped immediately after the pulse additions but were able to recover similarly to COD removal. After the first pulse addition, ammonia removal changed from 98% down to 97, 83, and 32% for citrate AgNPs, GA AgNPs, and Ag as AgNO₃, respectively, at the end of the first cycle. These results showed that Ag as AgNO₃ caused a statistically greater drop in ammonia removal than AgNPs ($p < 0.05$). Noticeably, Ag as AgNO₃ significantly disrupted nitrification, which is commonly carried out by sensitive wastewater autotrophic bacteria. This effect is congruent with our previous study that also found Ag as AgNO₃ to be lethal to *Nitrosomonas europaea*, a model wastewater bacterium, at 0.2 ppm [18]. Treatment recovery of the Ag as AgNO₃ spiked reactor took longer than the AgNP treated reactors, but after 8 d, all reactors were removing in excess of 88% of the influent ammonia. The second and third pulse additions had virtually no effect on ammonia removal, indicating that the SBRs may have had enough functional redundancy in their microbial communities to adapt and survive large spikes in AgNPs. The continuous spike of 0.2 ppm Ag did not appear to significantly affect ammonia removal, with the exception of the Ag as AgNO₃ treatment that lowered removal to 64% on day 55, but overall, the reactors were able to recover. Overall, these results were surprising since nitrifying autotrophic bacteria are much slower growers than heterotrophic bacteria, and are usually disrupted first and slow to recover [184, 185]. Our

results indicate that our sludge seed may have had some inherent Ag resistance that allowed it to nitrify consistently after the first spike.

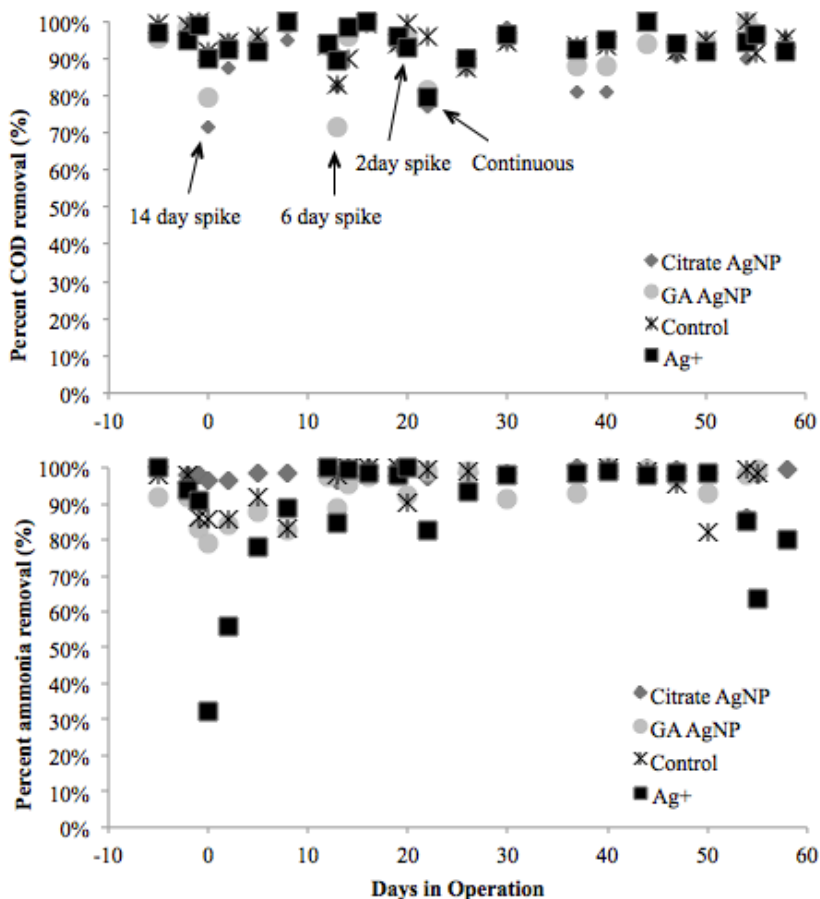


Figure 18: COD and ammonia removal percentages in SBRs during pulse and continuous inputs.

Nitrate and nitrite concentrations were more variable than COD and ammonia removal trends during SBR treatment. An increase in nitrate was observed in the presence of Ag⁺ and citrate AgNPs, which was attributed to the addition of nitrate from the Ag stock suspensions (approximately 6 ppm or 1mM contribution). This spike was not observed in

GA AgNP treated SBRs. Nitrite concentrations were relatively steady throughout Ag dosing, with some slight increases in the Ag^+ treatment during the second pulse addition and the beginning of the continuous spike. Since there was no surge in ammonia concentration during these time points, we speculate that this unusual effect was caused by a temporary shift in nitrite-oxidizing bacteria (NOB) metabolism causing ineffective nitrite removal.

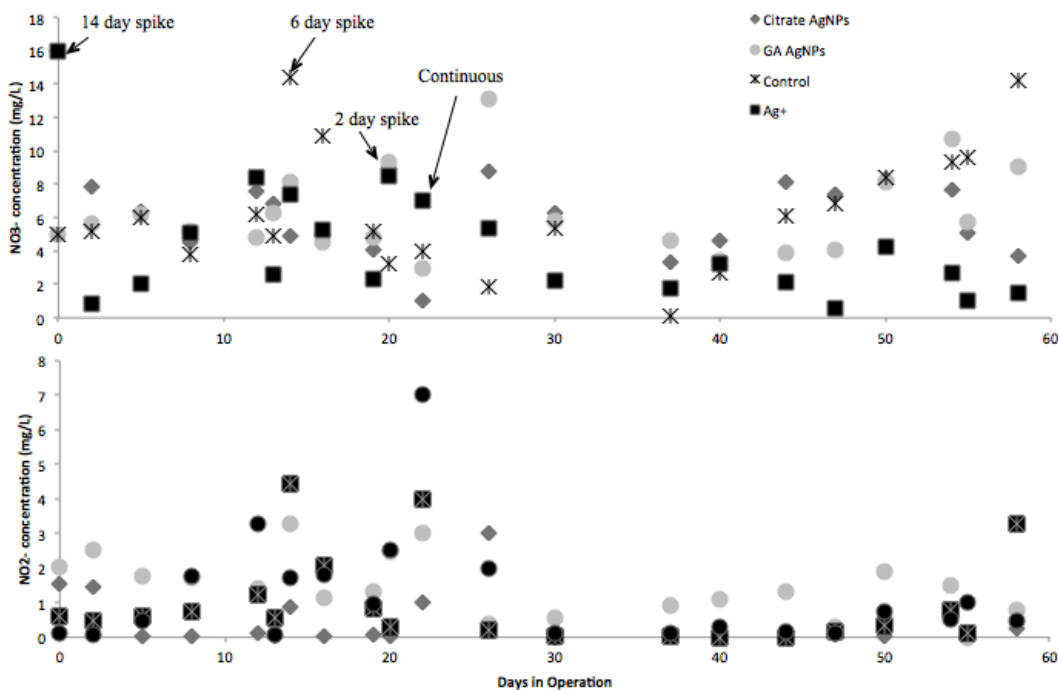


Figure 19: Nitrite and nitrate concentrations in SBRs during 0.2 ppm pulse and continuous Ag spikes.

Effects of AgNPs on Microbial Community Structure. T-RFLP was performed on DNA samples from the SBRs and analyzed for diversity and abundance. Microbial communities prior to the Ag spike were compared to communities at the end of each Ag

spike were compared to determine how the microbial community shifted in the SBRs. Table 3 shows a labeling guide for the T-RFLP principle coordinates diagram and clustering.

Table 3: Label guide for SBR T-RFLP sample

C	No Ag
CA	Citrate AgNP
GA	GA AgNP
AG	Ag ⁺ as AgNO ₃
Day 0	No Ag
Day 14	End of 14 d 0.2 ppm spike
Day 20	End of 6 d 0.2 ppm spike
Day 22	End of 2 d 0.2 ppm spike
Day 32	10 d after starting 0.2 ppm continuous spike
Day 56	34 d after starting 0.2ppm continuous spike

The first profiles assessed were the universal 16S SSU rDNA T-RFLP chromatograms, which provide a preliminary representation of bacterial clustering (Figure 20). The SBR communities before Ag spiking clearly clustered with each other but as Ag additions became more frequent, the Ag treated communities became less similar from the control communities. The first noticeable trend in clustering was the grouping of C14, CA14, and GA14 and distancing of AG14. Because the ionic Ag had the highest effect on ammonia removal following the first 0.2 ppm pulse addition, it is possible that several AOB or AOA in the population were eliminated, in addition to heterotrophic bacteria that are responsible for COD removal. After the second and third 0.2 ppm pulse additions (d 20 and 22) the GA and CA communities shifted more towards the AG14 community.

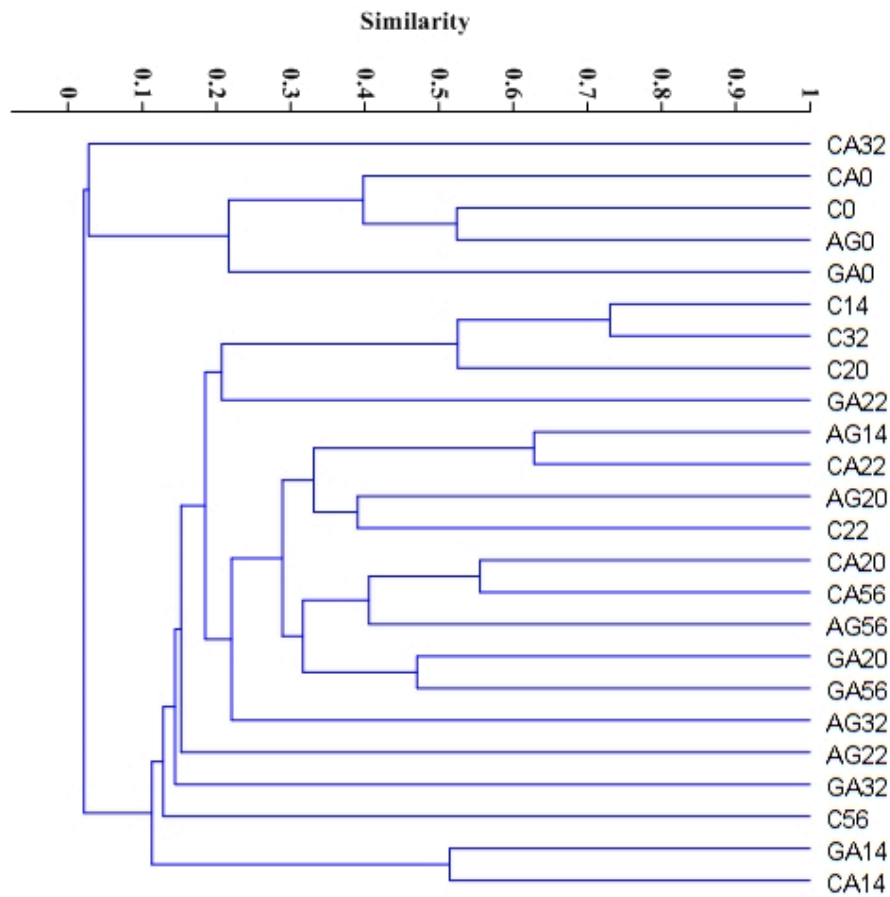


Figure 20: Bray-Curtis similarity indices of Ag treated SBRs

As the continuous 0.2 ppm Ag spike proceeded, the Ag treated communities clustered strongly while the control communities seemed more variable but still remained unclustered from the Ag samples. This could be due to the diversity of the controls, which was relatively higher than other groups for some time points such as day 32. Table 4 displays Simpson 1-D diversity indices. Overall, the Ag additions lowered diversity in all treatments during the first 22 d of Ag addition (pulses only). One interesting trend

observed in the diversity indices was the increase in diversity in the Ag⁺ treated SBR. One explanation for this increase could be the development of chromosomal Ag resistance genes as the selective pressure stayed constant during the 0.2 ppm continuous spike [186]. The citrate and GA AgNP treated SBRs never reached the same diversity it had before Ag addition, but they did appear to improve in diversity by the last day of continuous Ag feeding.

Table 4: Diversity indices of Ag treated SBRs

Sample ID	Simpson 1-D	Sample ID	Simpson 1-D
CA0	0.954	CA22	0.865
GA0	0.925	GA22	0.657
C0	0.934	C22	0.652
AG0	0.931	AG22	0.573
CA14	0.708	CA32	0.372
GA14	0.252	GA32	0.341
C14	0.597	C32	0.701
AG14	0.846	AG32	0.666
CA20	0.721	CA56	0.889
GA20	0.585	GA56	0.899
C20	0.816	C56	0.936
AG20	0.411	AG56	0.917

Implications of AgNPs on Wastewater Treatment Performance. Our results indicate that the AgNPs may disrupt COD and ammonia removal initially, but eventually microbial adaptation and Ag adsorption to biomass will reduced the overall impacts. While there may be brief upsets in treatment at 0.2 ppm Ag, it is likely that wastewater microbial communities have enough functional redundancy to recover quickly. Our results indicate that adsorption to microbial biomass and low dissolved Ag were important factors that

dictated AgNP interaction with microbial communities in sludge. In general, the microbial community diversities decreased with Ag spikes, but it is likely that starting communities had some inherent Ag resistance from exposure in the WWTP, and thus were able to survive Ag addition. It is likely that any Ag⁺ released from AgNPs will be bound by anions like sulfide and chloride, which are commonly present in wastewater. The microbial community analysis and treatment efficiency of the SBRs in this study indicate that COD removal may be more likely to face continuous upsets with AgNP addition. The microbes responsible for ammonia removal may not be as sensitive as previous studies have described [187]. Nitrification disruption is most likely a function of the starting community and the heavy metal resistance it has developed, so the effects of AgNPs on treatment efficiency could vary from case to case. Despite this, our results clearly indicate that wastewater microbial communities are able to recover from Ag and AgNP additions but their dynamics may shift. The results shown in this study suggest that wastewater treatment could be negatively impacted by Ag and AgNPs in the short term but the degree of treatment disruption will depend on the quantity of AgNPs and function of the microbial community. Further research is needed to test more types of AgNPs in different wastewater microbial communities.

6 Soil Bacterial Community Dynamics in Terrestrial Mesocosms treated with Biosolids Containing Ag Nanoparticles

6.1 Introduction

Ag nanoparticles (AgNPs) are progressively being added to consumer products to enhance their antimicrobial properties [28]. Their integration into fabrics, cosmetics, and a wide variety of items has caused a number of concerns about their long term impacts as the AgNP containing consumer product wash into wastewater treatment [36]. The EPA has examined biosolids from various wastewater treatment plants for Ag concentration, and measured values ranging from 1.94 to 856 mg/kg [35]. The ceiling concentration for Ag in sludge/biosolids has not been established; currently, only As, Cd, Cu, Pb, Hg, Mo, Ni, Se, and Zn are regulated in title 40, part 503 of federal regulation [36]. Recent research determined that AgNP treated socks were releasing anywhere from 0.3–377 μg Ag/g of cloth during washing [29]. Consequently, studies have begun to try to quantify the toxicity of AgNPs to model heterotrophic bacteria, wastewater organisms, and a host of ecologically relevant organisms [18, 112, 188]. The presence of AgNPs in sludge biosolids, the dewatered waste product from wastewater treatment plants, is also a concern since the solids contain many of the precipitated heavy metals found in wastewater [189]. Because the solids can be dried and land applied as fertilizer for plants, it is possible that Ag-spiked biosolids could alter the natural microbial communities found in soil and interrupt ecologically important functions. The unpredictability of how AgNPs will interact in different environments complicates risk assessment of AgNP usage.

The properties of the matrix in which the AgNPs are located are important for predicting AgNP dissolution, speciation and complexation. In particular, the pH, ionic strength, and natural organic matter, in addition to the AgNP coating dissolution rate, all play a role in controlling which forms of Ag are present [7, 105]. In another study performed by Fabrega et al. [106], high humic acid and pH levels showed an increase in aggregation, a decrease in dissolution of the coating, and a decrease in antimicrobial efficacy.

Recently, wastewater has been identified as a sink for Ag sulfide nanoparticles due to its high concentration of sulfide containing compounds [13, 108]. It is also possible for AgNPs to dissolve and release ionic Ag in the form of AgCl, a rather nonreactive form of Ag that is less of a threat to microbes [190]. Nevertheless, it is important to characterize the impacts of AgNPs in biosolids and their effects on the microbial ecology in which they are deposited. Previous studies have shown that the addition of heavy metals such as copper can lower enzymatic activity and biodiversity of soil bacteria, which could have negative implications on the environment [191, 192]. Lack of further research on the effects of AgNPs in soil bacterial communities confirms the research gap present in understanding the impacts of AgNPs in the environment and more specifically, land applied biosolids. In this study, terrestrial mesocosms were applied with AgNP biosolids slurries and bacterial community dynamics were monitored over 50 d. Diversity and phylogeny were examined to assess the impacts of AgNPs on bacterial structure.

6.2 Materials and Methods

Mesocosm setup. Terrestrial mesocosms were prepared in the Duke Forest by putting 21.5 gallon polyethylene tubs (Rubbermaid, Wooster, USA) equipped with drains at 10 cm and at the bottom. The total height of the boxes was approximately 42 cm tall. Boxes were filled with soil from the Sandy Creek Restoration in Durham, NC [193]. Soils were either Cartecay series (Coarse-loamy, mixed, semi-active, nonacid, thermic Aquic Udifluvents) or Chewacala series (Fine-loamy, mixed, active, thermic Fluvaquentic Dystrudepts) and had 63.5% sand, 10.5% silt, 26.2% clay, and 1.8% organic matter. Mesocosms plants were added in random placement to 16 slots in each tub. Plants species contained plants native to NC wet meadows (*Carex lurida*, sedge; *Juncus effusus*, rush; *Lobelia cardinalis*, forb; and *Panicum virgatum*, grass; purchased from Mellow Marsh Farm, Silk Hope, USA), as well as the non-native invasive C4 grass, *Microstegium vimineum*. Plants were watered and maintained until they were fully grown. Excess weeds were removed before experimentation.

Biosolids application. To test the impacts of land-applied biosolids containing AgNPs, biosolids were collected from a local wastewater treatment plant and then mixed with AgNPs or Ag as AgNO₃. The biosolids used in these experiments were rated Class A EQ, and were obtained from the South Cary Water Reclamation Facility (Apex, USA) as dried pellets. To create the biosolids slurry containing AgNPs, 200 g of dried pellets were first mixed with 750 mL of water and homogenized with an immersion blender (KitchenAid, St. Joseph, USA). Polyvinylpyrrolidone (PVP) AgNPs purchased from

Nanoamorphous Materials (Los Alamos, USA) were mixed with biosolids to simulate AgNP-contaminated biosolids. PVP AgNP powder was suspended in deionized water by sonicating them for 10 min at 100 W with a Sonicator 4000 equipped with a ½ inch diameter flat titanium tip (Misonix, QSonica LLC, Newton, USA). Particles in suspension had diameters of 21±17 nm as measured by TEM. Detailed particle characterization can be found in a previous publication [127] and in Chapter 3 of this dissertation. Ag as AgNO₃ (Sigma Aldrich, St. Louis, USA) was used as the positive control. Ag doses were based on realistic concentrations of Ag measured in the EPA's Targeted National Sewage Sludge Survey (TNSSS). In total, AgNP treated boxes received 11.5 ppm Ag/L biosolids slurry. Experimentation was started at the end of August 2009 and lasted until October 2009. There were four treatments in total, with 6 replicates each: controls, which received only 1500 mL DI water; slurry only, which received only 200 g biosolids slurry; slurry and AgNPs, which received 200 g biosolids and 9.9 mg AgNPs; and slurry and AgNO₃, which received 200 g biosolids and 44 mg Ag as AgNO₃. The biosolids in the slurry treatment samples were homogenized then promptly added to the soil surface of the mesocosms, below the plant growth.

DNA extraction and PCR Conditions. Soil samples were collected from the mesocosm the day before the Ag spike, the day after the Ag spike, and 50 d after the Ag spike. Approximately 10 g of soil from each mesocosm were removed using 10 cm corers and immediately stored at -80°C prior to DNA extraction. For each sampling point and treatment, total DNA was extracted from four 0.25 g replicates using the PowerSoil®

DNA Isolation Kit (MoBio Laboratories, Solana Beach, CA). All DNA extractions were performed following the manufacturer's protocol with slight modification. The manufacturer's bead beating step was extended to 15 min. Following extraction, DNA was stored in elution buffer at -20°C until further use. DNA purity and concentration was verified using an ND-1000 NanoDrop spectrophotometer (NanoDrop Technologies, Wilmington, DE). DNA concentrations ranged from 5 to 20 ng/μL and purity was verified to ensure no phenolic or protein contamination. PCR amplification of bacterial 16S SSU rDNA gene fragments was performed following the protocol described in Lukow et al. [172] with slight modification. The forward primer (27F) was fluorescently labeled with 6 – carboxyfluorescein. One μL of template DNA was utilized for each amplification in a 100 μL reaction. Bovine serum albumin (10 μg) was added to limit primer dimer formation and humic acid interference. The number of cycles was extended to 40 to ensure total amplification. The presence of PCR amplicons of the correct length was verified by visualization on a 1% agarose gel containing 0.1% ethidium bromide. PCR amplicons were purified using a Qiagen PCR Purification Kit (Qiagen, Hilden, Germany) following the manufacturer's protocol. Samples were eluted to a final volume of 50 μL in elution buffer. Final PCR product concentrations and purity was verified as described above.

T-RFLP Analysis. Restriction enzyme digests were obtained as described in Lukow et al. [172]. One hundred ng of purified PCR product and 10 U of *HaeII* and *MspI* (New England Bio-labs Inc., Beverly, MA, USA) were utilized for each reaction. The mixture

was incubated at 37°C for 2 h, followed by 15 min heating at 65°C for enzymatic inactivation. All samples were desalted by spin column filtration and fragment analysis was carried out using an Applied Biosystems 3100 capillary sequencer (Foster City, CA) with POP6 polymer and ROX-labeled MapMarker 1000 size standards (BioVentures, Inc., Murfreesboro, TN). All analyses were carried out at the Duke University DNA Analysis Facility (Durham, NC) following standard procedures. PCR amplicons were digested again with single restriction enzymes for use in taxonomic fragment matching. *MspI*, *HhaI*, and *AluI* (New England Bio-labs Inc., Beverly, MA, USA) were utilized for amplicons digestion of samples required for taxonomic analysis.

T-RFLP profiles were visualized using Applied Biosystems GeneScan v3.7.1 software (Foster City, CA). Raw data were imported into T-REX [176] in the following format: Dye/Peak, Sample File Name, Size, Height, Area, Data Point. T-REX was used to first select true peaks in all profiles and then T-RFs were aligned. Data analysis was performed in T-REX using the presence/absence feature. All T-RFs smaller than 50 bp were excluded to ensure primer dimer fragments were not included in the analysis. A minimum peak height threshold of 50 relative fluorescent units was also utilized. Data files were then imported into PC-ORD [194] for ordination plot generation. Raw data, in the form of binary code (for presence/absence), were analyzed using the nonmetric multidimensional scaling (NMS) feature using Sorenson distance and was run on the medium auto-pilot function [173]. NMS Ordination plots were analyzed for group clustering. Analysis of similarity (ANOSIM) statistical analysis was performed using the

PAST statistical software to determine if ordination clusters were statistically similar (Hammer, Ø. & Harper, D.A.T. 2006. *Paleontological Data Analysis*. Blackwell.). The null hypothesis (H_0) assumes that there are no differences between community composition at given sampling dates [195]. The Global R value is used to test the null hypothesis. Specifically, the R-value indicates how closely related the groups are to each and to their own replicates. R-values indicating similarity were output from the program, as well as significance p-values. R-values range from -1 to 1 and compare the similarity of the replicates in a group to the similarity of the selected groups. An R-value between 0 and 1 indicates that the groups are more similar to their own replicates than each other. And R-value of -1 to 0 indicates the groups are more similar to each other than their own replicates.

Data files were also imported into PAST statistical software to create Bray-Curtis cluster similarity (Hammer & Harper, D.A.T. 2006. *Paleontological Data Analysis*. Blackwell). For Bray-Curtis analysis, a transformation exponent of $c=2$ was selected. Samples run with individual restriction enzymes were used in a phylogenetic sorting algorithm that matched the 16S rDNA gene fragment lengths to the phylogeny given National Center for Biotechnology Information (NCBI) sequence database. These data were processed by Dr. Chris Ellis at Duke University and the methods are outlined in Johnson et al. [196]. Briefly, the restriction enzymes used bind and cleave specific recognition nucleotide sequences in amplicons. Since all bacteria will have different sequences and thus, different fragment lengths, the species of each fragment peak can be predicted by

matching the fragment length with known sequences in the NCBI database. While the program does not always match 100%, our files were able to get 60% or more matches on most treatments. Text files given by program include phylum, order, class, family, and genus of each microbe (fragment) characterized in the sample. This study only looks at the phylum level of bacteria because it gives overall information about diversity and function of the bacteria found in the sample.

6.3 Results and Discussion

Ordination, Clustering and ANOSIM results. Ordination plots were first created for all treatments and days to determine overall trends in community composition. Figure 21 shows the clustering of the treatments 1 d before, 1 d after, and 50 d after the Ag/biosolids addition. Overall, distinct patterns were noticeable between days and treatments. On day 0, it appears that there was no significant clustering, and the community variation is high. After spiking the samples with biosolids and Ag (day 1), discrete clustering is present between samples that differentiate them from the control samples, which still have the community composition similar day 1. By day 50, the spiked samples still appear to be clustered away from the control, but are not statistically different from each other. R-values given from the ANOSIM test are shown in Table 5. The values used for calculation of the R statistic were averaged for each group (treatment or date).

Table 5: R statistic similarity values for terrestrial mesocosms

	<i>R value</i>	<i>p value</i>
global R (all days)	0.677	0.000
global R (all treatments)	0.084	0.004

	<i>Day 0 (Pre-treatment)</i>		<i>Day 1</i>		<i>Day 50</i>	
	<i>R value</i>	<i>p value</i>	<i>R value</i>	<i>p value</i>	<i>R value</i>	<i>p value</i>
global R	0.059	0.214	0.622	0.000	0.368	0.000
control vs. ionic silver	0.048	0.317	1.000	0.002	0.748	0.002
control vs. PVP AgNP	-0.124	0.849	1.000	0.002	0.664	0.002
control vs. biosolids slurry	0.232	0.053	1.000	0.002	0.756	0.002
PVP AgNP vs. ionic silver	-0.059	0.617	0.496	0.004	-0.032	0.596
PVP AgNP vs. biosolids slurry	0.187	0.071	0.344	0.012	0.011	0.041
ionic silver vs. biosolids slurry	-0.004	0.452	0.302	0.005	-0.176	0.995

Before treatment on day 0, no box was significantly dissimilar from any others and ordination plots appear scattered (Figure 21). Post-dosing on day 1, all treatments were significantly dissimilar from the control samples and from each other. R values between the treated boxes ranged from 0.30 to 0.5 with a ~98% confidence interval, which is of particular interest since this indicates that the Ag treatments did affect the microbial community structure. More notable is that the highest dissimilarity was between the nanoAg and ionic Ag samples, indicating microbial community differences unique to each type of Ag slurry. At the end of experimentation on day 50, all communities appear to be dispersed and dissimilar from control samples. However, no noticeable patterns are present among the treated boxes in ordination graphs and R-values suggesting that the initial differences between AgNP and ionic Ag become attenuated overtime. The treated samples are however, still significantly dissimilar from the control samples on day 50.

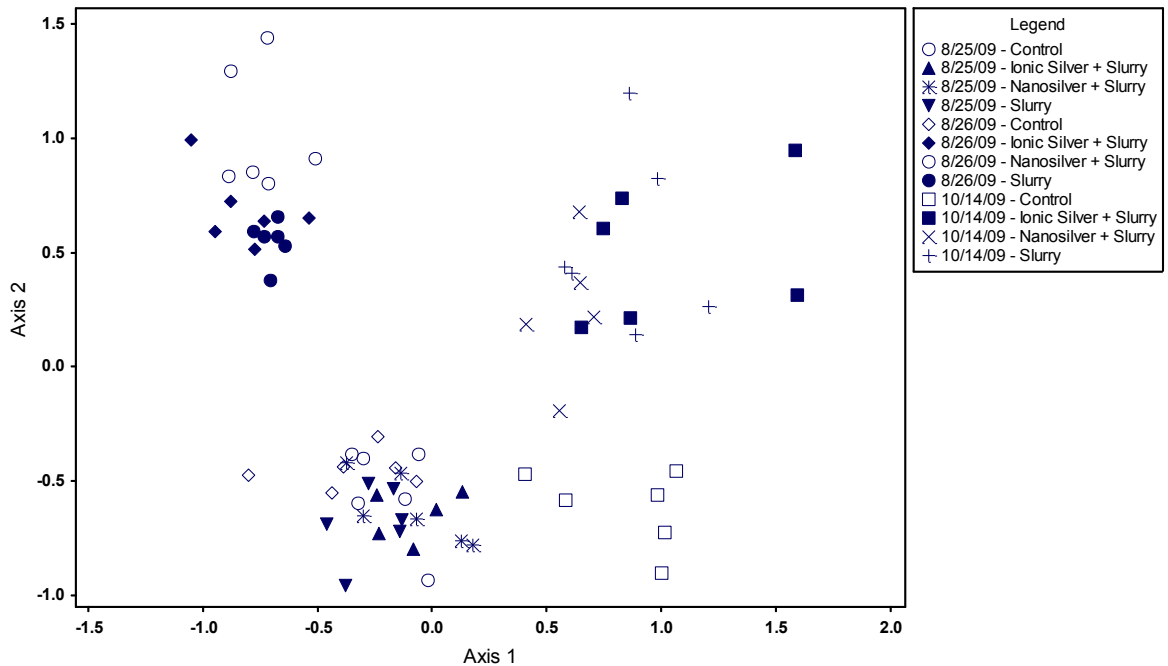


Figure 21: PC-ORD ordination diagram showing clustering of all communities and samples. Day 0 = 8/25/09, Day 1 = 8/26/09, and Day 50 = 10/14/09

Clustering results also showed the same trend as the ordination diagrams. All samples prior to Ag addition were clustered near each other, indicating they had a similar starting community. After the biosolids slurry and Ag addition, the AgNP and Ag as AgNO₃ treatments grouped, while the slurry and control boxes were less similar. After 50 d, all of the samples had re-clustered and their communities were interspersed. These trends confirm that the AgNP and Ag as AgNO₃ do affect the microbial community structure but over time, that distinction diminishes and the communities begin to cluster again. It also could suggest that as the AgNPs dissolve and

bind with components in soil (natural organic matter, metal ligands), their bioavailability decreases.

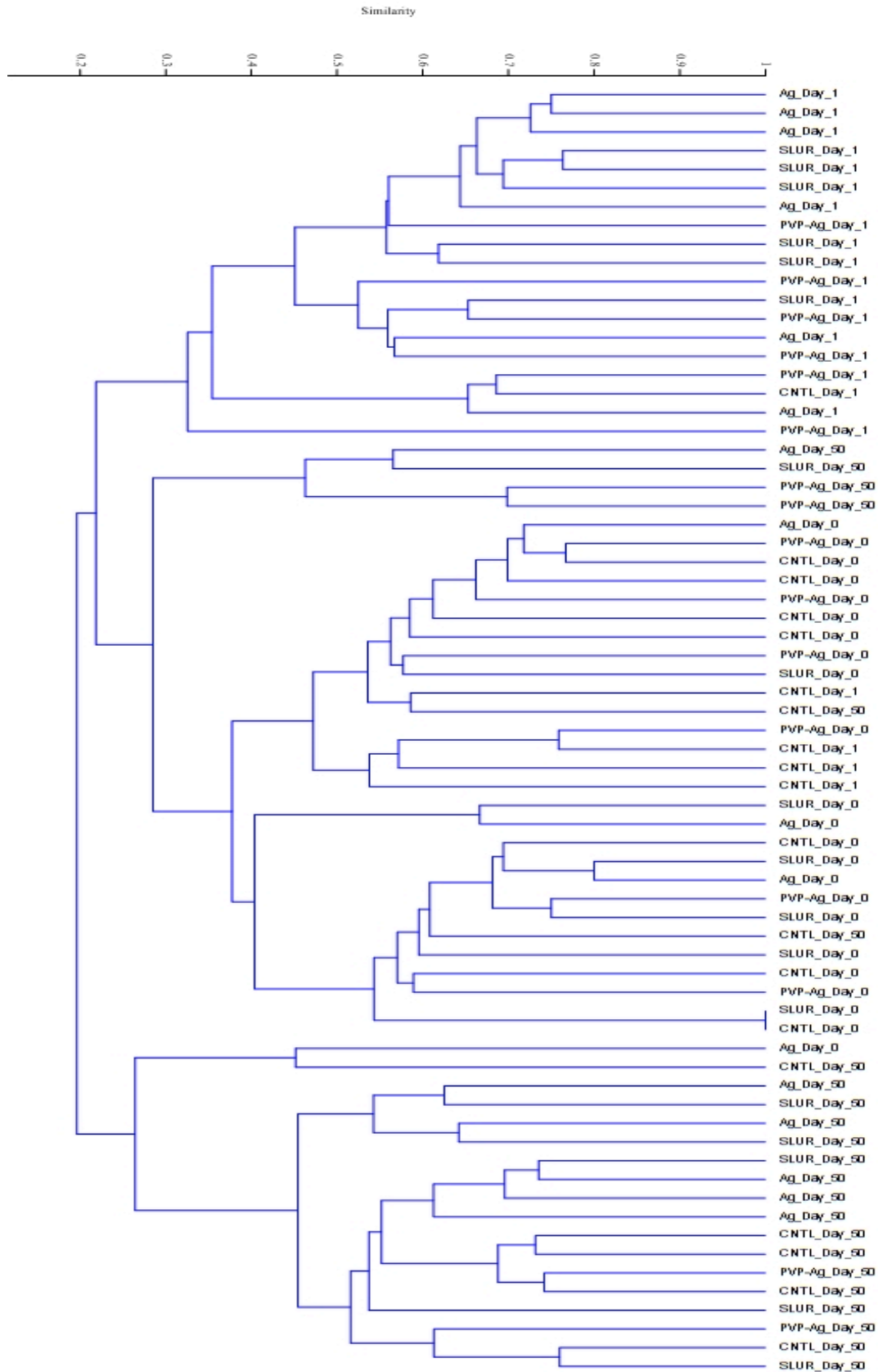


Figure 22: Cluster tree of Bray-Curtis similarity indices. “CNTL” = control boxes, “AG” = treated with Ag as AgNO₃ and biosolids slurry, “PVP” = treated with PVP AgNPs and biosolids slurry, “SLUR” = treated with only the biosolids slurry.

Taxonomic Analysis. Fragment matching of the 16S SSU rDNA gene was completed to identify taxonomic shifts in the bacterial community. In total, 26 phyla were identified in the 72 samples run: *Proteobacteria*, *Verrucomicrobia*, *Firmicutes*, *Planctomycetes*, *Tenericutes*, *Acidobacteria*, *Bacteroidetes*, *Chlorobi*, *Actinobacteria*, *Deinococcus-Thermus*, *Aquificae*, *Chloroflexi*, *Cyanobacteria*, *Gemmatimonadetes*, *Spirochaetes*, *Chrysiogenetes*, *Tenericutes*, *Bacillariophyta*, *Deinococcus*, *Fusobacteria*, *Deferribacteres*, *Synergistetes*, *Gemmatimonadetes*, *Nitrospirae*, *Thermotogae*, and *Lentisphaerae*. Figure 23 shows the percent of each phyla over the 3 time points and 4 treatments. In general, *Proteobacteria* was the most dominant phylum present in all cases, but especially before spiking in the biosolids slurry. Only 3 phyla were present in all the treatments and days: *Proteobacteria* (34.0 to 75.0%), *Firmicutes* (4.88 to 38.2%), and *Planctomycetes* (1.04 to 11.2%). The remaining phyla were in lower abundance for all samples, with the exception of *Verrucomicrobia*, which ranged from 0.0 to 25.1%. There was an apparent relationship between the biosolids slurry spike and the abundance of phyla in the sample. In the pre-slurry spike, the number of phyla ranged from 5 to 16. On day 1, the number of phyla expanded from 11 to 17 and on day 50 ranged from 8 to 17. The rapid increase in number of phyla on day 1 is likely due to the bacterial addition inherent in the biosolids slurry. All boxes with slurry additions were increased in *Firmicutes* and *Actinobacteria*. The PVP AgNP treated boxes saw a large increase in *Firmicutes* (38.2%) post treatment and a decrease in *Proteobacteria* (73.1 to 40.4%). These data suggest that *Firmicutes* may be more impervious to Ag than *Proteobacteria*, or that community was able to thrive in the Ag and slurry mixture. Denitrifying bacteria,

which are important for nitrogen cycling in soil, may have been negatively impacted AgNPs since those generally fall under the *Proteobacteria* phylum. *Firmicutes* have been well identified in wastewater and some species possess the mercuric resistance genes produce a stress response in the presence of heavy metals, which could add to their resilience in these mesocosms [197, 198]. The slurry boxes did not drastically change from day 0 to day 1, and appeared to be partially dominated by *Actinobacteria*. Also notable, the three dominant phyla found in the slurry, *Actinobacteria*, *Proteobacteria*, and *Firmicutes*, also contain strains of bacteria with copper resistance genes, which have been proven to function similarly in the presence of Ag [3, 199]. By day 50, *Verrucomicrobia* had increased drastically in the Ag as AgNO₃ treated boxes, from to 3.0 to 25.1%. Although little is known about this phylum, studies have speculated that *Verrucomicrobia* has shown resilience with several different types of contaminants, including Hg, which induces similar stress responses to Ag in bacteria [200-202]. *Planctomycetes* also increased in the Ag as AgNO₃ treated boxes, from to 3.0 to 11.2%, which may have been caused by the box becoming anoxic [203]. *Bacteroidetes* increased in all treatments by the day 50 time point, indicating a natural shift in community, possibly due to temperature shifts from late summer to early Fall.

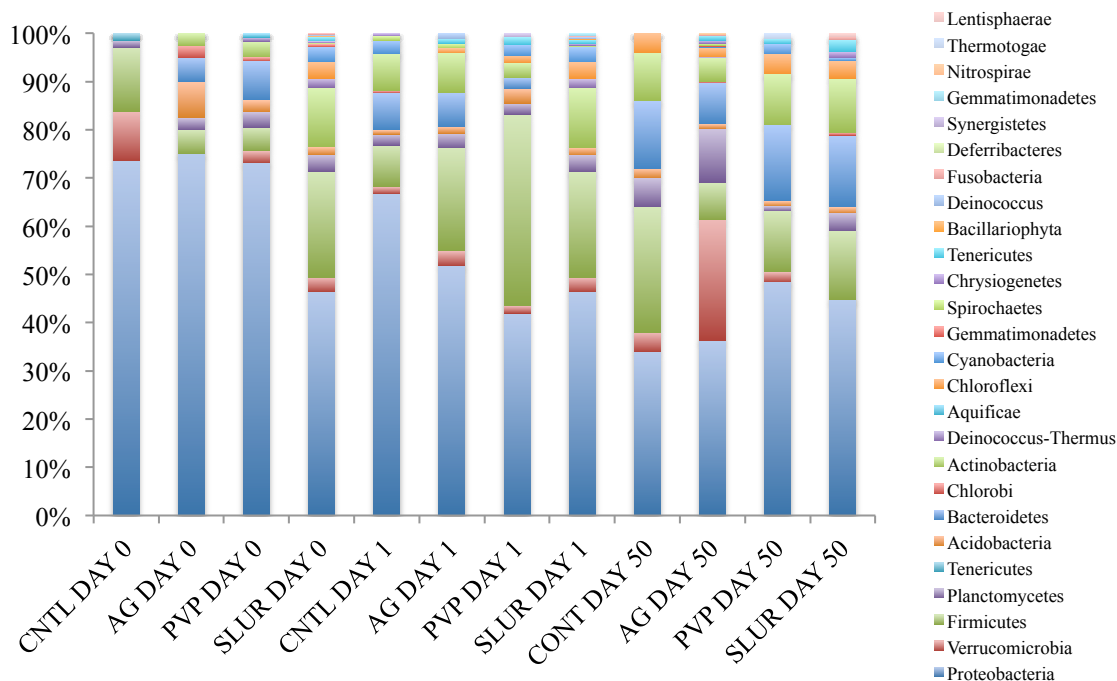


Figure 23: Phyla of bacteria found in terrestrial mesocosms, sorted by treatment and date. “CNTL” = control boxes, “AG” = treated with Ag as AgNO₃ and biosolids slurry, “PVP” = treated with PVP AgNPs and biosolids slurry, “SLUR” = treated with only the biosolids slurry.

Summary of Ag-spiked Biosolids in Land Applications. These results suggest that soil bacterial communities will be altered if Ag and AgNP spiked biosolids are land applied. It is possible that bacteria with metal resistance are most likely to initially persist in the presence of AgNPs. However, the microbial community will re-cluster after it has had time to adapt to environmental changes, which could be caused by Ag becoming less bioavailable. The final bacterial community profiles indicate that a new equilibrium is found after the communities have time to adjust to Ag input. From our data, *Proteobacteria* are likely to initially decrease and *Firmicutes* will become more dominant. While no overall decrease in diversity was observed, but rather an increase

likely due to the bacteria supplemented by the biosolids slurry, more in depth functional analyses should be performed to determine and compare short and long term ecological impacts of Ag and AgNP. It is also possible that repeat addition of biosolids containing AgNPs to soil and plants may encourage the spread of silver resistance genes and further alter microbial communities.

7 Conclusions and Engineering Significance

This dissertation was intended to provide a systematic examination of the effects AgNPs on bacteria relevant to wastewater treatment and their potentially harmful impacts to engineered wastewater treatment systems. Various types of AgNPs were shown to be toxic to model heterotrophic and autotrophic bacteria, but toxicity appeared to be a function of the coating dissolution rate and matrix properties such as ionic strength. Nitrification was found to be severely inhibited by AgNPs at concentrations of 2 ppm or higher, but the degree was dependent on the type of coating used to stabilize the AgNPs. Model heterotrophic organisms were all negatively affected by laboratory made and consumer product AgNPs, but the coating was also a major factor in determining mortality. Consumer product AgNPs proved to be even more toxic than laboratory AgNPs, possibly due to the high dissolved Ag concentration measured in consumer products. AgNPs also negatively impacted bench scale sequencing batch reactor performance, but Ag as AgNO₃ had a stronger effect on treatment efficiency. COD and ammonia removal were decreased with 0.2 ppm Ag and AgNP pulse and continuous spikes. Microbial community analysis of SBRs showed that AgNP addition lowered diversity and shifted those communities to cluster with each other. Lastly, it was shown that land applied biosolids containing AgNPs and Ag as AgNO₃ also caused communities shifts and clustering, indicating that Ag could be a selective pressure that could alter important microbial communities when AgNPs enter into the environment.

7.1 Key findings

Conclusion 1: Nitrification efficiency in *N. europaea* decreased with AgNP treatment and was a function of coating dissolution.

GA and citrate AgNPs inhibited nitrification most strongly ($67.9 \pm 3.6\%$ and $91.4 \pm 0.2\%$, respectively at 2 ppm). The data in this dissertation indicate that Ag^+ dissolution and colloid stability of AgNPs were the main factors in AgNP toxicity. CA AgNPs had a higher membrane loss at 2 ppm, and TEM imaging confirmed that most cells lost functionality through membrane loss. In general, low amounts of dissolved Ag initially cause a post-transcriptional interruption of membrane-bound nitrifying enzyme function, reducing nitrification by 10% or more. A further increase in dissolved Ag results in heavy metal stress response (e.g., *merA* up-regulation) and ultimately leads to membrane disruption. The highest effect on membrane disruption was observed for CA AgNPs ($64 \pm 11\%$ membranes compromised at 2 ppm), which had high colloidal stability.

Conclusion 2: Lab manufactured AgNPs and AgNP containing food supplements inhibit the growth of model heterotrophic bacteria. However, the toxicity is a function of the dissolved Ag concentration, and AgNP stability.

Consumer product (SS, SB, and MS) and laboratory made (GA and CA) AgNPs were found to slow the growth rates of *P. aeruginosa*, *B. subtilis*, and *E. coli*. In general, the consumer product containing AgNPs were more effective at inhibiting growth, and reduced the growth rate by up to 100% at 2 ppm. Our data suggest that AgNP toxicity to heterotrophic bacteria is linked to, but not exclusively, a function of dissolved Ag, which is in agreement with previous literature [14]. These results also highlight the importance

of AgNP coating on bacterial interactions and inhibition. Nevertheless, membrane integrity did not appear as dependent on dissolved Ag concentration, and may have been linked to the attachment efficiency of the AgNPs. Membrane loss results showed no statistical difference between consumer product AgNPs and laboratory made AgNPs. The highest AgNP membrane loss was $60.0 \pm 3.6\%$ in the 2 ppm MS treated sample. *P. aeruginosa* was more sensitive to AgNPs than *B. subtilis* and *E. coli*. Overall, it appears that the toxicity of AgNPs to heterotrophic bacteria is not primarily a function of the type of membrane, but rather the individual properties of the bacterium.

Conclusion 3: Bench scale SBR treatment efficiency and microbial community dynamics were altered by the addition of AgNPs, but the functional redundancy in wastewater allowed SBRs to recover from Ag additions.

COD and ammonia removal rates were disrupted immediately after the first spike of 0.2 ppm GA and CA AgNPs, but SBRs were able to recover from Ag spikes after 3 to 8 d. COD removal was affected more significantly than ammonia removal, possibly due to pre-existing Ag resistant nitrifiers present in SBRs. While there may be brief upsets in treatment at 0.2 ppm Ag, it is likely that wastewater microbial communities have enough functional redundancy to recover quickly. Ag measurements suggested that total Ag decreased most rapidly in the GA AgNP SBR. Dissolved Ag remained very low in all reactors and was not statistically different from the no-Ag control SBR ($p > 0.05$). Our results indicate that adsorption to microbial biomass and low dissolved Ag were important factors that dictated AgNP interaction with microbial communities in sludge. In general, the microbial community diversities decreased with Ag spikes, but it is likely

that starting communities had some inherent Ag resistance from exposure in the WWTP, and thus were able to survive Ag addition.

Conclusion 4: AgNPs in sludge biosolids could change the microbial communities found in sediments but natural microbial adaptation will return the community to a new equilibrium.

Bacterial communities in terrestrial mesocosms were altered by the spike of Ag or AgNP biosolids slurry. Diversity was increased by the addition of biosolids microbes and AgNP treated communities were statistically different from mesocosms treated with Ag as AgNO₃. However, after 50 d, the communities re-clustered into a new equilibrium and were no longer statistically different from each other. This result may have been due to Ag becoming less bioavailable as it bound with soil components like NOM or metal ligands. Our data indicate that Ag will cause a decrease in *Proteobacteria*, while *Firmicutes* will become more dominant. These results could lead to a decrease in important denitrifying bacteria, which are grouped under *Proteobacteria*.

7.2 Recommendations for AgNP usage limits and future work

Overall, this dissertation work shows that AgNPs could be very harmful to biological nutrient removal if concentrations are allowed to exceed 0.2 ppm, and regulation of Ag and AgNPs is needed. The results suggest AgNPs could have a significant impact on microbial communities in both wastewater and soil, but the functional redundancy of these complex systems and intrinsic heavy metal resistances should reestablish the

microbial communities to a new balance. Nevertheless, environmental standards for water and soil should be established to ensure that sensitive microbial systems are not disturbed so larger negative impacts, such as biological nutrient removal WWTP failure, are avoided. In general, we recommend that influent Ag and AgNP water concentrations stay below 200 ppb in wastewater treatment plants. This will ensure that nitrification and COD removal carry on effectively. Since the microbial resistance to heavy metals will be different in all wastewater communities, this Ag limit will ensure proper nitrification to even the more sensitive nitrifiers. We also recommend that biosolids be routinely measured for silver and that they also do not exceed 10 ppm, as tested in our terrestrial mesocosm experiments. This will ensure that microbial systems are not interrupted by AgNP or Ag addition. In addition to measuring Ag, WWTPs should report total Ag concentrations to help researchers identify if it has the potential to cause upsets on large scale WWTPs. As AgNPs continue to be produced with new coatings and properties, it is essential that AgNP characterization continues in order to assess how AgNPs will react with wastewater and effect essential microbial communities. Future studies should examine the prevalence of silver resistance in wastewater and determine if silver resistance genes are transferrable to other microbes as the community adapts.

Appendix A – Chapter 3 Supplemental Information

AgNP Synthesis. Citrate stabilized AgNPs were synthesized by reducing Ag nitrate in water with sodium citrate [126]. The starting concentrations were 1 mM Ag nitrate and 10 mM. Reaction caused a range of particles, from 1 to 50 nm in diameter and a concentration of 82.4 mg/L. Particle size was characterized by TEM (FEI Tecnai G² Twin, Hillsboro, Oregon). UV-VIS spectrum was acquired with a Varian Cary 300Bio Spectrophotometer (Cary, NC). Peak wavelength is at 406 nm. GA AgNPs were synthesized by mixing 304 mL of water, 60 mL of 10 g/L GA, and 30 mL of 0.1 M Ag nitrate. The solution was stirred for 10 min and then heated to boiling. Six mL of 1 M sodium citrate was added and the solution was further boiled for 10 min. The GA AgNPs were removed from heat, diluted 1:2 with water, and centrifuged for 1 h at 25,000 x g (Beckman Model J2-21, Miami, FL) three times before finally resuspending in water. The average particle size of these particles given by TEM imaging was 27 nm ± 6.5 nm. Polyvinylpyrrolidone (PVP) AgNPs were purchased from Nanostructured & Amorphous Materials, Inc. (Houston, TX) and are commercially available. The particles are described as 10 nm in size with 0.3 wt. % of PVP coating. They are spherical and have a cubic crystallographic structure. PVP AgNPs were weighed out and suspended in nanopure DI water. A probe sonicator was run at 100 A for 10 min to distribute the particles.

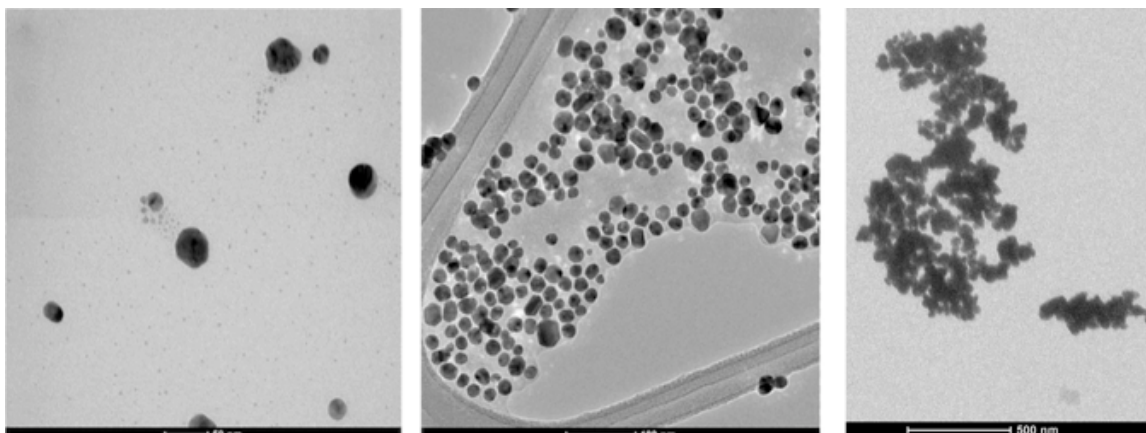


Figure A24: TEM imaging of AgNPs used. Right to left: Citrate coated, gum arabic coated, and PVP coated AgNPs. Please note the aggregation state of PVP particles. Individual particles can be seen but surface area was drastically reduced in these aggregates.

The hydrodynamic diameters of all the nanoparticles in the AOB growth medium was also measured using dynamic light scattering (DLS) with a 173° backscatter angle (Malvern Zetasizer, Worcestershire, United Kingdom). DLS estimated hydrodynamic diameters of approximately 25 and 68 nm for gum arabic and citrate coated AgNPs, respectively. PVP coated AgNPs showed two diameter peaks at 30 and 128 nm, indicating some aggregation after initial suspension.

AgNP coatings. For citrate and GA coating, the actual concentration of citrate and GA used to synthesize the AgNPs was tested as shown in Table A6.

Table A6: Ratio of Ag to nanoparticle coating and concentrations tested with *N. europaea*

	Amount of coating in AgNP	Concentrations tested
GA AgNPs	~ 1 Ag: 2 GA by weight	4 and 40 mg/L

Cit AgNPs	~ 1 Ag: 1 Citrate by weight	2 and 20 mg/L
PVP AgNPs	Unknown (estimated at less than 1% by weight)	1, 2, and 20 mg/L

LIVE/DEAD Microscopy. 0.2 mL of cells were harvested from each reactor and stained with the Live/Dead® BacLight™ reagents following the manufacturer’s protocol. After a 15 min incubation, 7 μL of cells were applied to glass slides and evaluated using a Zeiss Axio Imager wide-field fluorescence microscope (Carl Zeiss MicroImaging, Thornwood, NY). Stained cells were examined with fluorescence excitation wavelengths of 535 nm (green) and 642 nm (red). Six spots were chosen at random during microscopy from each slide and an image was taken for both the red and green excitations. Images were recorded using Metamorph Image software (Universal Imaging, Sunnyvale, CA). All membrane integrity tests were performed at the end of the 4 h exposure of *N. europaea* to AgNPs. In total, for each treatment, 18 “live” images were taken and 18 “dead” images were taken. Image J software (version 1.41, National Institute of Health, Bethesda, Maryland) was then used to count cells in each image and ratios of live/dead cells for each spot was calculated using the following equations:

$$\text{percent "live"} = \frac{\text{count of live cells}}{\text{count of live + dead cells (total)}} * 100\%$$

$$\text{percent "dead"} = \frac{\text{count of dead cells}}{\text{count of live + dead cells (total)}} * 100\%$$

Transmission Electron Microscopy (TEM). Cells of *N. europaea* from nitrite generation experiments were also harvested and pelletized for thin-section TEM imaging. Cell preparation and imaging was carried out at Duke's Shared Materials Instrumentation Facility (Durham, NC). Cells were fixed for 2 h at room temperature in a solution of 4% formaldehyde, 2% glutaraldehyde, phosphate buffered saline (PBS), and ultra pure water. Post fixation, cells were washed with PBS treated with 1% osmium tetroxide. Cells were washed with acetate buffer and stained with 0.5% uranyl acetate and then washed with acetate buffer again. Cells were dehydrated with ethanol washes, and embedded in epoxy resin. An ultra microtome cut thin sections of the resin sample and slices were inspected at 60 kV with a FEI Tecnai G² Twin TEM (Hillsboro, Oregon). Resulting images display the majority of characteristics found in samples; over ten images were taken for each sample after surveying a large amount of each TEM grid.

qRT-PCR. Cells were exposed to AgNP for 2 h before harvesting after examination of the nitrite inhibition data. At this time point, nitrification was significantly disrupted in several AgNP treatments. All treatments were performed in triplicates. Cells for RNA extraction were first centrifuged and washed with PBS buffer. Trizol (Invitrogen Co. Carlsbad, CA) was then used to stabilize, lyse cells, and separate RNA. RNA extraction was performed on the Trizol supernatant using the Qiagen RNeasy mini kit (Chatsworth, CA) following the manufacturer's instruction. Complementary DNA was synthesized within 24 h following RNA extraction using the iScript cDNA Synthesis kit

(Bio-Rad, Hercules, CA). Primer sequences for target genes in *N. europaea* are listed in Table A7.

Table A7: Primer sequences used for qRT-PCR.

<i>Gene</i>	<i>Forward primer</i>	<i>Reverse primer</i>	<i>Source</i>
16S	CAGCMGCCGCGGTAATWC	ATCTACGCATTTACCGCTAC	[204] and [205]
amoA	TGGCGACATACCTGTCACAT	ACAATGCATCTTTGGCTTC	[206]
hao	CAAACCTGCCGAAATGAACC	GCTGGTGATGTTCTCTGCAA	[206]
merA	GCTTTATCAAGCTGGTCATC	ACATCCTTGTTGAAGGTCTG	[206]

The annealing temperature for all primers was found to be optimal at 55°C, with the exception of the 16S rRNA primers, which were run at 51°C. Relative quantification was executed using the Stratagene Mx3000P qPCR system (La Jolla, CA) and iTaqTM SYBR₁ Green Supermix with ROX (Bio-Rad Laboratories, Hercules, CA). Conditions for qPCR were 95°C for 10 min, followed by 40 cycles at 95°C for 30 s, 1 min at respective annealing temperatures, 30 s at 72°C, and dissociation curve to assess quality of primers. All samples were run in duplicate wells and PCR efficiencies of 90% or greater were obtained.

Table A8: Dissolved Ag concentration after 4 h exposure period in AOB medium with *N. europaea*.

Target Concentration	Ag+ Concentration (ppb)
0.2 ppm GA AgNP	6.3 ± 3.4
0.2 ppm Cit AgNP	0.6 ± 0.8
0.2 ppm PVP AgNP	2.1 ± 0.9
2 ppm GA AgNP	16.1 ± 9.5
2 ppm Cit AgNP	63.5 ± 2.2
2 ppm PVP AgNP	21.6 ± 8.3
20 ppm GA AgNP	37.9 ± 1.3
20 ppm Cit AgNP	150.0 ± 3.2
20 ppm PVP AgNP	160.9 ± 10.3
0.2 ppm Ag+	45.4 ± 3.1

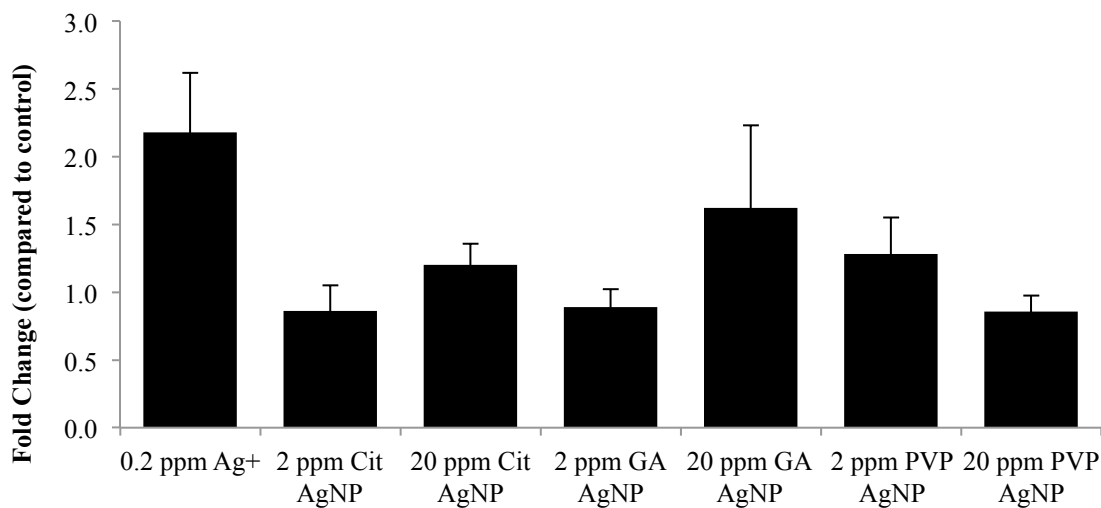


Figure A25: Gene expression of *amoA* relative to 16S rRNA reference gene. No treatments significantly changed with exposure to AgNPs. Error bars represent the standard deviation of triplicate samples.

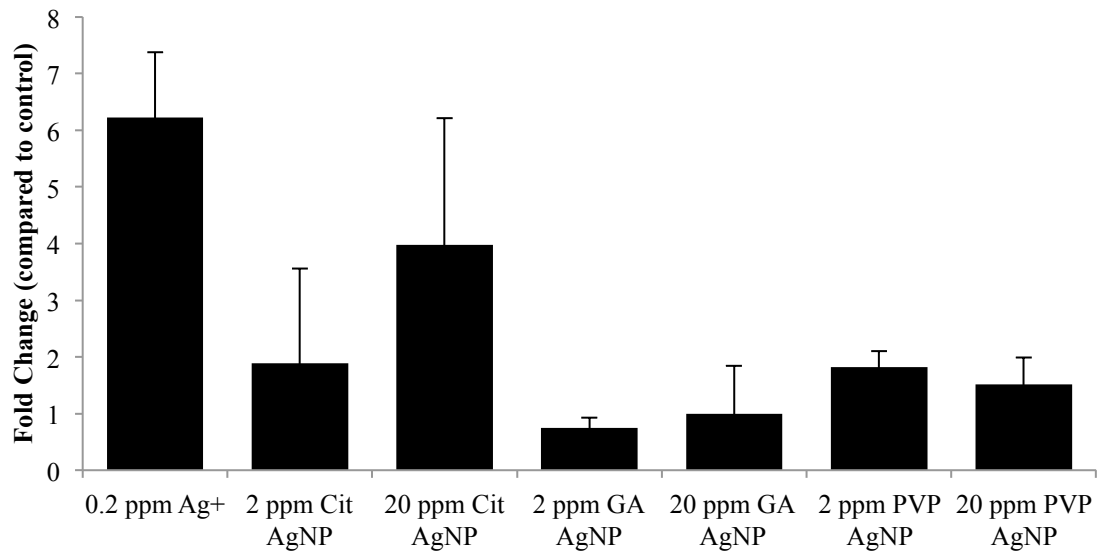


Figure A26: Gene expression of *hao* relative to 16S rRNA reference gene. The pure Ag⁺ as AgNO₃ treatment was significantly up-regulated. Error bars represent the standard deviation of triplicate samples.

Appendix B – Chapter 4 Supplemental Information

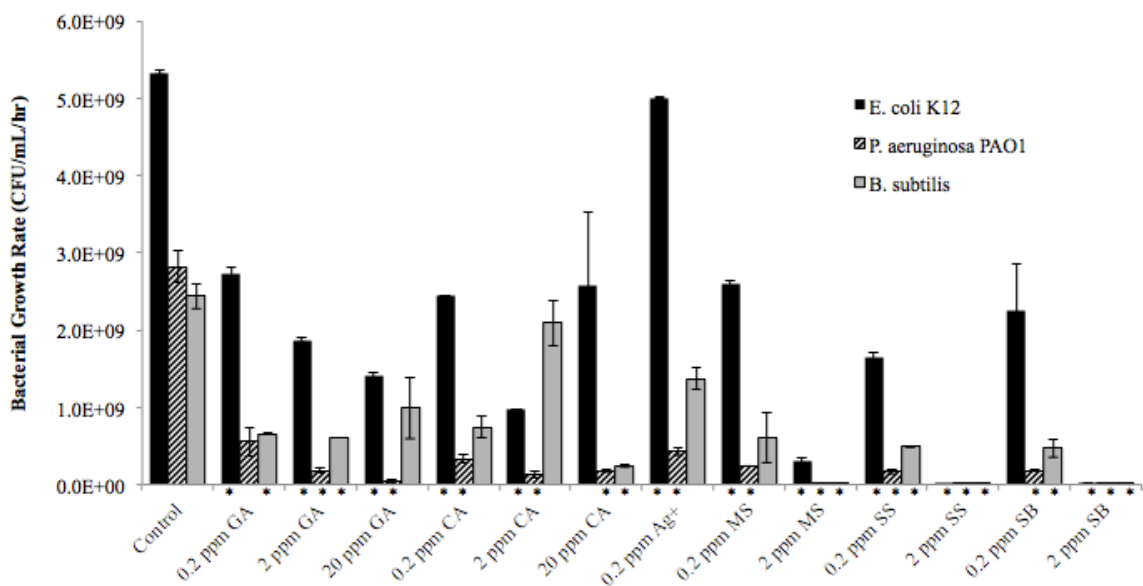


Figure B27: Growth rates of bacteria treated with AgNPs. Asterisks indicate statistical significance ($p < 0.05$) between no Ag samples and AgNP treatment samples. Error bars represent the standard deviation of triplicate samples.

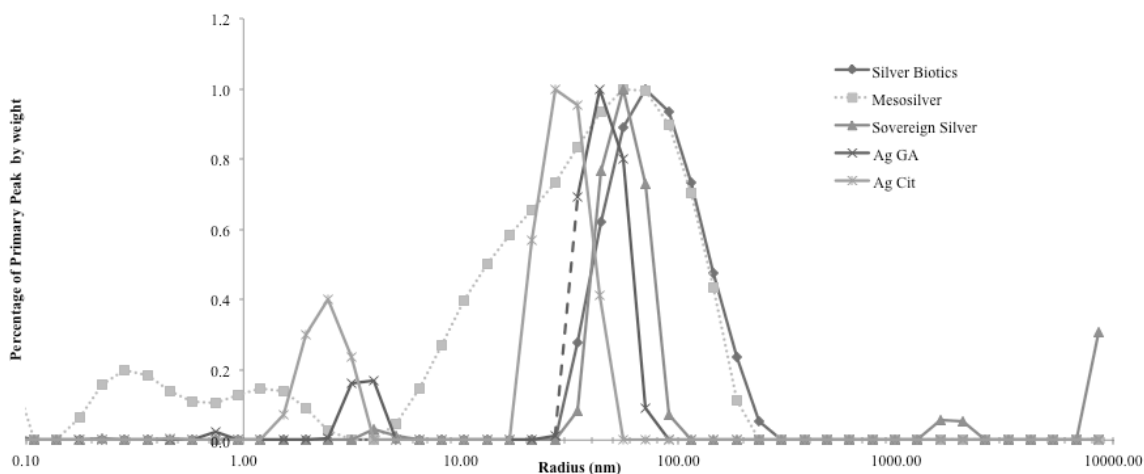


Figure B28: Primary peak weight percentage vs. particle radius (nm) of all AgNPs.

Appendix C – Chapter 6 Supplemental Information

Ordinations:

Three days compared:

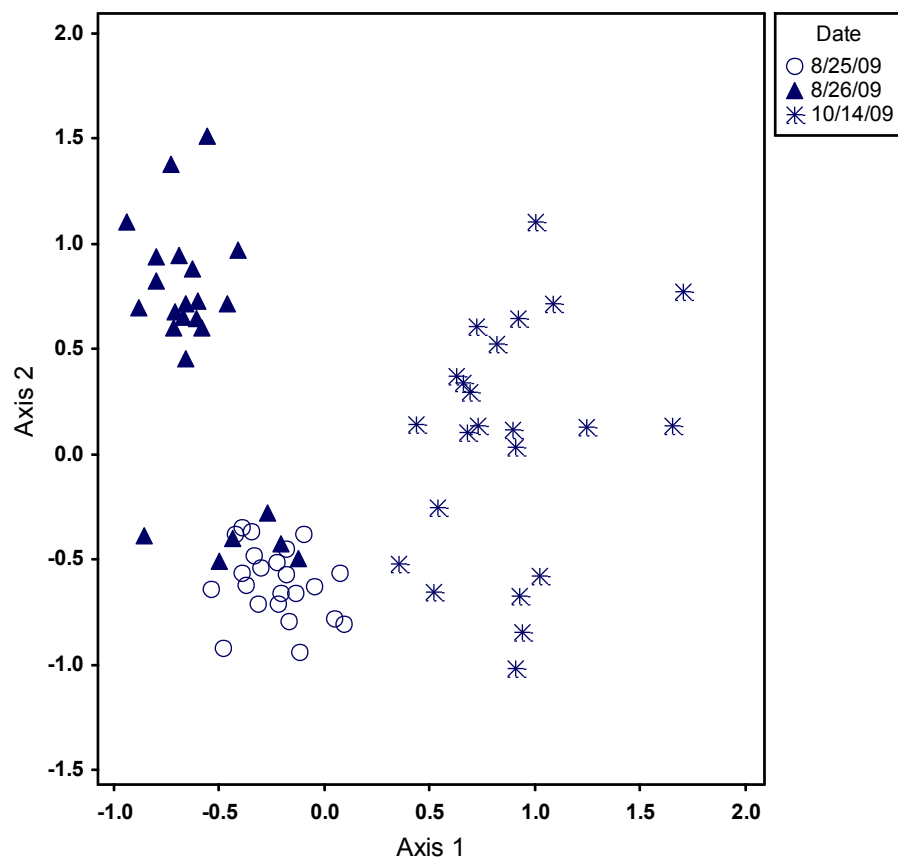


Figure B29: Ordination diagram of T-RFLP communities, sorted by day.

All treatments compared:

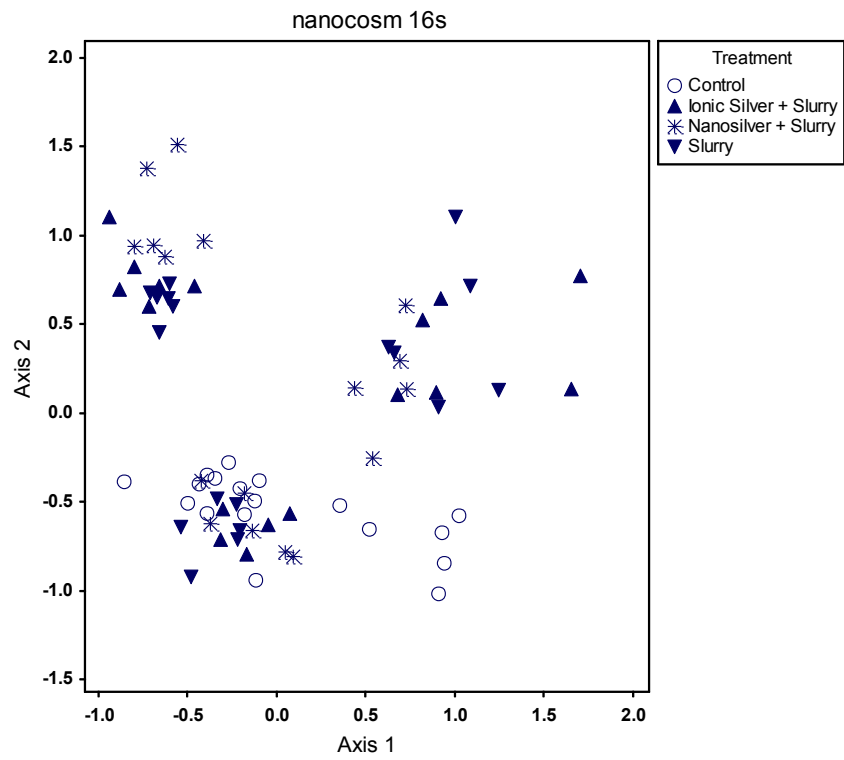


Figure B30: Ordination diagram of T-RFLP profile clusters, sorted by treatment

References

1. Wiesner, M. R.; Lowry, G. V.; Alvarez, P.; Dionysiou, D.; Biswas, P., Assessing the risks of manufactured nanomaterials. *Environmental Science & Technology* **2006**, *40*, (14), 4336-4345.
2. Choi, O.; Deng, K. K.; Kim, N. J.; Ross, L.; Surampalli, R. Y.; Hu, Z. Q., The inhibitory effects of silver nanoparticles, silver ions, and silver chloride colloids on microbial growth. *Water Res.* **2008**, *42*, (12), 3066-3074.
3. Silver, S., Bacterial silver resistance: molecular biology and uses and misuses of silver compounds. *FEMS Microbiology Reviews* **2003**, *27*, (2-3), 341-353.
4. Wang, S.; Gunsch, C. K., Effects of selected pharmaceutically active compounds on the ammonia oxidizing bacterium *Nitrosomonas europaea*. *Chemosphere In Press, Corrected Proof*.
5. Mullen, M. D.; Wolf, D. C.; Ferris, F. G.; Beveridge, T. J.; Flemming, C. A.; Bailey, G. W., Bacterial sorption of heavy metals. *Applied and Environmental Microbiology* **1989**, *55*, (12), 3143-3149.
6. Beveridge, T. J.; Fyfe, W. S., Metal fixation by bacterial cell walls. *Canadian Journal of Earth Sciences* **1985**, *22*, (12), 1893-1898.
7. Farre, M.; Gajda-Schranz, K.; Kantiani, L.; Barcelo, D., Ecotoxicity and analysis of nanomaterials in the aquatic environment. *Anal. Bioanal. Chem.* **2009**, *393*, (1), 81-95.
8. Sondi, I.; Salopek-Sondi, B., Silver nanoparticles as antimicrobial agent: a case study on *E. coli* as a model for Gram-negative bacteria. *Journal of Colloid and Interface Science* **2004**, *275*, (1), 177-182.
9. Kim, J. S.; Kuk, E.; Yu, K. N.; Kim, J.-H.; Park, S. J.; Lee, H. J.; Kim, S. H.; Park, Y. K.; Park, Y. H.; Hwang, C.-Y.; Kim, Y.-K.; Lee, Y.-S.; Jeong, D. H.; Cho, M.-H., Antimicrobial effects of silver nanoparticles. *Nanomedicine: Nanotechnology, Biology and Medicine* **2007**, *3*, (1), 95-101.
10. Maneerung, T.; Tokura, S.; Rujiravanit, R., Impregnation of silver nanoparticles into bacterial cellulose for antimicrobial wound dressing. *Carbohydrate Polymers* **2008**, *72*, (1), 43-51.
11. Jain, P.; Pradeep, T., Potential of silver nanoparticle-coated polyurethane foam as an antibacterial water filter. *Biotechnology and Bioengineering* **2005**, *90*, (1), 59-63.

12. Sambhy, V.; MacBride, M. M.; Peterson, B. R.; Sen, A., Silver Bromide Nanoparticle/Polymer Composites: Dual Action Tunable Antimicrobial Materials. *Journal of the American Chemical Society* **2006**, *128*, (30), 9798-9808.
13. Kim, B.; Park, C.-S.; Murayama, M.; Hochella, M. F., Discovery and Characterization of Silver Sulfide Nanoparticles in Final Sewage Sludge Products. *Environmental Science & Technology* **2010**, *44*, (19), 7509-7514.
14. Choi, O.; Deng, K. K.; Kim, N.-J.; Ross Jr, L.; Surampalli, R. Y.; Hu, Z., The inhibitory effects of silver nanoparticles, silver ions, and silver chloride colloids on microbial growth. *Water Research* **2008**, *42*, (12), 3066-3074.
15. Atiyeh, B. S.; Costagliola, M.; Hayek, S. N.; Dibo, S. A., Effect of silver on burn wound infection control and healing: Review of the literature. *Burns* **2007**, *33*, (2), 139-148.
16. Morones, J.; Elechiguerra, J.; Camacho, A.; Holt, K.; Kouri, J.; Ramirez, J.; Yacaman, M., The bactericidal effect of silver nanoparticles. *Nanotechnology* **2005**, *16*, (10), 2346-2353.
17. Navarro, E.; Piccapietra, F.; Wagner, B.; Marconi, F.; Kaegi, R.; Odzak, N.; Sigg, L.; Behra, R., Toxicity of Silver Nanoparticles to *Chlamydomonas reinhardtii*. *Environmental Science & Technology* **2008**, *42*, (23), 8959-8964.
18. Arnaout, C. L.; Gunsch, C. K., Impacts of Silver Nanoparticle Coating on the Nitrification Potential of *Nitrosomonas europaea*. *Environmental Science & Technology* **2012**, *46*, (10), 5387-5395.
19. Bhushan, B., Introduction to Nanotechnology. In *Springer Handbook of Nanotechnology*, Bhushan, B., Ed. Springer Berlin Heidelberg: 2010; pp 1-13.
20. Sharma, V.; Shukla, R. K.; Saxena, N.; Parmar, D.; Das, M.; Dhawan, A., DNA damaging potential of zinc oxide nanoparticles in human epidermal cells. *Toxicology Letters* **2009**, *185*, (3), 211-218.
21. Pyatenko, A.; Yamaguchi, M.; Suzuki, M., Synthesis of Spherical Silver Nanoparticles with Controllable Sizes in Aqueous Solutions. *The Journal of Physical Chemistry C* **2007**, *111*, (22), 7910-7917.
22. Chen, X.; Schluesener, H. J., Nanosilver: A nanoproduct in medical application. *Toxicology Letters* **2008**, *176*, (1), 1-12.
23. Morones, J. R.; Elechiguerra, J. L.; Camacho, A.; Holt, K.; Kouri, J. B.; Ramirez, J. T.; Yacaman, M. J., The bactericidal effect of silver nanoparticles. *Nanotechnology* **2005**, *16*, (10), 2346-2353.

24. Fröhlich, E.; Roblegg, E., Models for oral uptake of nanoparticles in consumer products. *Toxicology* **2012**, *291*, (1–3), 10-17.
25. Robertson, T. A.; Sanchez, W. Y.; Roberts, M. S., Are Commercially Available Nanoparticles Safe When Applied to the Skin? *J. Biomed. Nanotechnol.* **2010**, *6*, (5), 452-468.
26. Bystrzejewska-Piotrowska, G.; Golimowski, J.; Urban, P. L., Nanoparticles: Their potential toxicity, waste and environmental management. *Waste Management* **2009**, *29*, (9), 2587-2595.
27. Benn, T.; Cavanagh, B.; Hristovski, K.; Posner, J. D.; Westerhoff, P., The Release of Nanosilver from Consumer Products Used in the Home. *J. Environ. Qual.* **2010**, *39*, (6), 1875-1882.
28. Benn, T. M.; Westerhoff, P., Nanoparticle Silver Released into Water from Commercially Available Sock Fabrics. *Environmental Science & Technology* **2008**, *42*, (11), 4133-4139.
29. Geranio, L.; Heuberger, M.; Nowack, B., The Behavior of Silver Nanotextiles during Washing. *Environmental Science & Technology* **2009**, *43*, (21), 8113-8118.
30. Yu, D.-H.; Yu, X.; Wang, C.; Liu, X.-C.; Xing, Y., Synthesis of Natural Cellulose-Templated TiO₂/Ag Nanosponge Composites and Photocatalytic Properties. *ACS Applied Materials & Interfaces* **2012**, *4*, (5), 2781-2787.
31. Chen, X. J.; Sanchez-Gaytan, B. L.; Qian, Z. X.; Park, S. J., Noble metal nanoparticles in DNA detection and delivery. *Wiley Interdiscip. Rev.-Nanomed. Nanobiotechnol.* **2012**, *4*, (3), 273-290.
32. Brown, A. N.; Smith, K.; Samuels, T. A.; Lu, J. R.; Obare, S. O.; Scott, M. E., Nanoparticles Functionalized with Ampicillin Destroy Multiple-Antibiotic-Resistant Isolates of *Pseudomonas aeruginosa* and *Enterobacter aerogenes* and Methicillin-Resistant *Staphylococcus aureus*. *Appl. Environ. Microbiol.* **2012**, *78*, (8), 2768-2774.
33. Cao, X.; Tang, M.; Liu, F.; Nie, Y.; Zhao, C., Immobilization of silver nanoparticles onto sulfonated polyethersulfone membranes as antibacterial materials. *Colloids and Surfaces B: Biointerfaces* **2010**, *81*, (2), 555-562.
34. Agency, E. P. Secondary Drinking Water Regulations: Guidance for Nuisance Chemicals
35. Agency, E. P. Biosolids: Targeted National Sewage Sludge Survey Report - Overview.

36. Choi, O.; Clevenger, T. E.; Deng, B.; Surampalli, R. Y.; Ross Jr, L.; Hu, Z., Role of sulfide and ligand strength in controlling nanosilver toxicity. *Water Research* **2009**, *43*, (7), 1879-1886.
37. Lorenz, C.; Von Goetz, N.; Scheringer, M.; Wormuth, M.; Hungerbühler, K., Potential exposure of German consumers to engineered nanoparticles in cosmetics and personal care products. *Nanotoxicology* **2010**, *5*, (1), 12-29.
38. Huang, Y. M.; Chen, S. X.; Bing, X.; Gao, C. L.; Wang, T.; Yuan, B., Nanosilver Migrated into Food-Simulating Solutions from Commercially Available Food Fresh Containers. *Packaging Technology and Science* **2011**, *24*, (5), 291-297.
39. Quadros, M. E.; Marr, L. C., Environmental and Human Health Risks of Aerosolized Silver Nanoparticles. *Journal of the Air & Waste Management Association* **2010**, *60*, (7), 770-781.
40. Samberg, M. E.; Oldenburg, S. J.; Monteiro-Riviere, N. A., Evaluation of Silver Nanoparticle Toxicity in Skin in Vivo and Keratinocytes in Vitro. *Environ. Health Perspect.* **2010**, *118*, (3), 407-413.
41. Asare, N.; Instanes, C.; Sandberg, W. J.; Refsnes, M.; Schwarze, P.; Kruszewski, M.; Brunborg, G., Cytotoxic and genotoxic effects of silver nanoparticles in testicular cells. *Toxicology* **2012**, *291*, (1-3), 65-72.
42. Nangmenyi, G.; Yue, Z. R.; Mehrabi, S.; Mintz, E.; Economy, J., Synthesis and characterization of silver-nanoparticle-impregnated fiberglass and utility in water disinfection. *Nanotechnology* **2009**, *20*, (49).
43. Tiede, K.; Boxall, A. B. A.; Wang, X. M.; Gore, D.; Tiede, D.; Baxter, M.; David, H.; Tear, S. P.; Lewis, J., Application of hydrodynamic chromatography-ICP-MS to investigate the fate of silver nanoparticles in activated sludge. *Journal of Analytical Atomic Spectrometry* **2010**, *25*, (7), 1149-1154.
44. Tang, J. L.; Xiong, L.; Wang, S.; Wang, J. Y.; Liu, L.; Li, J. G.; Yuan, F. Q.; Xi, T. F., Distribution, Translocation and Accumulation of Silver Nanoparticles in Rats. *Journal of Nanoscience and Nanotechnology* **2009**, *9*, (8), 4924-4932.
45. Ladner, D. A.; Steele, M.; Weir, A.; Hristovski, K.; Westerhoff, P., Functionalized nanoparticle interactions with polymeric membranes. *J. Hazard. Mater.* **2012**, *211*, 288-295.
46. Chen, J. C.; Lin, Z. H.; Ma, X. X., Evidence of the production of silver nanoparticles via pretreatment of *Phoma* sp.3.2883 with silver nitrate. *Lett. Appl. Microbiol.* **2003**, *37*, (2), 105-108.

47. Zook, J. M.; Long, S. E.; Cleveland, D.; Geronimo, C. L. A.; MacCuspie, R. I., Measuring silver nanoparticle dissolution in complex biological and environmental matrices using UV-visible absorbance. *Anal. Bioanal. Chem.* **2011**, *401*, (6), 1993-2002.
48. Nayak, R. R.; Pradhan, N.; Behera, D.; Pradhan, K. M.; Mishra, S.; Sukla, L. B.; Mishra, B. K., Green synthesis of silver nanoparticle by *Penicillium purpurogenum* NPMF: the process and optimization. *J. Nanopart. Res.* **2011**, *13*, (8), 3129-3137.
49. Prathna, T. C.; Chandrasekaran, N.; Mukherjee, A., Studies on aggregation behaviour of silver nanoparticles in aqueous matrices: Effect of surface functionalization and matrix composition. *Colloids and Surfaces a-Physicochemical and Engineering Aspects* **2011**, *390*, (1-3), 216-224.
50. Rodriguez-Arguelles, M. C.; Sieiro, C.; Cao, R.; Nasi, L., Chitosan and silver nanoparticles as pudding with raisins with antimicrobial properties. *J. Colloid Interface Sci.* **2011**, *364*, (1), 80-84.
51. El Badawy, A. M.; Luxton, T. P.; Silva, R. G.; Scheckel, K. G.; Suidan, M. T.; Tolaymat, T. M., Impact of Environmental Conditions (pH, Ionic Strength, and Electrolyte Type) on the Surface Charge and Aggregation of Silver Nanoparticles Suspensions. *Environmental Science & Technology* **2010**, *44*, (4), 1260-1266.
52. Kvittek, L.; Panacek, A.; Soukupova, J.; Kolar, M.; Vecerova, R.; Pucek, R.; Holecova, M.; Zboril, R., Effect of surfactants and polymers on stability and antibacterial activity of silver nanoparticles (NPs). *Journal of Physical Chemistry C* **2008**, *112*, (15), 5825-5834.
53. Huang, H. H.; Ni, X. P.; Loy, G. L.; Chew, C. H.; Tan, K. L.; Loh, F. C.; Deng, J. F.; Xu, G. Q., Photochemical formation of silver nanoparticles in poly(N-vinylpyrrolidone). *Langmuir* **1996**, *12*, (4), 909-912.
54. Song, J. E.; Phenrat, T.; Marinakos, S.; Xiao, Y.; Liu, J.; Wiesner, M. R.; Tilton, R. D.; Lowry, G. V., Hydrophobic Interactions Increase Attachment of Gum Arabic- and PVP-Coated Ag Nanoparticles to Hydrophobic Surfaces. *Environmental Science & Technology* **2011**, *45*, (14), 5988-5995.
55. Sur, I.; Cam, D.; Kahraman, M.; Baysal, A.; Culha, M., Interaction of multi-functional silver nanoparticles with living cells. *Nanotechnology* **2010**, *21*, (17).
56. Tejamaya, M.; Römer, I.; Merrifield, R. C.; Lead, J. R., Stability of Citrate, PVP, and PEG Coated Silver Nanoparticles in Ecotoxicology Media. *Environmental Science & Technology* **2012**.

57. Wang, H.; Qiao, X.; Chen, J.; Ding, S., Preparation of silver nanoparticles by chemical reduction method. *Colloids and Surfaces A: Physicochemical and Engineering Aspects* **2005**, *256*, (2,Äi3), 111-115.
58. Piccapietra, F.; Sigg, L.; Behra, R., Colloidal Stability of Carbonate-Coated Silver Nanoparticles in Synthetic and Natural Freshwater. *Environmental Science & Technology* **2012**, *46*, (2), 818-825.
59. Kittler, S.; Greulich, C.; Diendorf, J.; Köller, M.; Epple, M., Toxicity of Silver Nanoparticles Increases during Storage Because of Slow Dissolution under Release of Silver Ions. *Chemistry of Materials* **2010**, *22*, (16), 4548-4554.
60. Zhao, C. M.; Wang, W. X., Importance of surface coatings and soluble silver in silver nanoparticles toxicity to *Daphnia magna*. *Nanotoxicology* **2012**, *6*, (4), 361-370.
61. Henglein, A.; Giersig, M., Formation of Colloidal Silver Nanoparticles: Capping Action of Citrate. *The Journal of Physical Chemistry B* **1999**, *103*, (44), 9533-9539.
62. Badawy, A. M. E.; Luxton, T. P.; Silva, R. G.; Scheckel, K. G.; Suidan, M. T.; Tolaymat, T. M., Impact of Environmental Conditions (pH, Ionic Strength, and Electrolyte Type) on the Surface Charge and Aggregation of Silver Nanoparticles Suspensions. *Environmental Science & Technology* **2010**, *44*, (4), 1260-1266.
63. Mulfinger, L.; Solomon, S. D.; Bahadory, M.; Jeyarajasingam, A. V.; Rutkowsky, S. A.; Boritz, C., Synthesis and Study of Silver Nanoparticles. *Journal of Chemical Education* **2007**, *84*, (2), 322.
64. Li, X.; Lenhart, J. J.; Walker, H. W., Dissolution-Accompanied Aggregation Kinetics of Silver Nanoparticles. *Langmuir* **2010**, *26*, (22), 16690-16698.
65. Liu, J.; Hurt, R. H., Ion Release Kinetics and Particle Persistence in Aqueous Nano-Silver Colloids. *Environmental Science & Technology* **2010**, *44*, (6), 2169-2175.
66. Stebounova, L.; Guio, E.; Grassian, V., Silver nanoparticles in simulated biological media: a study of aggregation, sedimentation, and dissolution. *J. Nanopart. Res.* **2011**, *13*, (1), 233-244.
67. Sondi, I.; Goia, D. V.; Matijević, E., Preparation of highly concentrated stable dispersions of uniform silver nanoparticles. *J. Colloid Interface Sci.* **2003**, *260*, (1), 75-81.
68. Scheckel, K. G.; Luxton, T. P.; El Badawy, A. M.; Impellitteri, C. A.; Tolaymat, T. M., Synchrotron Speciation of Silver and Zinc Oxide Nanoparticles Aged in a Kaolin Suspension. *Environmental Science & Technology* **2010**, *44*, (4), 1307-1312.

69. Impellitteri, C. A.; Tolaymat, T. M.; Scheckel, K. G., The Speciation Of Silver Nanoparticles In Antimicrobial Fabric Before And After Exposure To A Hypochlorite/detergent Solution. *J. Environ. Qual.* **2009**, *38*, (4), 1528-1530.
70. Kaegi, R.; Voegelin, A.; Sinnet, B.; Zuleeg, S.; Hagendorfer, H.; Burkhardt, M.; Siegrist, H., Behavior of Metallic Silver Nanoparticles in a Pilot Wastewater Treatment Plant. *Environmental Science & Technology* **2011**, *45*, (9), 3902-3908.
71. Gardea-Torresdey, J. L.; Gomez, E.; Peralta-Videa, J. R.; Parsons, J. G.; Troiani, H.; Jose-Yacaman, M., Alfalfa Sprouts: A Natural Source for the Synthesis of Silver Nanoparticles. *Langmuir* **2003**, *19*, (4), 1357-1361.
72. Gadd, G. M.; Griffiths, A. J., Microorganisms and heavy metal toxicity. *Microbial Ecology* **1977**, *4*, (4), 303-317.
73. Ercal, N.; Gurer-Orhan, H.; Aykin-Burns, N., Toxic Metals and Oxidative Stress Part I: Mechanisms Involved in Metal-induced Oxidative Damage. *Current Topics in Medicinal Chemistry* **2001**, *1*, (6), 529-539.
74. Wei, Y.-H.; Lu, C.-Y.; Lee, H.-C.; Pang, C.-Y.; Ma, Y.-S., Oxidative Damage and Mutation to Mitochondrial DNA and Age-dependent Decline of Mitochondrial Respiratory Function. *Annals of the New York Academy of Sciences* **1998**, *854*, (1), 155-170.
75. Wood, J. M.; Wang, H. K., MICROBIAL RESISTANCE TO HEAVY-METALS. *Environmental Science & Technology* **1983**, *17*, (12), A582-A590.
76. Xiang, L.; Chan, L. C.; Wong, J. W. C., Removal of heavy metals from anaerobically digested sewage sludge by isolated indigenous iron-oxidizing bacteria. *Chemosphere* **2000**, *41*, (1-2), 283-287.
77. Guibaud, G.; Comte, S.; Bordas, F.; Dupuy, S.; Baudu, M., Comparison of the complexation potential of extracellular polymeric substances (EPS), extracted from activated sludges and produced by pure bacteria strains, for cadmium, lead and nickel. *Chemosphere* **2005**, *59*, (5), 629-638.
78. Yee, N.; Fein, J. B., Quantifying Metal Adsorption onto Bacteria Mixtures: A Test and Application of the Surface Complexation Model. *Geomicrobiology Journal* **2003**, *20*, (1), 43-60.
79. Goncalves, M. D. S.; Sigg, L.; Reutlinger, M.; Stumm, W., Metal-Ion Binding by Biological Surfaces - Voltammetric Assessment in the Presence of Bacteria. *Science of the Total Environment* **1987**, *60*, 105-119.

80. Ferguson, G. P.; Booth, I. R., Importance of Glutathione for Growth and Survival of *Escherichia coli* Cells: Detoxification of Methylglyoxal and Maintenance of Intracellular K⁺. *J. Bacteriol.* **1998**, *180*, (16), 4314-4318.
81. Perr, A. C. F.; Bhriain, N. N.; Brown, N. L.; Rouch, D. A., Molecular characterization of the *gor* gene encoding glutathione reductase from *Pseudomonas aeruginosa*: determinants of substrate specificity among pyridine nucleotide-disulphide oxidoreductases. *Molecular Microbiology* **1991**, *5*, (1), 163-171.
82. Jones, D. P., [11] Redox potential of GSH/GSSG couple: Assay and biological significance. In *Methods in Enzymology*, Helmut, S.; Lester, P., Eds. Academic Press: 2002; Vol. Volume 348, pp 93-112.
83. Cooke, T. D.; Bruland, K. W., Aquatic Chemistry of Selenium - Evidence of Biomethylation. *Environmental Science & Technology* **1987**, *21*, (12), 1214-1219.
84. Schedlbauer, O. F.; Heumann, K. G., Biomethylation of thallium by bacteria and first determination of biogenic dimethylthallium in the ocean. *Applied Organometallic Chemistry* **2000**, *14*, (6), 330-340.
85. Compeau, G. C.; Bartha, R., Sulfate-Reducing Bacteria: Principal Methylators of Mercury in Anoxic Estuarine Sediment. *Appl. Environ. Microbiol.* **1985**, *50*, (2), 498-502.
86. Percival, S. L.; Bowler, P. G.; Russell, D., Bacterial resistance to silver in wound care. *Journal of Hospital Infection* **2005**, *60*, (1), 1-7.
87. Castellano, J. J.; Shafii, S. M.; Ko, F.; Donate, G.; Wright, T. E.; Mannari, R. J.; Payne, W. G.; Smith, D. J.; Robson, M. C., Comparative evaluation of silver-containing antimicrobial dressings and drugs. *International Wound Journal* **2007**, *4*, (2), 114-122.
88. Carlson, C.; Hussain, S. M.; Schrand, A. M.; K. Braydich-Stolle, L.; Hess, K. L.; Jones, R. L.; Schlager, J. J., Unique Cellular Interaction of Silver Nanoparticles: Size-Dependent Generation of Reactive Oxygen Species. *The Journal of Physical Chemistry B* **2008**, *112*, (43), 13608-13619.
89. Jung, W. K.; Koo, H. C.; Kim, K. W.; Shin, S.; Kim, S. H.; Park, Y. H., Antibacterial Activity and Mechanism of Action of the Silver Ion in *Staphylococcus aureus* and *Escherichia coli*. *Appl. Environ. Microbiol.* **2008**, *74*, (7), 2171-2178.
90. Slawson, R. M.; Lee, H.; Trevors, J. T., Bacterial interactions with silver. *BioMetals* **1990**, *3*, (3), 151-154.

91. Arakawa, H.; Neault, J. F.; Tajmir-Riahi, H. A., Silver(I) Complexes with DNA and RNA Studied by Fourier Transform Infrared Spectroscopy and Capillary Electrophoresis. *Biophysical Journal* **2001**, *81*, (3), 1580-1587.
92. Hossain, Z.; Huq, F., Studies on the interaction between Ag⁺ and DNA. *Journal of Inorganic Biochemistry* **2002**, *91*, (2), 398-404.
93. Hussain, S.; Anner, R. M.; Anner, B. M., Cysteine protects Na,K-ATPase and isolated human lymphocytes from silver toxicity. *Biochemical and Biophysical Research Communications* **1992**, *189*, (3), 1444-1449.
94. Matsumura, Y.; Yoshikata, K.; Kunisaki, S.-i.; Tsuchido, T., Mode of Bactericidal Action of Silver Zeolite and Its Comparison with That of Silver Nitrate. *Appl. Environ. Microbiol.* **2003**, *69*, (7), 4278-4281.
95. Jin, X.; Li, M.; Wang, J.; Marambio-Jones, C.; Peng, F.; Huang, X.; Damoiseaux, R.; Hoek, E. M. V., High-Throughput Screening of Silver Nanoparticle Stability and Bacterial Inactivation in Aquatic Media: Influence of Specific Ions. *Environmental Science & Technology* **2010**, *44*, (19), 7321-7328.
96. Zeng, W.; Zhang, Y.; Li, L.; Peng, Y. Z.; Wang, S. Y., Control and optimization of nitrifying communities for nitrification from domestic wastewater at room temperatures. *Enzyme Microb. Technol.* **2009**, *45*, (3), 226-232.
97. Hooper, A. B.; Vannelli, T.; Bergmann, D. J.; Arciero, D. M. In *Enzymology of the oxidation of ammonia to nitrite by bacteria*, Feb, 1997; 1997; pp 59-67.
98. Park, H. D.; Noguera, D. R., Characterization of two ammonia-oxidizing bacteria isolated from reactors operated with low dissolved oxygen concentrations. *Journal of Applied Microbiology* **2007**, *102*, (5), 1401-1417.
99. Bedard, C.; Knowles, R., Physiology, biochemistry, and Specific Inhibitors of CH₄, NH₄⁺, and Co-oxidation by Methanotrophs and Nitrifiers *Microbiological Reviews* **1989**, *53*, (1), 68-84.
100. Blum, D. J. W.; Speece, R. E., The Toxicity of Organic Chemicals to Treatment Processes. *Water Science and Technology* **1992**, *25*, (3), 23-31.
101. Lee, Y. W.; Tian, Q.; Ong, S. K.; Sato, C.; Chung, J., Inhibitory Effects of Copper on Nitrifying Bacteria in Suspended and Attached Growth Reactors. *Water Air Soil Pollut.* **2009**, *203*, (1-4), 17-27.
102. Riggle, P. J.; Kumamoto, C. A., Role of a *Candida albicans* P1-Type ATPase in Resistance to Copper and Silver Ion Toxicity. *J. Bacteriol.* **2000**, *182*, (17), 4899-4905.

103. Lodi, A.; Solisio, C.; Converti, A.; Del Borghi, M., Cadmium, Zinc, Copper, Silver and Chromium(III) removal from wastewaters by *Sphaerotilus natans*. *Bioprocess and Biosystems Engineering* **1998**, *19*, (3), 197-203.
104. Ghandour, W.; Hubbard, J. A.; Deistung, J.; Hughes, M. N.; Poole, R. K., The uptake of silver ions by *Escherichia coli* K12: toxic effects and interaction with copper ions. *Applied Microbiology and Biotechnology* **1988**, *28*, (6), 559-565.
105. Gao, J.; Youn, S.; Hovsepyan, A.; Llaneza, V. L.; Wang, Y.; Bitton, G.; Bonzongo, J. C. J., Dispersion and Toxicity of Selected Manufactured Nanomaterials in Natural River Water Samples: Effects of Water Chemical Composition. *Environmental Science & Technology* **2009**, *43*, (9), 3322-3328.
106. Fabrega, J.; Fawcett, S. R.; Renshaw, J. C.; Lead, J. R., Silver Nanoparticle Impact on Bacterial Growth: Effect of pH, Concentration, and Organic Matter. *Environmental Science & Technology* **2009**, *43*, (19), 7285-7290.
107. Tien, D. C.; Tseng, K. H.; Liao, C. Y.; Tsung, T. T., Identification and quantification of ionic silver from colloidal silver prepared by electric spark discharge system and its antimicrobial potency study. *J. Alloy. Compd.* **2009**, *473*, (1-2), 298-302.
108. Blaser, S. A.; Scheringer, M.; MacLeod, M.; Hungerbühler, K., Estimation of cumulative aquatic exposure and risk due to silver: Contribution of nano-functionalized plastics and textiles. *Science of The Total Environment* **2008**, *390*, (2-3), 396-409.
109. Gheju, M.; Pode, R.; Manea, F., Comparative heavy metal chemical extraction from anaerobically digested biosolids. *Hydrometallurgy* **2011**, *108*, (1-2), 115-121.
110. Sambhy, V.; MacBride, M. M.; Peterson, B. R.; Sen, A., Silver Bromide Nanoparticle/Polymer Composites: A Dual Action Tunable Antimicrobial Materials. *Journal of the American Chemical Society* **2006**, *128*, (30), 9798-9808.
111. Marambio-Jones, C.; Hoek, E., A review of the antibacterial effects of silver nanomaterials and potential implications for human health and the environment. *Journal of Nanoparticle Research* **2010**, *12*, (5), 1531-1551.
112. Pal, S.; Tak, Y. K.; Song, J. M., Does the Antibacterial Activity of Silver Nanoparticles Depend on the Shape of the Nanoparticle? A Study of the Gram-Negative Bacterium *Escherichia coli*. *Applied and Environmental Microbiology* **2007**, *73*, (6), 1712-1720.
113. Lu, W.; Senapati, D.; Wang, S.; Tovmachenko, O.; Singh, A. K.; Yu, H.; Ray, P. C., Effect of surface coating on the toxicity of silver nanomaterials on human skin keratinocytes. *Chemical Physics Letters* **2010**, *487*, (1-3), 92-96.

114. Sheng, Z.; Liu, Y., Effects of silver nanoparticles on wastewater biofilms. *Water Research* **2011**, *45*, (18), 6039-6050.
115. Arciero, D.; Vannelli, T.; Logan, M.; Hopper, A. B., Degradation of trichloroethylene by the ammonia-oxidizing bacterium *Nitrosomonas europaea*. *Biochemical and Biophysical Research Communications* **1989**, *159*, (2), 640-643.
116. Kim, J. Y.; Lee, C.; Cho, M.; Yoon, J., Enhanced inactivation of *E. coli* and MS-2 phage by silver ions combined with UV-A and visible light irradiation. *Water Research* **2008**, *42*, (1-2), 356-362.
117. Bedard, C.; Knowles, R., Physiology, biochemistry, and specific inhibitors of CH₄, NH₄⁺, and CO oxidation by methanotrophs and nitrifiers. *Microbiol. Mol. Biol. Rev.* **1989**, *53*, (1), 68-84.
118. DiSpirito, A. A.; Taaffe, L. R.; Hooper, A. B., Localization and concentration of hydroxylamine oxidoreductase and cytochromes c-552, c-554, cm-553, cm-552 and a in *Nitrosomonas europaea*. *Biochimica et Biophysica Acta (BBA) - Bioenergetics* **1985**, *806*, (2), 320-330.
119. Choi, O. K.; Hu, Z. Q., Nitrification inhibition by silver nanoparticles. *Water Science and Technology* **2009**, *59*, (9), 1699-1702.
120. Radniecki, T. S.; Stankus, D. P.; Neigh, A.; Nason, J. A.; Semprini, L., Influence of liberated silver from silver nanoparticles on nitrification inhibition of *Nitrosomonas europaea*. *Chemosphere* **2011**, *85*, (1), 43-49.
121. Teske, A.; Alm, E.; Regan, J. M.; Toze, S.; Rittmann, B. E.; Stahl, D. A., Evolutionary Relationships Among Ammonia-Oxidizing and Nitrite-Oxidizing Bacteria. *Journal of Bacteriology* **1994**, *176*, (21), 6623-6630.
122. Mota, C.; Head, M. A.; Ridenoure, J. A.; Cheng, J. J.; de los Reyes, F. L., Effects of aeration cycles on nitrifying bacterial populations and nitrogen removal in intermittently aerated reactors. *Applied and Environmental Microbiology* **2005**, *71*, (12), 8565-8572.
123. Wang, H.; Qiao, X.; Chen, J.; Wang, X.; Ding, S., Mechanisms of PVP in the preparation of silver nanoparticles. *Materials Chemistry and Physics* **2005**, *94*, (2-3), 449-453.
124. Henglein, A.; Giersig, M., Formation of Colloidal Silver Nanoparticles: Capping Action of Citrate. *The Journal of Physical Chemistry B* **1999**, *103*, (44), 9533-9539.

125. Liu, J.; Sonshine, D. A.; Shervani, S.; Hurt, R. H., Controlled Release of Biologically Active Silver from Nanosilver Surfaces. *ACS Nano* **2010**, *4*, (11), 6903-6913.
126. Lee, P. C.; Meisel, D., Adsorption and surface-enhanced Raman of dyes on silver and gold sols. *The Journal of Physical Chemistry* **1982**, *86*, (17), 3391-3395.
127. Meyer, J. N.; Lord, C. A.; Yang, X. Y.; Turner, E. A.; Badireddy, A. R.; Marinakos, S. M.; Chilkoti, A.; Wiesner, M. R.; Auffan, M., Intracellular uptake and associated toxicity of silver nanoparticles in *Caenorhabditis elegans*. *Aquatic Toxicology* **2010**, *100*, (2), 140-150.
128. Yin, L.; Cheng, Y.; Espinasse, B.; Colman, B. P.; Auffan, M.; Wiesner, M.; Rose, J.; Liu, J.; Bernhardt, E. S., More than the Ions: The Effects of Silver Nanoparticles on *Lolium multiflorum*. *Environmental Science & Technology* **2011**, *45*, (6), 2360-2367.
129. Skotnicka-Pitak, J.; Khunjar, W. O.; Love, N. G.; Aga, D. S., Characterization of Metabolites Formed During the Biotransformation of 17 β E \pm -Ethinylestradiol by *Nitrosomonas europaea* in Batch and Continuous Flow Bioreactors. *Environmental Science & Technology* **2009**, *43*, (10), 3549-3555.
130. Ensign, S. A.; Hyman, M. R.; Arp, D. J., In vitro activation of ammonia monooxygenase from *Nitrosomonas europaea* by copper. *Journal of bacteriology* **1993**, *175*, (7), 1971-1980.
131. Park, S.; Ely, R. L., Candidate stress genes of *Nitrosomonas europaea* for monitoring inhibition of nitrification by heavy metals. *Applied and Environmental Microbiology* **2008**, *74*, (17), 5475-5482.
132. Radniecki, T. S.; Dolan, M. E.; Semprini, L., Physiological and Transcriptional Responses of *Nitrosomonas europaea* to Toluene and Benzene Inhibition. *Environmental Science & Technology* **2008**, *42*, (11), 4093-4098.
133. Park, S.; Ely, R., Genome-wide transcriptional responses of *Nitrosomonas europaea* to zinc. *Archives of Microbiology* **2008**, *189*, (6), 541-548.
134. Hyman, M. R.; Russell, S. A.; Ely, R. L.; Williamson, K. J.; Arp, D. J., Inhibition, inactivation, and recovery of ammonia-oxidizing activity in cometabolism of trichloroethylene by *Nitrosomonas europaea*. *Applied and Environmental Microbiology* **1995**, *61*, (4), 1480-1487.
135. Zhao, C.-M.; Wang, W.-X., Comparison of acute and chronic toxicity of silver nanoparticles and silver nitrate to *Daphnia magna*. *Environmental Toxicology and Chemistry* **2011**, *30*, (4), 885-892.

136. Bott, C. B.; Love, N. G., Implicating the glutathione-gated potassium efflux system as a cause of electrophile-induced activated sludge deflocculation. *Applied and Environmental Microbiology* **2004**, *70*, (9), 5569-5578.
137. Wang, S.; Gunsch, C. K., Effects of selected pharmaceutically active compounds on the ammonia oxidizing bacterium *Nitrosomonas europaea*. *Chemosphere* **2011**, *82*, (4), 565-572.
138. Sayavedra-Soto, L. A.; Hommes, N. G.; Alzerreca, J. J.; Arp, D. J.; Norton, J. M.; Klotz, M. G., Transcription of the amoC, amoA and amoB genes in *Nitrosomonas europaea* and *Nitrosospira* sp. NpAV. *FEMS Microbiology Letters* **1998**, *167*, (1), 81-88.
139. Sayavedra-Soto, L. A.; Hommes, N. G.; Arp, D. J., Characterization of the gene encoding hydroxylamine oxidoreductase in *Nitrosomonas europaea*. *Journal of bacteriology* **1994**, *176*, (2), 504-510.
140. Peirson, S. N.; Butler, J. N.; Foster, R. G., Experimental validation of novel and conventional approaches to quantitative realtime PCR data analysis. *Nucleic Acids Research* **2003**, *31*, (14), e73.
141. Kvittek, L.; PanacÅ&oscar;ek, A.; Soukupova, J.; Kolar, M.; VecÅ&oscar;erova, R.; Pucek, R.; Holecova, M.; Zboril, R., Effect of Surfactants and Polymers on Stability and Antibacterial Activity of Silver Nanoparticles (NPs). *The Journal of Physical Chemistry C* **2008**, *112*, (15), 5825-5834.
142. Stein, L. Y.; Arp, D. J., Loss of Ammonia Monooxygenase Activity in *Nitrosomonas europaea* upon Exposure to Nitrite. *Applied and Environmental Microbiology* **1998**, *64*, (10), 4098-4102.
143. Thurman, R. B.; Gerba, C. P.; Bitton, G., The molecular mechanisms of copper and silver ion disinfection of bacteria and viruses. *Critical Reviews in Environmental Control* **1989**, *18*, (4), 295-315.
144. Premuzic, E. T.; Francis, A. J.; Lin, M.; Schubert, J., Induced formation of chelating agents by *Pseudomonas aeruginosa* grown in presence of thorium and uranium. *Archives of Environmental Contamination and Toxicology* **1985**, *14*, (6), 759-768.
145. Kim, S.; Choi, J. E.; Choi, J.; Chung, K.-H.; Park, K.; Yi, J.; Ryu, D.-Y., Oxidative stress-dependent toxicity of silver nanoparticles in human hepatoma cells. *Toxicology in Vitro* **2009**, *23*, (6), 1076-1084.
146. Xiu, Z.-M.; Ma, J.; Alvarez, P. J. J., Differential Effect of Common Ligands and Molecular Oxygen on Antimicrobial Activity of Silver Nanoparticles versus Silver Ions. *Environmental Science & Technology* **2011**, *45*, (20), 9003-9008.

147. Jose Ruben, M.; Jose Luis, E.; Alejandra, C.; Katherine, H.; Juan, B. K.; Jose Tapia, R. r.; Miguel Jose, Y., The bactericidal effect of silver nanoparticles. *Nanotechnology* **2005**, *16*, (10), 2346.
148. Marden, P.; Tunlid, A.; Malmcrona-Friberg, K.; Odham, G.; Kjelleberg, S., Physiological and morphological changes during short term starvation of marine bacterial isolates. *Archives of Microbiology* **1985**, *142*, (4), 326-332.
149. Kittler, S.; Greulich, C.; Diendorf, J.; KoÅäller, M.; Epple, M., Toxicity of Silver Nanoparticles Increases during Storage Because of Slow Dissolution under Release of Silver Ions. *Chemistry of Materials* **2010**, *22*, (16), 4548-4554.
150. Rosen, B. P., Bacterial resistance to heavy metals and metalloids. *Journal of Biological Inorganic Chemistry* **1996**, *1*, (4), 273-277.
151. Jeffrey, W. H.; Nazaret, S.; Barkay, T., Detection of the *merA* gene and its expression in the environment. *Microbial Ecology* **1996**, *32*, (3), 293-303.
152. Greer, S.; Perham, R. N., Glutathione reductase from *Escherichia coli*: cloning and sequence analysis of the gene and relationship to other flavoprotein disulfide oxidoreductases. *Biochemistry* **1986**, *25*, (9), 2736-2742.
153. Su, H.-L.; Chou, C.-C.; Hung, D.-J.; Lin, S.-H.; Pao, I. C.; Lin, J.-H.; Huang, F.-L.; Dong, R.-X.; Lin, J.-J., The disruption of bacterial membrane integrity through ROS generation induced by nanohybrids of silver and clay. *Biomaterials* **2009**, *30*, (30), 5979-5987.
154. Fabrega, J.; Renshaw, J. C.; Lead, J. R., Interactions of Silver Nanoparticles with *Pseudomonas putida* Biofilms. *Environmental Science & Technology* **2009**, *43*, (23), 9004-9009.
155. Furno, F.; Morley, K. S.; Wong, B.; Sharp, B. L.; Arnold, P. L.; Howdle, S. M.; Bayston, R.; Brown, P. D.; Winship, P. D.; Reid, H. J., Silver nanoparticles and polymeric medical devices: a new approach to prevention of infection? *Journal of Antimicrobial Chemotherapy* **2004**, *54*, (6), 1019-1024.
156. Choi, O.; Hu, Z., Size Dependent and Reactive Oxygen Species Related Nanosilver Toxicity to Nitrifying Bacteria. *Environmental Science & Technology* **2008**, *42*, (12), 4583-4588.
157. Zook, J.; Long, S.; Cleveland, D.; Geronimo, C.; MacCusprie, R., Measuring silver nanoparticle dissolution in complex biological and environmental matrices using UV-visible absorbance. *Anal. Bioanal. Chem.* **2011**, *401*, (6), 1993-2002.

158. Kim, S.; Baek, Y.-W.; An, Y.-J., Assay-dependent effect of silver nanoparticles to <i>Escherichia coli</i> and <i>Bacillus subtilis</i>. *Applied Microbiology and Biotechnology* **2011**, *92*, (5), 1045-1052.
159. Sondi, I.; Salopek-Sondi, B., Silver nanoparticles as antimicrobial agent: a case study on *E. coli* as a model for Gram-negative bacteria. *J. Colloid Interface Sci.* **2004**, *275*, (1), 177-182.
160. Kumar, C. G.; Mamidyala, S. K., Extracellular synthesis of silver nanoparticles using culture supernatant of *Pseudomonas aeruginosa*. *Colloids and Surfaces B: Biointerfaces* **2011**, *84*, (2), 462-466.
161. Husseiny, M. I.; El-Aziz, M. A.; Badr, Y.; Mahmoud, M. A., Biosynthesis of gold nanoparticles using *Pseudomonas aeruginosa*. *Spectrochimica Acta Part A: Molecular and Biomolecular Spectroscopy* **2007**, *67*, (3-4), 1003-1006.
162. Kelly, R.; Love, N., The Role of Glutathione Mediated Oxidative Stress Response Mechanisms in Nitrifying Bacteria. *Proceedings of the Water Environment Federation* **2006**, *2006*, 6574-6592.
163. Leichert, L. I. O.; Scharf, C.; Hecker, M., Global Characterization of Disulfide Stress in *Bacillus subtilis*. *Journal of Bacteriology* **2003**, *185*, (6), 1967-1975.
164. Caro, C.; López-Cartes, C.; Zaderenko, P.; Mejías, J. A., Thiol-immobilized silver nanoparticle aggregate films for surface enhanced Raman scattering. *Journal of Raman Spectroscopy* **2008**, *39*, (9), 1162-1169.
165. Van Hying, D. L.; Klemperer, W. G.; Zukoski, C. F., Silver Nanoparticle Formation: Predictions and Verification of the Aggregative Growth Model. *Langmuir* **2001**, *17*, (11), 3128-3135.
166. Teitzel, G. M.; Parsek, M. R., Heavy Metal Resistance of Biofilm and Planktonic *Pseudomonas aeruginosa*. *Applied and Environmental Microbiology* **2003**, *69*, (4), 2313-2320.
167. Ahmad, A.; Mukherjee, P.; Senapati, S.; Mandal, D.; Khan, M. I.; Kumar, R.; Sastry, M., Extracellular biosynthesis of silver nanoparticles using the fungus *Fusarium oxysporum*. *Colloids and Surfaces B: Biointerfaces* **2003**, *28*, (4), 313-318.
168. Gurunathan, S.; Kalishwaralal, K.; Vaidyanathan, R.; Venkataraman, D.; Pandian, S. R. K.; Muniyandi, J.; Hariharan, N.; Eom, S. H., Biosynthesis, purification and characterization of silver nanoparticles using *Escherichia coli*. *Colloids and Surfaces B: Biointerfaces* **2009**, *74*, (1), 328-335.

169. Wastewater Technology Fact Sheet: Sequencing Batch Reactors. In Water, O. o., Ed. Environmental Protection Agency: Washington, D.C., 1999.
170. Kos, P., Short SRT (solids retention time) nitrification process/flowsheet. *Water Science and Technology* **1998**, *38*, (1), 23-29.
171. Zeng, R. J.; Lemaire, R.; Yuan, Z.; Keller, J., Simultaneous nitrification, denitrification, and phosphorus removal in a lab-scale sequencing batch reactor. *Biotechnology and Bioengineering* **2003**, *84*, (2), 170-178.
172. Lukow, T.; Dunfield, P. F.; Liesack, W., Use of the T-RFLP technique to assess spatial and temporal changes in the bacterial community structure within an agricultural soil planted with transgenic and non-transgenic potato plants. *FEMS Microbiol. Ecol.* **2000**, *32*, (3), 241-247.
173. Culman, S. W.; Gauch, H. G.; Blackwood, C. B.; Thies, J. E., Analysis of T-RFLP data using analysis of variance and ordination methods: A comparative study. *Journal of Microbiological Methods* **2008**, *75*, (1), 55-63.
174. Rothauwe, J. H.; Witzel, K. P.; Liesack, W., The ammonia monooxygenase structural gene amoA as a functional marker: molecular fine-scale analysis of natural ammonia-oxidizing populations. *Applied and Environmental Microbiology* **1997**, *63*, (12), 4704-12.
175. Jin, T.; Zhang, T.; Yan, Q., Characterization and quantification of ammonia-oxidizing archaea (AOA) and bacteria (AOB) in a nitrogen-removing reactor using T-RFLP and qPCR. *Applied Microbiology and Biotechnology* **2010**, *87*, (3), 1167-1176.
176. Culman, S.; Bukowski, R.; Gauch, H.; Cadillo-Quiroz, H.; Buckley, D., T-REX: software for the processing and analysis of T-RFLP data. *BMC Bioinformatics* **2009**, *10*, (1), 171.
177. Balantrapu, K.; Goia, D. V., Silver nanoparticles for printable electronics and biological applications. *Journal of Materials Research* **2009**, *24*, (9), 2828-2836.
178. Lin, S.; Cheng, Y.; Liu, J.; Wiesner, M. R., Polymeric Coatings on Silver Nanoparticles Hinder Autoaggregation but Enhance Attachment to Uncoated Surfaces. *Langmuir* **2012**, *28*, (9), 4178-4186.
179. Hou, L. L.; Li, K. Y.; Ding, Y. Z.; Li, Y.; Chen, J.; Wu, X. L.; Li, X. Q., Removal of silver nanoparticles in simulated wastewater treatment processes and its impact on COD and NH₄ reduction. *Chemosphere* **2012**, *87*, (3), 248-252.

180. Kiser, M. A.; Ryu, H.; Jang, H. Y.; Hristovski, K.; Westerhoff, P., Biosorption of nanoparticles to heterotrophic wastewater biomass. *Water Research* **2010**, *44*, (14), 4105-4114.
181. Adams, N. W. H.; Kramer, J. R., Silver speciation in wastewater effluent, surface waters, and pore waters. *Environmental Toxicology and Chemistry* **1999**, *18*, (12), 2667-2673.
182. Ratte, H. T., Bioaccumulation and toxicity of silver compounds: A review. *Environmental Toxicology and Chemistry* **1999**, *18*, (1), 89-108.
183. Trevors, J. T., Silver Resistance and Accumulation in Bacteria *Enzyme Microb. Technol.* **1987**, *9*, (6), 331-333.
184. Kindaichi, T.; Ito, T.; Okabe, S., Ecophysiological Interaction between Nitrifying Bacteria and Heterotrophic Bacteria in Autotrophic Nitrifying Biofilms as Determined by Microautoradiography-Fluorescence In Situ Hybridization. *Applied and Environmental Microbiology* **2004**, *70*, (3), 1641-1650.
185. Hagopian, D. S.; Riley, J. G., A closer look at the bacteriology of nitrification. *Aquacultural Engineering* **1998**, *18*, (4), 223-244.
186. Silver, S., Bacterial silver resistance: molecular biology and uses and misuses of silver compounds. *FEMS Microbiology Reviews* **2003**, *27*, (2-3), 341-353.
187. Liang, Z.; Das, A.; Hu, Z., Bacterial response to a shock load of nanosilver in an activated sludge treatment system. *Water Research* **2010**, *44*, (18), 5432-5438.
188. Laban, G.; Nies, L.; Turco, R.; Bickham, J.; Sepúlveda, M., The effects of silver nanoparticles on fathead minnow (<i>Pimephales promelas) embryos. *Ecotoxicology* **2010**, *19*, (1), 185-195.
189. Kao, P.-H.; Huang, C.-C.; Hseu, Z.-Y., Response of microbial activities to heavy metals in a neutral loamy soil treated with biosolid. *Chemosphere* **2006**, *64*, (1), 63-70.
190. Impellitteri, C. A.; Tolaymat, T. M.; Scheckel, K. G., The Speciation Of Silver Nanoparticles In Antimicrobial Fabric Before And After Exposure To A Hypochlorite/detergent Solution. *J. Environ. Qual.* **2009**, *38*, (4), 1528-1530.
191. Wang, Y.; Shi, J.; Wang, H.; Lin, Q.; Chen, X.; Chen, Y., The influence of soil heavy metals pollution on soil microbial biomass, enzyme activity, and community composition near a copper smelter. *Ecotoxicology and Environmental Safety* **2007**, *67*, (1), 75-81.

192. Gao, Y.; Zhou, P.; Mao, L.; Zhi, Y.-e.; Shi, W.-j., Assessment of effects of heavy metals combined pollution on soil enzyme activities and microbial community structure: modified ecological dose–response model and PCR-RAPD. *Environmental Earth Sciences* **2010**, *60*, (3), 603-612.
193. Bernhardt, E. S.; Colman, B. P.; Hochella Jr, M. F.; Cardinale, B. J.; Nisbet, R. M.; Richardson, C. J.; Yin, L., An Ecological Perspective on Nanomaterial Impacts in the Environment. *J. Environ. Qual* **2010**, *39*, 1-12.
194. McCune B; Mefford, M. *PC-ORD. Multivariate Analysis of Ecological Data*, 4; MjM Software Design: Gleneden Beach, Oregon, USA, 1999.
195. Clarke, K. R., Nonparametric multivariate analyses of changes in community structure. *Australian Journal of Ecology* **1993**, *18*, (1), 117-143.
196. Johnson, M. C.; Devine, A. A.; Ellis, J. C.; Grunden, A. M.; Fellner, V., Effects of antibiotics and oil on microbial profiles and fermentation in mixed cultures of ruminal microorganisms. *Journal of Dairy Science* **2009**, *92*, (9), 4467-4480.
197. Venkata Mohan, S.; Agarwal, L.; Mohanakrishna, G.; Srikanth, S.; Kapley, A.; Purohit, H. J.; Sarma, P. N., Firmicutes with iron dependent hydrogenase drive hydrogen production in anaerobic bioreactor using distillery wastewater. *International Journal of Hydrogen Energy* **2011**, *36*, (14), 8234-8242.
198. Permina, E.; Kazakov, A.; Kalinina, O.; Gelfand, M., Comparative genomics of regulation of heavy metal resistance in Eubacteria. *BMC Microbiology* **2006**, *6*, (1), 49.
199. Sun, L.-N.; Zhang, Y.-F.; He, L.-Y.; Chen, Z.-J.; Wang, Q.-Y.; Qian, M.; Sheng, X.-F., Genetic diversity and characterization of heavy metal-resistant-endophytic bacteria from two copper-tolerant plant species on copper mine wasteland. *Bioresource Technology* **2010**, *101*, (2), 501-509.
200. Vishnivetskaya, T. A.; Mosher, J. J.; Palumbo, A. V.; Yang, Z. K.; Podar, M.; Brown, S. D.; Brooks, S. C.; Gu, B.; Southworth, G. R.; Drake, M. M.; Brandt, C. C.; Elias, D. A., Mercury and Other Heavy Metals Influence Bacterial Community Structure in Contaminated Tennessee Streams. *Applied and Environmental Microbiology* **2011**, *77*, (1), 302-311.
201. Silver, S.; Misra, T. K., Plasmid-Mediated Heavy Metal Resistances. *Annual Review of Microbiology* **1988**, *42*, (1), 717-743.
202. Sitte, J.; Akob, D. M.; Kaufmann, C.; Finster, K.; Banerjee, D.; Burkhardt, E.-M.; Kostka, J. E.; Scheinost, A. C.; Büchel, G.; Küsel, K., Microbial Links between Sulfate Reduction and Metal Retention in Uranium- and Heavy Metal-Contaminated Soil. *Applied and Environmental Microbiology* **2010**, *76*, (10), 3143-3152.

203. Freitag, T. E.; Prosser, J. I., Community Structure of Ammonia-Oxidizing Bacteria within Anoxic Marine Sediments. *Applied and Environmental Microbiology* **2003**, *69*, (3), 1359-1371.
204. Baker, G. C.; Smith, J. J.; Cowan, D. A., Review and re-analysis of domain-specific 16S primers. *Journal of Microbiological Methods* **2003**, *55*, (3), 541-555.
205. Klijn, N.; Weerkamp, A. H.; de Vos, W. M., Identification of mesophilic lactic acid bacteria by using polymerase chain reaction-amplified variable regions of 16S rRNA and specific DNA probes. *Appl. Environ. Microbiol.* **1991**, *57*, (11), 3390-3393.
206. Radniecki, T. S.; Semprini, L.; Dolan, M. E., Expression of merA, amoA and hao in Continuously Cultured *Nitrosomonas europaea* Cells Exposed to Zinc Chloride Additions. *Biotechnology and Bioengineering* **2009**, *102*, (2), 546-553.

Biography

Christina Lee Arnaout was born in Arlington, TX, USA on December 10, 1985. The universities attended and degrees obtained as well as her publications and academic honors are listed below.

EDUCATION

Doctor of Philosophy in Civil and Environmental Engineering (Sept 2012)

Duke University, Durham, NC

Focus: Biological Nutrient Removal in Wastewater Treatment

Tentative dissertation thesis title: Assessing the Impacts of Silver Nanoparticles on the Growth, Diversity, and Function of Wastewater Bacteria

Graduate Advisor: Claudia K. Gunsch, PhD

GPA: 3.6/4.0

Master of Science in Civil and Environmental Engineering

Duke University, Durham, NC

GPA: 3.5/4.0

Bachelor of Science in Civil and Environmental Engineering

University of Texas at Austin

PUBLICATIONS

“Impacts of Silver Nanoparticle Coating on the Nitrification Potential of *Nitrosomonas europaea*.” Christina L. Arnaout, and Claudia K. Gunsch *Environmental Science & Technology*, **DOI:** 10.1021/es204540z

GRADUATE SCHOOL AWARDS AND NOTABLE RECOGNITIONS

Poster Competition Winner, *Association of Environmental Engineering and Science Professors* (2011)

Honorable Mention - National Science Foundation Graduate Research Fellowship (2010)

2nd Place Winner for Research Poster Contest, *American Water Works Association - North Carolina Branch* (2009)